Università degli studi di Pavia
Dipartimento di Matematica
Corso di Laurea Magistrale in Matematica

UNIVERSITÀ
DI PAVIA

Kinetic modelling and mathematical study of CubeSat-atmosphere interaction in Very Low Earth Orbit

Tesi di Laurea Magistrale in Matematica

Relatore (Supervisor):
Francesco Salvarani

Tesi di Laurea di:
Maria Laura Deiana
Matricola 544657

Anno Accademico 2024-2025

"I mostri che c'ho dentro
che mi fanno cadere,
questa mania che devi andare solo bene.
A chi mi salva ogni volta che tocco il fondo,
A chi comunque vada mi rimane accanto.
E se questa vita è un viaggio,
meno male siete qui
ogni volta che non so
volare."

— Enrico Nigiotti, Ogni volta che non so volare

A mamma, papà e Davide.

Contents

Introduction

The aim of this thesis is to analyze atmospheric behavior within the Very Low Earth Orbit (VLEO) regime and, more specifically, to investigate the complex interaction between the atmosphere and CubeSat satellites.
Originally developed for academic purposes due to their reduced and standardized dimensions, CubeSats are cubic nanosatellites that have undergone rapid evolution. Today, these platforms are widely deployed in sophisticated scientific missions and commercial applications, owing to their capacity for rapid and efficient communication with Earth.

Particular attention is devoted to VLEO orbits, characterized by altitudes ranging from 100 km to 450 km. In this region, the atmospheric composition varies significantly with altitude, necessitating the use of distinct kinetic models for an accurate description. Notably, at approximately 400 km, the predominance of atomic oxygen introduces significant technical challenges related to the degradation of satellite surfaces.

The first chapter provides a general introduction to satellite systems and CubeSats, complemented by an analysis of atmospheric composition based on data from [18]. This analysis demonstrates that, near 100 km, the atmosphere is primarily composed of O_2 and N_2. In this region, the mean free path is relatively small compared to the characteristic dimensions of the satellite, rendering particle collisions a non-negligible phenomenon. Conversely, at an altitude of about 400 km, atomic oxygen (O) becomes predominant, and the mean free path increases significantly, such that the gas can be treated as collisionless.

The second chapter reviews the state of the art and provides the theoretical background necessary to interpret the results presented in subsequent chapters. First, the kinetic equations for monatomic gases are introduced, progressing from the transport equation to the Boltzmann equation, including an analysis of the corresponding H-theorem. This framework is then extended to polyatomic gas mixtures. Subsequently, the fundamentals of two-scale convergence are presented, followed by a theoretical overview of the Direct Simulation Monte Carlo (DSMC) method for the numerical solution of the Boltzmann equation, accounting for diffuse reflection at the boundaries.

The third chapter presents the theoretical results of this work.
First, an existence and uniqueness theorem is proved for the solution of the

system governed by the monatomic transport equation, subject to appropriate initial and boundary conditions, describing the atmospheric composition at approximately 100 km. In this analysis, a diffuse reflection condition is assumed on the surface of a convex obstacle with a C^1 boundary.
The second part of the chapter investigates the convergence of this solution in cases where the surface temperature exhibits oscillatory behavior. Since such oscillations preclude strong convergence, the existence of a two-scale limit is established and its structure is characterized.
In the final section, a functional is introduced that depends on the particle flux and incorporates a kernel increasing with temperature, in order to model the degradation dynamics of the satellite surface. Given the functional's dependence on temperature and the assumption of periodic oscillations, the existence of the two-scale limit and its convergence properties are examined.

The final chapter presents our numerical results.
Through the implementation of a DSMC code, the system governed by the polyatomic Boltzmann equation is simulated under initial conditions appropriate for gas mixtures, accurately reflecting the atmosphere at 100 km. Specifically, the convergence to equilibrium of the gas in the region surrounding the satellite is analyzed.
Subsequently, using a second DSMC code, the satellite's surface degradation caused by atomic oxygen at an altitude of approximately 400 km is simulated, modeling the problem via the monatomic transport equation with suitable initial and boundary conditions. In this phase, interactions with the satellite are weighted according to several factors, including temperature, kinetic energy, and the cosine of the angle between the surface normal at the impact point and the incident velocity vector, accounting for the potential contribution of drift.
In the final analysis, degradation is simulated for a satellite rotating around the z-axis. This rotation induces oscillations in the surface temperature, and the overall evolution of the oxidation process over a complete rotation is investigated.

Chapter 1

Space Systems and Environmental Context

Given the objective of this work, namely the study of the atmosphere's interaction with the surface of a satellite at low altitude, it is necessary to delve into some physical aspects in this section, focusing on the family of satellites and the composition of the atmosphere as altitude varies.

1.1 Satellites

We define a satellite as a body, both natural and artificial, that orbits around a celestial body [10]. A primary example of a natural satellite is the Moon, which revolves around the Earth, but in this thesis work, we focus on man-made satellites. These are complex machines designed and launched from Earth by public institutions or private organizations for scientific, military, and commercial purposes, depending on the specific mission objectives. Communication with the Earth occurs via radio waves, and this allows knowing where they are located, their physical state, and the retrieval of mission data.

1.1.1 Nanosatellites: CubeSats

The landscape of man-made satellites is extremely various, in particular it is possible to classify them by their mass. Indeed, the SmallSat family [11] is defined as small spacecrafts with a mass of less than 180 kg; they, in turn, can be further differentiated into:

- Minisatellite, 100-180 kg
- Microsatellite, 10-100 kg
- Nanosatellite, 1-10 kg
- Picosatellite, 0.01-1 kg
- Femtosatellite, 0.001-0.01 kg

Of particular interest for this thesis work are CubeSats. These are cubic nanosatellites whose standard unit, "1U", is $10 \times 10 \times 10$ cm.

The CubeSat unit was developed in 1999 for educational purposes by California Polytechnic State University in San Luis Obispo (Cal Poly) and Stanford University [11]. It was suitable for this purpose given its compact and standardized shape, which reduces both technical and scientific developments and costs.

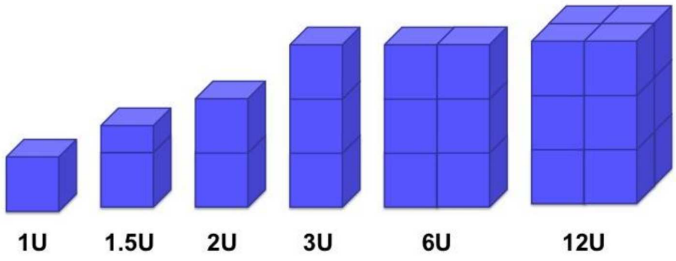

Figure 1.1: The standard CubeSat formats

But, although the primary interest was academic, this family of satellites immediately attracted the attention of government agencies and large commercial companies worldwide, leading it to evolve by combining various units: 1.5, 2, 3, 6, and even 12U, as shown in Figure 1.1. This evolution allowed for more advanced payloads and propulsion systems, essential for more complex space missions while still lowering the costs of access to space.

Among the main fields in which they have been of particular interest in recent decades are meteorology, Earth sciences, and telecommunication. For further info on CubeSats, their development process, and launch, see [12].

The evolution of CubeSats over the last few decades has been explored in depth in [5]; we report two graphs here. From Figure 1.2 we can notice how the number of CubeSat launches has increased in recent years, while from Figure 1.3 the great variety of mission types for which they have been used.

1.2 Very Low Earth Orbit

In this paper, we will focus our attention on CubeSats in VLEO (Very Low Earth Orbit).
The Very Low Earth Orbit (VLEO) [9] is an orbit around the Earth, located at an altitude between 100 and about 450 km; this type of orbit presents numerous advantages, useful for both commercial and scientific activities, such as:

- the reduction of launch costs, given the low altitude, which allows the use of numerous more accessible launch options such as micro-launchers;
- the greater ease and speed of Earth-satellite communication;

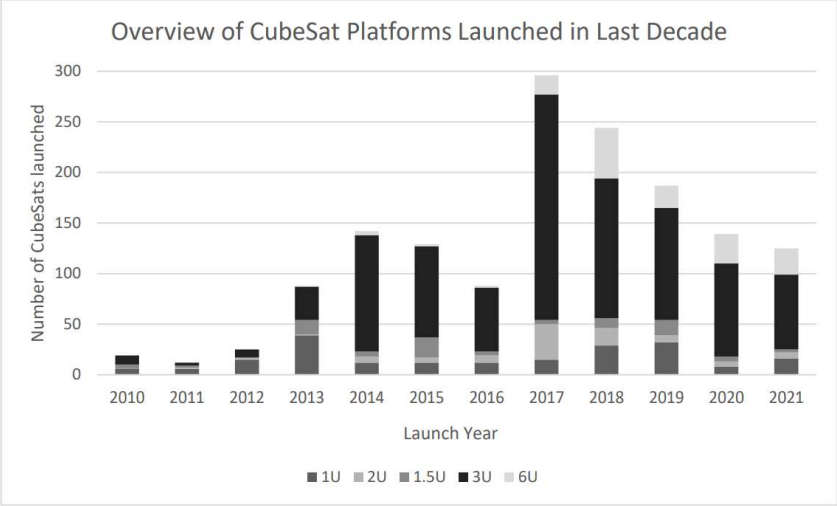

Figure 1.2: Number of CubeSat launches from 2010 to 2021. See source [5]

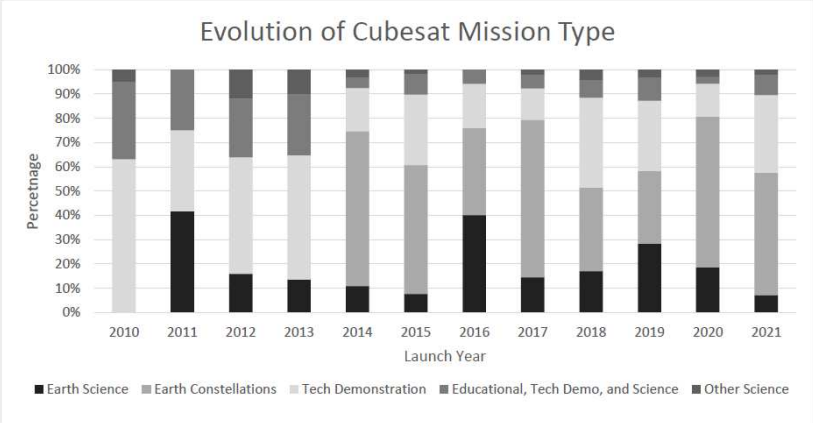

Figure 1.3: Evolution of CubeSat missions from 2010 to 2021. See source [5]

- obtaining high-resolution images for terrestrial observation through smaller and lighter lenses.

Other advantages of VLEOs are:

- relative safety from collisions with space debris;
- a more favorable radiation environment, which makes it possible to use general-purpose terrestrial-grade electronic components.

However, operating at such altitudes involves non-negligible technological challenges, including:

- a reduction in lifespan caused by residual aerodynamic drag;
- the active maintenance of the orbit (station keeping) through propulsion systems;

- the oxidation of exposed surfaces due to interaction with atomic oxygen O.

We will focus on this last point later, creating a Monte Carlo simulation that simulates the effects of degradation, given the stochastic nature of atomic collisions on an external body in rarefied environments.

1.2.1 Chemical composition of the atmosphere in VLEO

In this section, we will examine the constitutive analysis of the atmosphere at two VLEO altitudes, which will be those analyzed later in our study: 100 km and 400 km. For this purpose, we use data and graphs taken from the U.S. Standard Atmosphere [18].

First, we analyze Figure 1.4 which shows the density of molecules as a function of altitude.

- At altitudes below 100 km, the atmosphere is predominantly composed of N_2 ($\sim 78\%$), with the remainder consisting of O_2. So the atmosphere can be approximated as a mixture of diatomic gases.

  Furthermore, it can be observed that the molecular diameters σ of O_2 and N_2 are comparable, measuring approximately 3.63 Å and 3.75 Å, respectively (see Appendix A.1). This information will be crucial for determining the collision cross section.

- At 400 km, the situation is remarkably different: O is the most abundant species in the atmosphere; indeed, at these altitudes, solar radiation possesses sufficient energy to allow the photodissociation of diatomic oxygen. Therefore, at altitudes above 400 km, the atmosphere can be approximated as a monatomic gas.

A further parameter, which is useful to examine, is the mean free path as a function of altitude in Figure 1.5.

- At an altitude of 100 km, we have molecules with a mean free path in the order of 10^{-2} m; therefore, at these heights, intermolecular collision is not negligible;

- At 400 km, however, the mean free path of atmospheric molecules is of an order greater than 10^4 m. Therefore, contrary to what happens at 100 km, we could neglect intermolecular collisions.

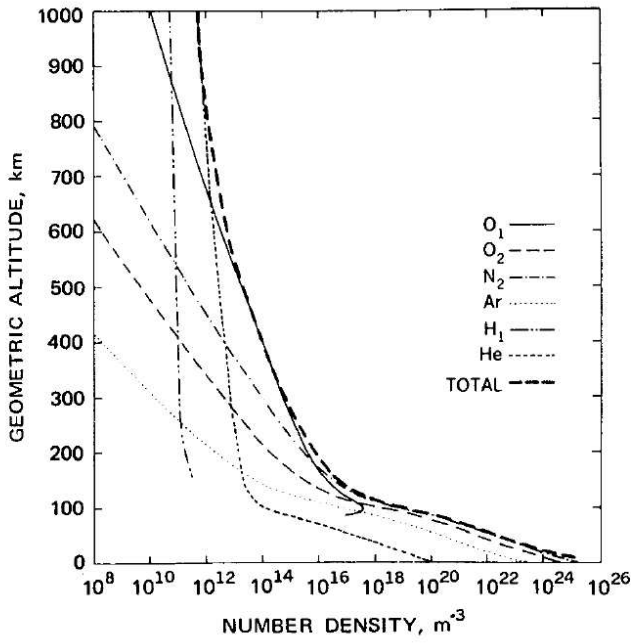

Figure 1.4: Density of each species and total density as a function of altitude. Taken from [18]

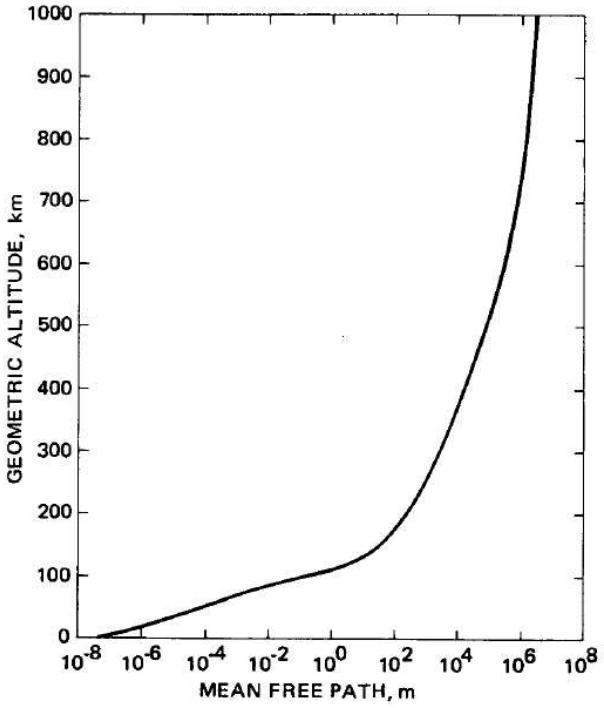

Figure 1.5: Mean free path of the atmosphere as a function of altitude. From [18]

Another crucial aspect to consider is the kinetic temperature of the gas in the atmosphere. As illustrated in Figure 1.6, the kinetic temperature varies significantly depending on the altitude:

- At an altitude of 100 km, the temperature is approximately 200 K;
- At an altitude of 400 km, the kinetic temperature reaches approximately 1000 K.

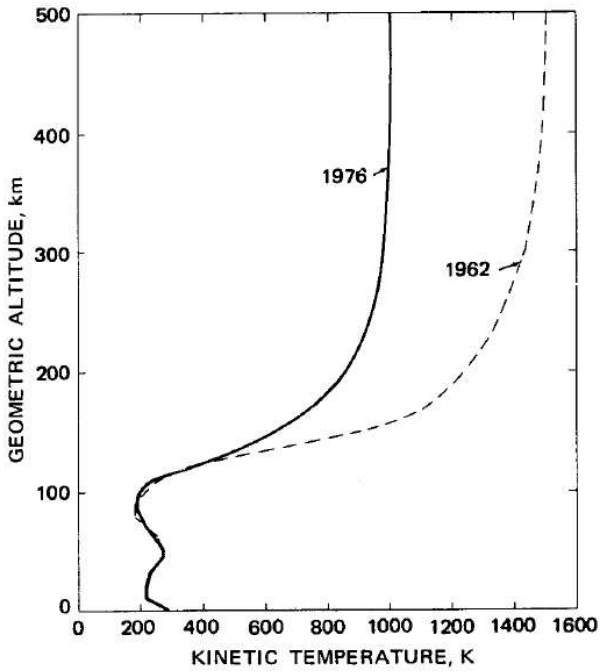

Figure 1.6: Kinetic temperature as a function of altitude. From [18]

Chapter 2

Mathematical and Numerical Framework

2.1 Kinetic equation for a monoatomic gas

Consider a monoatomic gas with mass m; the distribution function is defined as:

$$f : \mathbb{R}^+ \times \mathbb{R}^3_x \times \mathbb{R}^3_v \to [0, +\infty)$$

such that the value $f(t, x, v)\, dx\, dv$ represents the number of particles contained in the phase-space volume element $dx\, dv$ centered at (x, v) at time t.

2.1.1 Linear Transport

The distribution function f is a solution to the transport problem if it satisfies the equation:

$$\frac{\partial f}{\partial t}(t, x, v) + v \cdot \nabla_x f(t, x, v) = 0 \quad \forall (t, x, v) \in \mathbb{R}^+ \times \mathbb{R}^3_x \times \mathbb{R}^3_v. \tag{2.1}$$

Given an initial distribution f_{in}, we consider the following Cauchy problem:

$$\begin{cases} \dfrac{\partial f}{\partial t} + v \cdot \nabla_x f = 0 & (t, x, v) \in \mathbb{R}^+ \times \mathbb{R}^3_x \times \mathbb{R}^3_v \\ f(0, x, v) = f_{in}(x, v) & (x, v) \in \mathbb{R}^3_x \times \mathbb{R}^3_v. \end{cases} \tag{2.2}$$

To solve this system, it is essential to define the **characteristic curve**. Given $(y, v) \in \mathbb{R}^3_x \times \mathbb{R}^3_v$, the characteristic curve passing through y with velocity v is the trajectory:

$$\gamma(s) = y + vs, \quad \forall s \in \mathbb{R}^+. \tag{2.3}$$

Assuming $f \in C^1(\mathbb{R}^+ \times \mathbb{R}^3_x \times \mathbb{R}^3_v)$ is a solution to the free transport equation, it remains constant along these characteristics. Indeed, the total derivative with respect to time is:

$$\frac{d}{dt} f(t, \gamma(t), v) = \frac{\partial f}{\partial t}(t, \gamma(t), v) + \sum_{k=1}^{3} \frac{\partial f}{\partial x_k}(t, \gamma(t), v) \frac{d\gamma_k}{dt} =$$

$$= \frac{\partial f}{\partial t}(t, \gamma(t), v) + v \cdot \nabla_x f(t, \gamma(t), v) = 0,$$

where the vanishing of the expression is guaranteed by the fact that f satisfies the transport equation.

Boundary Conditions and the Generalized Solution

Suppose we have a bounded domain $D \subset \mathbb{R}^3$ with C^1 boundary, let $n(x)$ the outward unit normal to ∂D, which is well defined and continuous since ∂D is C^1.

We also introduce the outflow and the inflow phase-space boundary sets:

$$\Gamma_\pm := \{(x, v) \in \partial D \times \mathbb{R}^3 : \ \pm n(x) \cdot v > 0\},$$

where Γ_+ (resp. Γ_-) corresponds to molecules incoming to (resp. outgoing from) the boundary.

To complete the partition of the phase-space boundary, we define the characteristic boundary Γ_0 as the set:

$$\Gamma_0 := \{(x, v) \in \partial D \times \mathbb{R}^3 : n(x) \cdot v = 0\}, \tag{2.4}$$

which accounts for particles moving strictly tangent to the surface ∂D. It follows that the disjoint union $\Gamma_+ \cup \Gamma_- \cup \Gamma_0$ fully covers the phase-space boundary $\partial D \times \mathbb{R}^3$.

Therefore, the system must be supplemented with appropriate boundary conditions to describe the interaction between the gas and the wall of D:

$$\begin{cases} \dfrac{\partial f}{\partial t} + v \cdot \nabla_x f = 0 & \text{for } (t, x, v) \in \mathbb{R}^+ \times D \times \mathbb{R}^3_v \\ f(0, x, v) = f_{in}(x, v) & \text{for } (x, v) \in D \times \mathbb{R}^3_v \\ f(t, x, v) = f_b(t, x, v) & \text{for } (t, x, v) \in \mathbb{R}^+ \times \Gamma_-. \end{cases} \tag{2.5}$$

In cases where the solution to the system (3.13) does not belong to C^1, it is not possible to define a solution in the classical sense; instead, it is defined in a mild sense.

Definition (Mild Solution)

A function f is a **mild solution** to the transport equation [2]:

$$\frac{\partial f}{\partial t} + v \cdot \nabla_x f = 0 \quad \text{a.e. } (t, x, v) \in \mathbb{R}^+ \times D \times \mathbb{R}^3_v$$

if and only if:

1. D is an open set with a C^1 boundary ∂D;
2. $s \mapsto f(t + s, x + sv, v)$ is of class C^1 for almost every $(t, x, v) \in \mathbb{R}^+ \times D \times \mathbb{R}^3_v$;
3. $\dfrac{d}{ds} f(t + s, x + sv, v) = 0$ holds almost everywhere.

where the initial and boundary conditions are understood in the sense of traces along characteristics:

$$\lim_{t \to 0^+} f(t, x + tv, v) = f_{in}(x, v) \text{ a.e. in } x \in D$$

$$\lim_{s \to 0^+} f(t + s, y + sv, v) = f_b(t, y, v) \text{ a.e. on } (t, y, v) \in \mathbb{R}^+ \times \Gamma_-.$$

Furthermore, we introduce the concept of **backward exit time** as the function:

$$\tau : D \times \mathbb{R}^3 \to \mathbb{R}^+ \tag{2.6}$$

such that:

$$\tau_{x,v} := \tau(x, v) = \inf\{t \geq 0 : x - vt \notin \overline{D}\}. \tag{2.7}$$

It represents the time elapsed for a particle, located at position x at time t with velocity v, to reach its current state since its last interaction with the boundary ∂D.

Being inside a bounded domain D, the particles undergo reflections at the boundary.

Reflection condictions

The simplest boundary condition for gas-surface interaction is the specular reflection. In this model, each molecule hitting the surface with a pre-collisional velocity v is reflected with a post-collisional velocity v' that is symmetric to v with respect to the tangent plane at the impact point x, i.e.:

$$v' = v - 2(v \cdot n(x))n(x).$$

At the level of the kinetic description, this condition implies that the distri-

bution function f for the reflected particles is given by:

$$f(t,x,v) = f(t,x,v-2\,[v\cdot n(x)]\,n(x)), \quad (x,v)\in\Gamma_-, \tag{2.8}$$

for every $t \geq 0$.

Another commonly used boundary condition is the diffusion reflection. In this case, the incident particles lose all memory of their incoming direction; all outgoing directions are equally probable, provided that the mass flux is conserved.

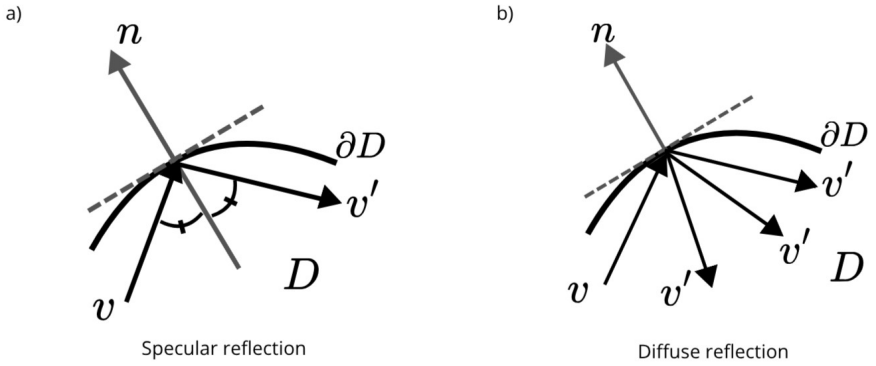

Figure 2.1: Specular *a*) and diffuse *b*) reflection models inside the domain D.

From a physical perspective, in a purely diffuse reflection, the particles are re-emitted according to a Maxwellian distribution at the wall temperature T_w:

$$f(t,x,v) = \mu(t,x)M_w(v), \quad (x,v)\in\Gamma_-, \tag{2.9}$$

where:

$$M_w(v) = (2\pi RT_w)^{-3/2}\exp\left(\frac{-|v|^2}{2RT_w}\right)$$

and $\mu(t,x)$ is a normalization parameter determined by the conservation of the flux:

$$\mu(t,x) = \frac{\displaystyle\int_{v\cdot n(x)<0} |v\cdot n(x)| f(t,x,v)\,dv}{\displaystyle\int_{v\cdot n(x)>0} (v\cdot n(x))M_w(v)\,dv}. \tag{2.10}$$

Finally, a more general boundary condition is the Maxwellian reflection, which consists of a linear combination of the specular and diffuse models [13]. By introducing an accommodation coefficient $\alpha \in [0,1]$, the distribution function at the boundary is defined as:

$$f(t,x,v) = (1-\alpha)f(t,x,v-2(v\cdot n_x)n_x) + \alpha\mu(t,x)M_w(v), \quad (x,v)\in\Gamma_- \tag{2.11}$$

where $\alpha = 0$ corresponds to purely specular reflection and $\alpha = 1$ to purely diffuse reflection.

External domain

Let $\Omega \subset \mathbb{R}^3$ an open set with C^1 boundary and assume that the density f is defined in the exterior domain $D = \mathbb{R}^3 \setminus \Omega$:

$$f : \mathbb{R}^+ \times (\mathbb{R}^3_x \setminus \Omega) \times \mathbb{R}^3_v \to [0, +\infty).$$

Let $n(x)$ be the outward unit normal to Ω (so it is inward with respect to the gas domain D), which is well-defined and continuous because $\partial\Omega$ is C^1. Since the gas occupies the exterior domain $\mathbb{R}^3 \setminus \Omega$, we consequently define:

$$\Gamma_\pm := \{(x, v) \in \partial\Omega \times \mathbb{R}^3 : \ \pm n(x) \cdot v > 0\},$$

where Γ_- (resp. Γ_+) corresponds to molecules incoming to (resp. outgoing from) the boundary of Ω.

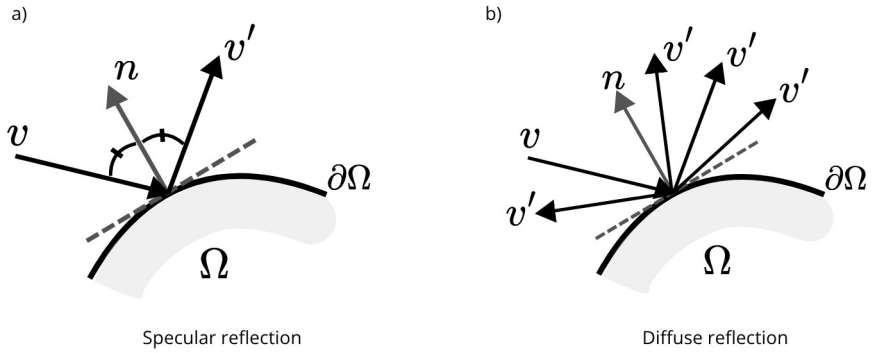

Figure 2.2: Specular a) and diffuse b) reflection models outside the domain Ω.

Therefore, the density satisfies the following system with initial and boundary conditions:

$$\begin{cases} \dfrac{\partial f}{\partial t} + v \cdot \nabla_x f = 0 & \text{for } (t, x, v) \in \mathbb{R}^+ \times (\mathbb{R}^3 \setminus \Omega) \times \mathbb{R}^3, \\ f(0, x, v) = f_{in}(x, v) & \text{for } (x, v) \in (\mathbb{R}^3 \setminus \Omega) \times \mathbb{R}^3, \\ f(t, x, v) = f_b(t, x, v) & \text{for } (t, x, v) \in \mathbb{R}^+ \times \Gamma_+. \end{cases} \tag{2.12}$$

The rest of the theory described in the previous sections remains unchanged when considering the domain $D = \mathbb{R}^3 \setminus \Omega$, except for a redefinition of the backward exit time in the case of an exterior domain.

We define the **backward exit time** as the function:

$$\tau : (\mathbb{R}^3 \setminus \Omega) \times \mathbb{R}^3 \to \mathbb{R}^+, \tag{2.13}$$

such that:

$$\tau(x, v) := \inf\{t \geq 0 : \ x - tv \notin \overline{D}\},$$

with the convention $\inf \varnothing = +\infty$. When $\tau(x, v) < +\infty$ we also define the

boundary footpoint

$$x_b(x,v) := x - \tau(x,v)v \in \partial D.$$

2.1.2 The Bolzmann equation

When the mean free path between molecules is no longer negligible, binary collisions must also be taken into account.

In this case, the distribution function f satisfies the Boltzmann equation:

$$\frac{\partial f}{\partial t} + v \cdot \nabla_x f = Q(f,f), \tag{2.14}$$

where Q is the collision operator, defined by:

$$Q(f,f)(t,x,v) = \int_{\mathbb{R}^3} \int_{\mathbb{S}^2} \left[f(t,x,v') f(t,x,v'_*) - f(t,x,v) f(t,x,v_*) \right] \mathcal{B}(v, v_*, \omega)\, d\omega\, dv_*. \tag{2.15}$$

Here, the pairs (v', v'_*) and (v, v_*) denote the pre- and post-collisional velocities and are related through the conservation of momentum and kinetic energy:

$$v + v_* = v' + v'_*, \tag{2.16}$$

$$|v|^2 + |v_*|^2 = |v'|^2 + |v'_*|^2. \tag{2.17}$$

From these relations, we can also deduce that

$$v' = \frac{v + v_*}{2} + \frac{|v - v_*|}{2}\,\omega, \tag{2.18}$$

$$v'_* = \frac{v + v_*}{2} - \frac{|v - v_*|}{2}\,\omega, \tag{2.19}$$

where $\omega \in \mathbb{S}^2$ represents the post-collisional direction of the relative velocity.

The collision kernel $\mathcal{B}$ measures the interaction frequency; it is assumed to satisfy the microreversibily condiction: $\mathcal{B}(v, v_*, \omega) = \mathcal{B}(v_*, v, \omega)$.

We now introduce the notion of **collision invariant**. A function $\varphi(v)$ is called a collision invariant if:

$$\int_{\mathbb{R}^3} \varphi(v)\, Q(f,f)(v)\, dv = 0. \tag{2.20}$$

Using the weak form of the collision operator, one obtains

$$\int_{\mathbb{R}^3} \varphi(v)\, Q(f,f)(v)\, dv = \frac{1}{4} \iiint_{\mathbb{R}^3 \times \mathbb{R}^3 \times \mathbb{S}^2} \left[\varphi(v') + \varphi(v'_*) - \varphi(v) - \varphi(v_*) \right] \times f(v) f(v_*) \mathcal{B}(v, v_*, \omega)\, d\omega\, dv_*\, dv. \tag{2.21}$$

Therefore, φ is a collision invariant if and only if

$$\varphi(v') + \varphi(v'_*) = \varphi(v) + \varphi(v_*). \tag{2.22}$$

From the conservation of momentum and kinetic energy, it follows that:

$$\varphi(v) = 1, \qquad \varphi(v) = v_i \ (i = 1, 2, 3), \qquad \varphi(v) = |v|^2$$

are collision invariants. Moreover, any collision invariant necessarily belongs to $\text{span}\{1, v, |v|^2\}$.

Macroscopic quantities

Given the distribution function f, the local macroscopic quantities are defined as:

$$n(t,x) = \int_{\mathbb{R}^3} f(t,x,v)\,dv \qquad \text{(Number density)} \tag{2.23}$$

$$\rho(t,x) = m\int_{\mathbb{R}^3} f(t,x,v)\,dv \qquad \text{(Mass density)} \tag{2.24}$$

$$u(t,x) = \frac{m}{\rho(t,x)}\int_{\mathbb{R}^3} v f(t,x,v)\,dv \qquad \text{(Bulk velocity)} \tag{2.25}$$

$$e(t,x) = \frac{m}{2\rho(t,x)}\int_{\mathbb{R}^3} |v-u|^2 f(t,x,v)\,dv = \frac{3}{2}\frac{k_B}{T}(t,x) \qquad \text{(Internal energy per particle)} \tag{2.26}$$

where k_B is the Boltzmann constant.

Theorem: H-Theorem for a monoatomic gas

Let

$$H(f)(t) = \int_{\mathbb{R}^3} f(v,t)\log f(v,t)\,dv$$

be the *H-functional*. Then, for the spatially homogeneous Boltzmann equation, one has

$$\frac{d}{dt}H(f)(t) = \int_{\mathbb{R}^3} Q(f,f)(v,t)\,\log f(v,t)\,dv \le 0.$$

Moreover,

$$\frac{d}{dt}H(f)(t) = 0$$

if and only if f is a Maxwellian distribution:

$$f(v,t) = \frac{\rho}{(2\pi RT)^{3/2}}\exp\left(-\frac{|v-u|^2}{2RT}\right).$$

Proof.

$$\int_{\mathbb{R}^3} Q(f,f)(v)\log(f(v))\,dv =$$
$$= \frac{1}{4}\iiint_{\mathbb{R}^3\times\mathbb{R}^3\times\mathbb{S}^2} \left(\log f(v) + \log f(v_*) - \log f(v') - \log f'(v'_*)\right) \times \tag{2.27}$$
$$\times \left[f(v')f(v'_*) - f(v)f(v_*)\right] \mathcal{B}\,d\omega\,dv_*\,dv \tag{2.28}$$
$$= \frac{1}{4}\iiint_{\mathbb{R}^3\times\mathbb{R}^3\times\mathbb{S}^2} \log\left(\frac{f(v)f(v_*)}{f(v')f(v'_*)}\right)\left[f(v')f(v'_*) - f(v)f(v_*)\right] \mathcal{B}\,d\omega\,dv_*\,dv. \tag{2.29}$$

Let

$$\lambda = \frac{f(v)f(v_*)}{f(v')f(v'_*)} \geq 0$$

Then

$$\Big[f(v')f(v'_*) - f(v)f(v_*)\Big] = f(v')f(v'_*)(1-\lambda)$$

and therefore

$$\int_{\mathbb{R}^3} Q(f,f)(v)\log(f(v))\,dv = \frac{1}{4}\iiint_{\mathbb{R}^3\times\mathbb{R}^3\times\mathbb{S}^2} f(v')f(v'_*)(1-\lambda)\log(\lambda)\mathcal{B}\,d\omega\,dv_*\,dv. \tag{2.30}$$

Since for all $\lambda > 0$

$$(1-\lambda)\log(\lambda) \leq 0,$$

it follows that

$$\frac{dH(f)}{dt} \leq 0.$$

Moreover, $\frac{dH(f)}{dt} = 0$ if and only if

$$(1-\lambda)\log(\lambda) = 0 \quad\Longleftrightarrow\quad \lambda = 1 \quad\Longleftrightarrow\quad f(v)f(v_*) = f(v')f(v'_*)$$

By taking the logarithm of both sides, we obtain the characterization of the equilibrium state:

$$\log f(v) + \log f(v_*) = \log f(v') + \log f(v'_*). \tag{2.31}$$

Therefore, $\varphi(v) = \log f(v)$ satisfies the defining relation of a collision invariant, and there exist$a, b, c \in \mathbb{R}$ such that

$$\log f(v) = a_i + b\cdot v + c|v|^2.$$

The constants are determined by requiring that f is consistent with the macroscopic quantities, which yields:

$$f(v,t) = \frac{\rho}{(2\pi RT)^{\frac{3}{2}}}\exp\frac{-|u-v|^2}{2RT}.$$

□

2.2 Mathematical Model for polyatomic gas mixtures

Let us now focus on the interaction between the satellite and the atmosphere at an altitude of 100 km. At these heights, as analyzed in the previous chapter, the atmosphere is composed of O_2 (22%), and N_2 (78%) with a non-negligible mean free path. Given the level of rarefaction and the chemical composition of the atmosphere, the evolution of the system is modeled using the Boltzmann equation for polyatomic gas mixtures.

Suppose we have a gas mixture composed of n different polyatomic species, with $n \geq 2$. For each species $i = 1, \ldots, n$, we define the distribution function

$$f_i : \mathbb{R}^+ \times \mathbb{R}^3_x \times \mathbb{R}^3_v \times \mathbb{R}^+ \to [0, +\infty)$$

representing the distribution function of species i, such that $f_i(t, x, v, I)\, dx\, dv\, dI$ is the number of particles contained in the phase-space volume element $dx\, dv$ centered at (x, v) at time t and internal energy $I \in \mathbb{R}^+$.

2.2.1 Macroscopic quantities

For each species i, with mass m_i, the local macroscopic quantities are defined as:

$$n_i(t,x) = \int_{\mathbb{R}_+} \int_{\mathbb{R}^3} f_i(t,x,v,I)\, dv\, dI \qquad \text{(Number density)} \tag{2.32}$$

$$\rho_i(t,x) = m_i \int_{\mathbb{R}_+} \int_{\mathbb{R}^3} f_i(t,x,v,I)\, dv\, dI \qquad \text{(Mass density)} \tag{2.33}$$

$$u_i(t,x) = \frac{m_i}{\rho_i(t,x)} \int_{\mathbb{R}_+} \int_{\mathbb{R}^3} v f_i(t,x,v,I)\, dv\, dI \qquad \text{(Species bulk velocity)} \tag{2.34}$$

$$e_i(t,x) = \frac{m_i}{2\rho_i(t,x)} \int_{\mathbb{R}_+} \int_{\mathbb{R}^3} |v - u_i|^2 f_i(t,x,v,I)\, dv\, dI \qquad \text{(Species thermal energy)} \tag{2.35}$$

where u is the mixture bulk velocity defined below.

Once the quantities for each species are established, the macroscopic variables for the entire gas mixture can be derived:

$$n(t,x) = \sum_{i=1}^{n} n_i(t,x) \qquad \text{(Number density)} \tag{2.36}$$

$$\rho(t,x) = \sum_{i=1}^{n} \rho_i(t,x) \qquad \text{(Total density)} \tag{2.37}$$

$$u(t,x) = \frac{1}{\rho} \sum_{i=1}^{n} \rho_i(t,x) u_i(t,x). \qquad \text{(Mixture bulk velocity)} \tag{2.38}$$

2.2.2 The Boltzmann system for gaseous mixtures

In the absence of external forces, the evolution of the gas mixture is governed by a system of n coupled Boltzmann equations:

$$\frac{\partial f_i}{\partial t} + v \cdot \nabla_x f_i = \sum_{j=1}^{n} \mathcal{Q}_{ij}(f_i, f_j) \quad i = 1, \dots, n. \tag{2.39}$$

The left-hand side represents the transport term, describing the free streaming of particles, while the right-hand side accounts for binary collisions between particles of species i and j.

$$\begin{aligned} &\mathcal{Q}_{ij}(f_i, f_j)(t, x, v, I) = \\ &\quad = \int_{\Omega} \int_{\mathbb{S}^2} \left[f_i(t, x, v', I') f_j(t, x, v'_*, I'_*) - f_i(t, x, v, I) f_j(t, x, v_*, I_*) \right] \times \\ &\qquad\qquad \times \mathcal{B}_{ij}(v, v_*, r, R, I, I_*, \omega) \frac{(1 - R)}{|v - v_*| \varphi_i(I)} \, dv_* \, dI_* \, dr \, dR \, d\omega. \end{aligned} \tag{2.40}$$

Here $\Omega = \{v_* \in \mathbb{R}^3;\, r, R \in [0, 1],\, I_* \in \mathbb{R}_+\}$ and $\varphi_i(I)dI$ represents a non-negative measure that varies according to the molecular structure of the gas.

The term $\mathcal{B}_{ij}$ denotes the collision cross section, which is assumed to satisfy the principles of microreversibility:

$$\mathcal{B}_{ij}(v, v_*, r, R, I, I_*, \omega) = \mathcal{B}_{ij}(v', v'_*, r', R', I', I'_*, \omega)$$

$$\mathcal{B}_{ij}(v, v_*, r, R, I, I_*, \omega) = \mathcal{B}_{ij}(v, v_*, 1 - r, R, I, I_*, \omega).$$

The tuples $(\mathbf{v}, \mathbf{v}_*, I, I_*, r, R)$ and $(\mathbf{v}', \mathbf{v}'_*, I', I'_*, r', R')$ denote the pre- and post-collisional variables of the model. In this work we adopt the **Borgnakke-Larsen model** [8].

First, the velocities and the internal energy must satisfy the conservation of momentum and total energy:

$$m_i v + m_j v_* = m_i v' + m_j v'_*, \tag{2.41}$$

$$\frac{1}{2} m_i |v|^2 + \frac{1}{2} m_j |v_*|^2 + I + I_* = \frac{1}{2} m_i |v'|^2 + \frac{1}{2} m_j |v'_*|^2 + I' + I'_*. \tag{2.42}$$

Let $\mu_{ij} = \frac{m_i m_j}{m_i + m_j}$ be the reduced mass and let $\varepsilon = \frac{1}{2} \mu_{ij} |v - v_*|^2 + I + I_*$ denotes the total energy in the center of mass frame.
A fraction $1 - R$, with $R \in [0, 1]$, of the total energy is assigned to the internal energy,

$$I' + I'_* = (1 - R)\varepsilon.$$

The remaining fraction of energy is distributed between the outgoing molecules

according to an additional parameter $r \in [0,1]$:

$$I' = r(1-R)\varepsilon \qquad I'_* = (1-r)(1-R)\varepsilon.$$

Therefore, the kinetic energy associated with the relative motion after the collision is

$$\frac{1}{2}\mu_{ij}|v' - v'_*|^2 = \varepsilon - (I' + I'_*) = R\varepsilon.$$

From these relations, the post-collisional velocities v' and v'_* can be expressed as functions of the pre-collisional quantities as follows:

$$v' = \frac{m_i v + m_j v_*}{m_i + m_j} + \frac{m_j}{m_i + m_j}\sqrt{\frac{2R\varepsilon}{\mu_{ij}}}\, T_\omega\left(\frac{v - v_*}{|v - v_*|}\right), \tag{2.43}$$

$$v'_* = \frac{m_i v + m_j v_*}{m_i + m_j} - \frac{m_i}{m_i + m_j}\sqrt{\frac{2R\varepsilon}{\mu_{ij}}}\, T_\omega\left(\frac{v - v_*}{|v - v_*|}\right), \tag{2.44}$$

where $\omega \in \mathbb{S}^2$ represents the direction of the relative velocity after the collision, and

$$T_\omega(x) = x - 2(\omega \cdot x)\omega$$

denotes the reflection of the vector x with respect to the plane orthogonal to ω.

2.2.3 Collision invariant

Definition: Collision invariant

A family of functions

$$\psi = (\psi_1, \dots, \psi_n), \qquad \varphi_i : \mathbb{R}^3 \to \mathbb{R},$$

is defined as a collisional invariant for a mixture if

$$\sum_{i=1}^{n}\sum_{j=1}^{n}\int_{\mathbb{R}_+}\int_{\mathbb{R}^3} \psi_i(v,I)\, \mathcal{Q}_{ij}(f_i, f_j)(v,I)\varphi_i(I)dI\, dv = 0,$$

for any choice of the distribution functions $(f_1, \dots, f_n)$.

Using the explicit form of the collision operator $Q_{ij}(f_i, f_j)$ and the microre-

versibility of the collision kernel, we obtain:

$$\begin{aligned}
&\int_{\mathbb{R}_+}\int_{\mathbb{R}^3} \psi_i(v,I)\, Q_{ij}(f_i,f_j)(v,I)\varphi_i(I)\,dv\,dI = \\
&\qquad = \int_{\mathbb{R}_+}\int_{\mathbb{R}^3}\int_{\Omega}\int_{\mathbb{S}^2} \psi_i(v,I)\,\left[f_i(v',I')f_j(v'_*,I'_*) - f_i(v,I)f_j(v_*,I_*)\right] \\
&\qquad\qquad \times \mathcal{B}_{ij}(v,v_*,r,R,I,I_*,\omega)\frac{(1-R)}{|v-v_*|}\,dv_*\,dI_*\,dr\,dR\,d\omega\,dv\,dI = \\
&= \frac{1}{2}\int_{\mathbb{R}_+}\int_{\mathbb{R}^3}\int_{\Omega}\int_{\mathbb{S}^2} \left(\psi_i(v,I)+\psi_j(v_*,I_*)\right)\left[f_i(v',I')f_j(v'_*,I'_*) - f_i(v,I)f_j(v_*,I_*)\right] \\
&\qquad\qquad \times \mathcal{B}_{ij}(v,v_*,r,R,I,I_*,\omega)\frac{(1-R)}{|v-v_*|}\,dv_*\,dI_*\,dr\,dR\,d\omega\,dv\,dI = \\
&= \frac{1}{4}\int_{\mathbb{R}_+}\int_{\mathbb{R}^3}\int_{\Omega}\int_{\mathbb{S}^2} \left(\psi_i(v)+\psi_j(v_*)-\psi_i(v')-\psi_j(v'_*)\right)\left[f_i(v',I')f_j(v'_*,I'_*)-f_i(v,I)f_j(v_*,I_*)\right] \\
&\qquad\qquad \times \mathcal{B}_{ij}(v,v_*,r,R,I,I_*,\omega)\frac{(1-R)}{|v-v_*|}\,dv_*\,dI_*\,dr\,dR\,d\omega\,dv\,dI. \quad (2.45)
\end{aligned}$$

Based on this formulation and by exploiting the conservation laws, we search for a base for the space of invariant operators.

Per $\psi_i(v) = 1$ e $\psi_j(v) = 0$ $\forall i,j = 1,\dots,n \quad i \neq j$:

$$\int_{\mathbb{R}_+}\int_{\mathbb{R}^3} Q_{ij}(f_i,f_j)(v,I)\psi_i(I)\varphi_i(I)\,dv\,dI = 0. \quad (2.46)$$

For $\psi_i(v,I) = m_i v_k$, with $k = 1,2,3$ and $i = 1,\dots,n$, by conservation of momentum we obtain:

$$\begin{aligned}
&\sum_{i=1}^{n}\sum_{j=1}^{n}\int_{\mathbb{R}_+}\int_{\mathbb{R}^3} m_i v_k\, Q_{ij}(f_i,f_j)(v,I)\,\varphi_i(I)dv\,dI = \\
&= \frac{1}{4}\sum_{i=1}^{n}\sum_{j=1}^{n}\int_{\mathbb{R}_+}\int_{\mathbb{R}^3}\int_{\Omega}\int_{\mathbb{S}^2} \left(m_i v_k + m_j(v_*)_k - m_i v'_k - m_j(v'_*)_k\right) \\
&\quad \times \left[f_i(v',I')f_j(v'_*,I'_*) - f_i(v,I)f_j(v_*,I_*)\right]\mathcal{B}_{ij}\frac{(1-R)}{|v-v_*|}\,dv_*\,dI_*\,dr\,dR\,d\omega\,dv\,dI = 0
\end{aligned} \quad (2.47)$$

Per $\varphi_i(v) = \frac{1}{2}m_i|v|^2 + I$ $\forall i = 1,\dots,n$ by conservation of energy we obtain:

$$\begin{aligned}
&\sum_{i=1}^{n}\sum_{j=1}^{n}\int_{\mathbb{R}_+}\int_{\mathbb{R}^3} \left(\frac{1}{2}m_i|v|^2 + I\right)\, Q_{ij}(f_i,f_j)(v,I)\varphi_i(I)\,dv\,dI = \\
&= \frac{1}{4}\sum_{i=1}^{n}\sum_{j=1}^{n}\int_{\mathbb{R}_+}\int_{\mathbb{R}^3}\int_{\Omega}\int_{\mathbb{S}^2} \left(\frac{1}{2}m_i|v|^2 + \frac{1}{2}m_j|v_*|^2 + I + I_* - \frac{1}{2}m_i|v'|^2 - \frac{1}{2}m_j|v'_*|^2 - I' - I'_*\right) \\
&\qquad\qquad \times \left[f_i(v')f_j(v'_*) - f_i(v)f_j(v_*)\right]\mathcal{B}_{ij}\,\frac{(1-R)}{|v-v_*|}\,dv_*\,dI_*\,dr\,dR\,d\omega\,dv\,dI = 0.
\end{aligned}$$

We have thus found $n + 4$ linearly independent vectors: n vectors related to the conservation of mass, 3 related to the conservation of momentum across the three velocity components, and the last one corresponding to the conservation of energy. Therefore, we construct a generic invariant $\psi(v, I) = (\psi_1(v, I), \dots, \psi_n(v, I))$ by a linear combination of these in the following form:

$$\psi_i(v, I) = a_i + b \cdot (m_i v) + c(m_i |v|^2 + I), \qquad i = 1, \dots, n$$

where $a_i \in \mathbb{R}$ are n scalars, $b \in \mathbb{R}^3$ is a constant vector, and $c \in \mathbb{R}$ is a scalar constant.

2.2.4 H-Theorem

Definition:

For a gas mixture composed of n different species, e $f_i \in L_1$ be the respective distribution functions, which are assumed to vanish at infinity, the entropy production functional is defined as:

$$D(f_1, \dots, f_n)(t) = \sum_{i,j=1}^{n} \int_{\mathbb{R}^3} \int_{\mathbb{R}_+} \int_{\mathbb{R}^3} Q_{ij}(f_i, f_j)(t, x, v, I) \times \\ \times \log\left(\frac{f_i(t, x, v, I)}{m_i}\right) \varphi_i(I)\, dx\, dv\, dI \tag{2.48}$$

while the entropy functional (or H-functional) is defined as:

$$H(t) = \sum_{i=1}^{n} \int_{\mathbb{R}^3} \int_{\mathbb{R}_+} \int_{\mathbb{R}^3_v} f_i \log\left(\frac{f_i}{m_i}\right) \varphi_i(I)\, dx\, dv\, dI \tag{2.49}$$

To study the time evolution of the entropy functional, we differentiate with respect to t:

$$\begin{aligned} \frac{dH}{dt} = &\sum_{i=1}^{n} \iiint \partial_t f_i \log\left(\frac{f_i(t, x, v, I)}{m_i}\right) dx\, dv\, dI \\ &+ \sum_{i=1}^{n} \iiint f_i\, \partial_t \left[\log\left(\frac{f_i(t, x, v, I)}{m_i}\right)\right] dx\, dv\, dI. \end{aligned} \tag{2.50}$$

Since

$$\partial_t \left(\log \frac{f_i}{m_i}\right) = \frac{\partial_t f_i}{f_i},$$

we obtain:

$$\frac{dH}{dt} = \sum_{i=1}^{n} \iiint \partial_t f_i \left(\log \frac{f_i}{m_i} + 1\right) \varphi_i(I)\, dx\, dv\, dI. \tag{2.51}$$

Using the Boltzmann equation $\partial_t f_i - v \cdot \nabla_x f_i = \sum_{j=1}^n \mathcal{Q}_{ij}(f_i, f_j)$ it follows that:

$$\begin{aligned}\frac{dH}{dt} &= \sum_{i=1}^n \iiint \left(\sum_{j=1}^n \mathcal{Q}_{ij}(f_i, f_j) + v \cdot \nabla_x f_i \right) \left(\log \frac{f_i}{m_i} + 1 \right) \varphi_i(I)\, dx\, dv\, dI = \\ &= \underbrace{\sum_{i=1}^n \sum_{j=1}^n \iiint \mathcal{Q}_{ij}(f_i, f_j) \left(\log \frac{f_i}{m_i} + 1 \right) \varphi_i(I)\, dx\, dv\, dI}_{=:T_1(t)} + \\ &\quad + \underbrace{\sum_{i=1}^n \iiint v \cdot \nabla_x f_i \left(\log \frac{f_i}{m_i} + 1 \right) \varphi_i(I)\, dx\, dv\, dI}_{=:T_2(t)}.\end{aligned} \tag{2.52}$$

Let us now focus on the transport term $T_2(t)$. Since

$$\nabla_x \left(f_i \log \frac{f_i}{m_i} \right) = \nabla_x f_i \left(\log \frac{f_i}{m_i} + 1 \right),$$

we can rewrite $T_2(t)$ as

$$\begin{aligned}T_2(t) &= \sum_{i=1}^n \iiint v \cdot \nabla_x \left(f_i \log \frac{f_i}{m_i} \right) \varphi_i(I)\, dx\, dv\, dI \\ &= \sum_{i=1}^n \iiint \nabla_x \cdot \left(v\, f_i \log \frac{f_i}{m_i} \right) \varphi_i(I)\, dx\, dv\, dI.\end{aligned} \tag{2.53}$$

Therefore, by the divergence theorem,

$$T_2(t) = \sum_{i=1}^n \iint_{\partial\Omega \times \mathbb{R}^3 \times \mathbb{R}_+} (v \cdot n(x))\, f_i \log \frac{f_i}{m_i}\, \varphi_i(I)\, d\sigma(x)\, dv\, dI. \tag{2.54}$$

Under suitable decay assumptions at infinity, this boundary contribution vanishes, and hence $T_2(t) = 0$.

As a consequence, using also (2.46), we deduce

$$\frac{dH}{dt} = \sum_{i=1}^n \sum_{j=1}^n \int_{\mathbb{R}_+} \int_{\mathbb{R}^3} \mathcal{Q}_{ij}(f_i, f_j)\, \log f_i\, dv\, dI =: D(f_1, \ldots, f_n). \tag{2.55}$$

Theorem: H-Theorem for Polyatomic Gas Mixtures

In the case of a mixture composed of n different species of polyatomic gas, the entropy functional $H(t)$ is non-increasing:

$$\frac{dH}{dt} = D(f_1, \dots, f_n) \leq 0.$$

Furthermore,

$$D(f_1, \dots, f_n) = 0$$

if and only if there exist the number density $n_i \geq 0$, a common velocity $u \in \mathbb{R}^3$, a common temperature $T > 0$ such that the distribution functions take the form:

$$f_i(v, I) = \frac{n_i}{q_i(T)} \left(\frac{m_i}{2\pi k_B T}\right)^{3/2} \exp\left[-\frac{1}{k_B T}\left(\frac{m_i}{2}|v-u|^2 + I\right)\right] \quad i = 1, \dots, n \tag{2.56}$$

where $q_i(T) = \int_0^\infty \varphi_i(I) \exp\frac{-I}{Tk_B}\, dI$ is the Laplace transform of φ_i.

Proof. Using the identity obtained in (2.45) with $\phi_i(v, I) = \log\Big(\frac{f_i(v,I)}{m_i}\Big)$, we obtain:

$$\sum_{i=1}^n \sum_{j=1}^n \int_{\mathbb{R}_+} \int_{\mathbb{R}^3} Q_{ij}(f_i, f_j)(v) \log\left(\frac{f_i(v,I)}{m_i}\right) dv\, dI =$$

$$= \frac{1}{4} \sum_{i=1}^n \sum_{j=1}^n \iiiint \left(\log\left(\frac{f_i}{m_i}\right) + \log\left(\frac{f_{j,*}}{m_j}\right) - \log\left(\frac{f_i'}{m_i}\right) - \log\left(\frac{f_{j,*}'}{m_j}\right)\right) \tag{2.57}$$

$$\times \left[f_i' f_{j,*}' - f_i f_{j,*}\right] \mathcal{B}_{ij} \frac{(1-R)}{|v - v_*|}\, dv_*\, dI_*\, dr\, dR\, d\omega\, dv\, dI \tag{2.58}$$

$$= \frac{1}{4} \sum_{i=1}^n \sum_{j=1}^n \iiiint \log\left(\frac{f_i f_{j,*}}{f_i' f_{j,*}'}\right) \left[f_i' f_{j,*}' - f_i f_{j,*}\right] \mathcal{B}_{ij} \frac{(1-R)}{|v - v_*|}\, dv_*\, dI_*\, dr\, dR\, d\omega\, dv\, dI \tag{2.59}$$

Let

$$\lambda_{ij} = \frac{f_i(v, I) f_j(v_*, I_*)}{f_i(v', I') f_j(v_*', I_*')} \geq 0 \quad \forall i, j = 1, \dots, n.$$

Then

$$\left[f_i(v', I') f_j(v_*', I_*') - f_i(v, I) f_j(v_*, I_*)\right] = f_i(v', I') f_j(v_*', I_*')(1 - \lambda_{ij}), \quad \forall i, j = 1, \dots, n$$

and therefore

$$D(f_1,\dots,f_n) = \frac{1}{4}\sum_{i=1}^{n}\sum_{j=1}^{n}\iiint f_i(v',I')f_j(v'_*,I'_*)(1-\lambda_{ij})\log(\lambda_{ij}) \tag{2.60}$$

$$\times\mathcal{B}_{ij}\frac{(1-R)}{|v-v_*|}\,dv_*\,dI_*\,dr\,dR\,d\omega\,dv\,dI. \tag{2.61}$$

Since for all $\lambda > 0$

$$(1-\lambda)\log(\lambda) \leq 0,$$

It follows that

$$D(f_1,\dots,f_n) \leq 0.$$

Moreover, $D(f_1,\dots,f_n) = 0$ if and only if $\forall i,j = 1,\dots,n$

$$(1-\lambda_{ij})\log(\lambda_{ij}) = 0 \quad\Longleftrightarrow\quad \lambda = 1 \quad\Longleftrightarrow\quad f_i(v,I)f_j(v_*,I_*) = f_i(v',I')f_j(v'_*,I'_*)$$

By taking the logarithm of both sides, we obtain the characterization of the equilibrium state:

$$\log f_i(v) + \log f_j(v_*) = \log f_i(v') + \log f_j(v'_*). \tag{2.62}$$

Relation (2.62) shows that, at the equilibrium state ($D = 0$), the family of functions $\phi = (\log f_1,\dots,\log f_n)$ satisfies the functional equation of collisional invariants. Consequently, ϕ must belong to the $(n+4)$-dimensional subspace of invariants. This implies that there exist $n+4$ scalars $(a_1,\dots,a_n,b,c)$ such that:

$$\log f_i(v,I) = a_i + b\cdot(m_i v) + c\left(\frac{1}{2}m_i|v|^2 + I\right), \quad i = 1,\dots,n.$$

By imposing the definitions of the macroscopic, the explicit values of the constants are obtained, leading to the following form:

$$f_i(v,I) = \frac{n_i}{q_i(T)}\left(\frac{m_i}{2\pi k_B T}\right)^{3/2}\exp\left[-\frac{1}{k_B T}\left(\frac{m_i}{2}|v-u|^2 + I\right)\right].$$

It remains to be proved that $T_i = T_j \quad$ and $\quad u_i = u_j \quad$ for $i \neq j$.
Using that $f_i(v,I)f_j(v_*,I_*) = f_i(v',I')f_j(v'_*,I'_*)$ we have that:

$$\begin{aligned}&\exp\left[-\frac{1}{k_B T}\Big(\frac{m_i}{2}|v-u_i|^2 + I + \frac{m_j}{2}|v_*-u_j|^2 + I_*\Big)\right] = \\ &\exp\left[-\frac{1}{k_B T}\Big(\frac{m_i}{2}|v'-u_i|^2 + I' + \frac{m_j}{2}|v'_*-u_j|^2 + I'_*\Big)\right].\end{aligned} \tag{2.63}$$

$$\frac{1}{T_i}\left[\frac{m_i}{2}\left|\frac{m_iv+m_jv_*}{m_i+m_j}+\frac{m_j}{m_i+m_j}\sqrt{\frac{2R\varepsilon}{\mu_{ij}}}\,T_\omega\left(\frac{v-v_*}{|v-v_*|}\right)-u_i\right|^2+r(1-R)\varepsilon\right]$$
$$+\frac{1}{T_j}\left[\frac{m_j}{2}\left|\frac{m_iv+m_jv_*}{m_i+m_j}-\frac{m_i}{m_i+m_j}\sqrt{\frac{2R\varepsilon}{\mu_{ij}}}\,T_\omega\left(\frac{v-v_*}{|v-v_*|}\right)-u_j\right|^2+(1-r)(1-R)\varepsilon\right]$$
$$=\frac{1}{T_i}\left[\frac{m_i}{2}|v-u_i|^2+I\right]+\frac{1}{T_j}\left[\frac{m_j}{2}|v_*-u_j|^2+I_*\right]. \tag{49}$$

By isolating the first-degree terms in r, we obtain:

$$\frac{1}{T_i}-\frac{1}{T_j}=0 \quad\Longrightarrow\quad T_i=T_j.$$

While isolating the terms of degree lower than $\sqrt{R}$, it follows that:

$$u_i=u_j.$$

It should be noted that the mean velocity u and the temperature T are common to all species $i=1,\dots,n$, representing the global mechanical and thermal equilibrium attained by the mixture.

□

Remark: In the present setting we consider classical diatomic gases, for which the internal density satisfies $\varphi_i(I)=1$. Consequently, the equilibrium distribution takes the form

$$f(t,x,v,I)=n_i(t,x)\left(\frac{m}{2\pi k_BT(t,x)}\right)^{3/2}\frac{1}{k_BT(t,x)}\exp\left(-\frac{m|v|^2}{2k_BT(t,x)}-\frac{I}{k_BT(t,x)}\right)=$$
$$=f_v(t,x,v)\cdot f_I(t,x,I)$$

where

$$f_v(t,x,v)=n_i(t,x)\left(\frac{m}{2\pi k_BT(t,x)}\right)^{3/2}\exp\left(-\frac{m|v|^2}{2k_BT(t,x)}\right)$$

and

$$f_I(t,x,I)=\frac{1}{k_BT(t,x)}\exp\left(-\frac{I}{k_BT(t,x)}\right).$$

Note: integrating $f$with respect to the internal energy I we have:

$$\int_0^\infty f(t,x,v,I)\,dI=f_v(t,x,v)\int_0^\infty\frac{1}{k_BT(t,x)}\exp\left(-\frac{I}{k_BT(t,x)}\right)dI$$
$$=f_v(t,x,v)\left[-\exp\left(-\frac{I}{k_BT(t,x)}\right)\right]_0^\infty=f_v(t,x,v)\,(0-(-1))$$
$$=f_v(t,x,v).$$

Conversely, integrating with respect to the velocity v, we obtainf_I:

$$\int_{\mathbb{R}^3} f(t,x,v,I)\,dv = f_I(t,x,I)\int_{\mathbb{R}^3}\left(\frac{m}{2\pi k_B T(t,x)}\right)^{3/2}\exp\left(-\frac{m|v|^2}{2k_B T(t,x)}\right)dv = f_I(t,x,I)$$

since the Maxwellian distribution is normalized to unity over the velocity space $\mathbb{R}^3$.

2.3 Two-scale convergence

If the boundary temperature of the satellite varies periodically in time, it can be the subject of study of the 2-scale convergence of the solution.

2.3.1 The importance of rigorous homogenisation

There are many physical phenomena, such as the propagation of Lamb waves in multiresonant metamaterials [14], in which the model is described by differential equations with oscillating coefficients. In this setting, one investigates how the microscopic oscillations of a "forest" of resonators can effectively isolate the plate from external vibrations.

More generally, we are concerned with processes in which microscopic oscillations determine fundamental macroscopic properties. The transition from the microscopic to the macroscopic scale is mathematically formalized through the homogenization process. Intuitively, one might assume that this simply amounts to replacing the oscillating term with its average; however, this approach is often insufficient. As demonstrated in the following, the homogenization limit can lead to effective systems with entirely different mathematical structures.

We now examine in detail two examples by Tartar [16, 17], the treatment of which has been drawn from [4]. In these examples, the homogenisation processes lead to different effective systems, thereby highlighting the importance of establishing a rigorous homogenisation.

Consider the following family of ODEs with the unknown u_ε. Let $a \in L^\infty(\mathbb{T}^N)$ be such that $a(y) \geq 0$ for almost every $y \in \mathbb{T}^N$.

$$\begin{cases} \frac{du_\epsilon}{dt} + a\left(\frac{z}{\epsilon}\right)u_\epsilon = 0, \\ u_\epsilon(0,z) = u^{in}(z), \end{cases} \qquad t>0,\ z\in\mathbb{R}^N \tag{2.64}$$

where $u^{in} \in L^2(\mathbb{R}^N) \cap L^\infty(\mathbb{R}^N)$.

For all $\varepsilon > 0$, the explicit solution is given by:

$$u_\epsilon(t,z) = u^{in}(z)e^{-ta(z/\epsilon)}, \quad t>0,\ z\in\mathbb{R}^N \tag{2.65}$$

In the limit as $\epsilon \to 0^+$, the sequence u_ϵ converges to u in $L^\infty(\mathbb{R}_+ \times \mathbb{R}^N)$ weak-*:

$$u(t,z) = u^{in}(z)\Phi(t), \quad t \geq 0,\ z \in \mathbb{R}^N \tag{2.66}$$

with Φ defined by:

$$\Phi(t) = \int_{\mathbb{T}^N} e^{-ta(y)} dy, \quad t \geq 0 \tag{2.67}$$

Tarar proved that the homogenized solution satisfies this integro-differential equation:

$$\begin{cases} \dfrac{du}{dt}(t,z) + \bar{a}u(t,z) = \displaystyle\int_0^t K(t-s)u(s,z)ds, \quad t > 0,\ z \in \mathbb{R}^N, \\ u(0,z) = u^{in}(z), \end{cases}$$

which does not satisfy the differential equation $\frac{du}{dt} + \bar{a}u = 0$ with $\bar{a} = \int_{\mathbb{T}^N} a(y)dy$.

We shall now examine a further problem, where the unknown is $v_\varepsilon \equiv v_\varepsilon(t) \in \mathbb{R}$:

$$\begin{cases} \dfrac{dv_\varepsilon}{dt} + b\left(\dfrac{t}{\varepsilon}\right) v_\varepsilon = 0, \quad t > 0, \\ v_\varepsilon(0) = v^{in}, \end{cases}$$

where $b \in L^\infty(\mathbb{T}^1)$.

In this case

$$v_\varepsilon(t) = v^{in} \exp\left(-\int_0^t b(s/\varepsilon)ds\right) \to v^{in}e^{-Bt} = v(t)$$

for each $t \geq 0$ as $\varepsilon \to 0^+$, where$B := \int_0^1 b(\sigma)d\sigma$. In this case the homogenized solution takes the form:

$$\begin{cases} \dfrac{dv}{dt} + Bv = 0, \quad t > 0, \\ v(0) = v^{in}, \end{cases}$$

It is worth noting that the systems satisfied by the homogenized equations in these two examples exhibit profoundly different behaviors. Consequently, we have chosen to employ two-scale convergence to correctly identify the behavior of the homogenized solution.

2.3.2 Definition and theorems

In this section, we present the fundamental definitions and theorems regarding two-scale convergence.[1]

Definition: two-scale convergence

Let consider Ω an open set of $\mathbb{R}^n$ and the unit cube $Y = [0,1]^n$.
We say that a sequence of functions $u_\epsilon \in L^2(\Omega)$ two-scale converges to $u_0(x,y)$ if

$$\lim_{\epsilon\to 0}\int_\Omega u_\epsilon(x)\psi\left(x,\frac{x}{\epsilon}\right)dx = \int_\Omega\int_Y u_0(x,y)\psi(x,y)\,dx\,dy \tag{2.68}$$

$\forall\psi$ test function in $D[\Omega; C^\infty_\#(Y)]$,where $D[\Omega; C^\infty_\#(Y)]$ denotes the space of smooth functions with compact support in Ω, taking values in the set of periodic functions $C^\infty_\#(Y)$.

Note that if Y is not the unit cube, the second term in (2.68) must be divided by $|Y|$, which represents the Lebesgue measure of the periodicity cell Y.

It is important to note that if the two-scale limit exists, it is unique. Suppose, by contradiction, that the sequence u_ϵ two-scale converges to both $u_0(x,y)$ and $v_0(x,y)$. By the definition of two-scale convergence, for any test function $\psi(x,y) \in \mathcal{D}[\Omega; C^\infty_\#(Y)]$, we have:

$$\lim_{\epsilon\to 0}\int_\Omega u_\epsilon(x)\psi\left(x,\frac{x}{\epsilon}\right)dx = \int_\Omega\int_Y u_0(x,y)\psi(x,y),dx,dy$$

$$\lim_{\epsilon\to 0}\int_\Omega u_\epsilon(x)\psi\left(x,\frac{x}{\epsilon}\right)dx = \int_\Omega\int_Y v_0(x,y)\psi(x,y),dx,dy$$

$$\Rightarrow \int_\Omega\int_Y \left[u_0(x,y) - v_0(x,y)\right]\psi(x,y),dx,dy = 0, \quad \forall\psi \in \mathcal{D}[\Omega; C^\infty_\#(Y)]$$

Since this equality holds for every test function, we conclude that:

$$u_0(x,y) = v_0(x,y) \quad \text{a.e. in } \Omega\times Y.$$

One of the most important result is the following theorem:

Theorem of compactness

For every *bounded sequence* $u_\epsilon \in L^2(\Omega)$, up to a subsequence, there exists the two-scale limit $u_0(x,y) \in L^2(\Omega\times Y)$.

The following lemma gives the link between the 2-scale convergence and the weak convergence:

Lemma

Given a sequence of functions $u_\epsilon \in L^2(\Omega)$ such that $u_\epsilon \xrightarrow{2-sc} u_0$, then $u_\epsilon(x,\frac{x}{\epsilon}) \rightharpoonup u(x) := \int_Y u_0(x,y)\,dy$ weak in $L^2(\Omega)$.

2.4 Direct Monte Carlo Simulation

Monte Carlo methods (DMCS) represent numerical techniques based on random sampling that enable the simulation of complex phenomena across diverse fields, ranging from statistical physics and biology to finance. These methods are widely employed because, unlike deterministic numerical approaches, they are particularly effective at solving high-dimensional problems, thereby circumventing the so-called *curse of dimensionality*.

In the present work, this approach is utilized to approximate the solution of partial differential equations starting from a discrete particle representation. Indeed, the Boltzmann equation can be interpreted as the kinetic limit of a system of particles interacting through collisions, both among themselves and with the domain boundaries.

2.4.1 The splitting approach

The standard approach to numerically solve the Boltzmann equation consists of splitting the equation into two distinct time steps and iterating this procedure to obtain the solution at subsequent times [13].

In the first time step, the spatially homogeneous Boltzmann equation for a monoatomic gas is solved, given the initial condition f_0:

$$\frac{\partial \tilde{f}}{\partial t} = \tilde{Q}(\tilde{f}, \tilde{f})$$

$$\tilde{f}(x, v, t) = f_0(x, v)$$

In this phase, the velocity distribution changes due to particle collisions, while the spatial positions remain constant.

For the following interval Δt, the pure transport equation is solved, using the output of the previous step as the initial condition:

$$\frac{\partial f}{\partial t} + v \cdot \nabla_x f = 0$$

$$f(0, x, v) = \tilde{f}(x, v, \Delta t)$$

This step accounts for the change in spatial positions, whereas the velocities of the particles remain unchanged.

At a numerical level, the method consists of dividing the domain into a certain number of cells. In each cell, an algorithm is applied to simulate collisions, followed by the transport step. Before repeating the splitting method, it is necessary to update the positioning of the particles within each cell. We shall now detail the numerical aspects of the two steps of the splitting approach.

2.4.2 DSMC for the spatially homogeneous Boltzmann equation

The Variable Hard Sphere (VHS) method is a molecular interaction model commonly used in gas kinetic theory. It is a variant of the Hard Spheres method where, however, the molecules have a variable cross section σ and collision kernel B:

$$\sigma\left(|v - v_*|\right) = C_\alpha |v - v_*|^{\alpha - 1}$$
$$B(v, v_*) = C_\alpha |v - v_*|^{\alpha},$$

where C_α is a positive constant.

At a computational level, the ideal choice of the upper bound Σ is:

$$\Sigma = B(2\Delta v)$$

where

$$\Delta v = \max_i |v_i - \bar{v}| \qquad \bar{v} = \frac{1}{N}\sum_i v_i.$$

The conservative DSMC scheme for simulating collisional interactions according to the VHS model is structured as follows:

Nanbu-Babovsky for VHS molecules [13]

1. From the initial density $f_0(v)$, sample the initial velocities of the particles $\{v_i^0, i = 1, \ldots, N\}$.
2. For each time step $n = 1$ to n_{Step}:
   Given $\{v_i^n, i = 1, \ldots, N\}$
   - Compute the upper bound Σ for the cross section
   - Set the number of collisions $N_c = round\left(\frac{N\rho\Sigma\Delta t}{2}\right)$
   - Randomly select N_c pairs (i, j), and for those molecules
     - Compute the relative cross section $B_{ij} = B(|v_i - v_j|)$
     - **If** $\Sigma\xi < B_{ij}$ (acceptance condition for real collision)
       - Perform the collision of i, j and calculate the post-collisional velocities v_i' and v_j' according to the collision laws of the model used
       - $v_i^{n+1} = v_i'$ and $v_j^{n+1} = v_j'$
     - **else** for the particles that did not collide, set $v_i^{n+1} = v_i^n$

   end for

Observation: the numerical treatment presented so far applies to the monospecies Boltzmann equation. In the multispecies polyatomic case, it suffices to determine the post-collisional velocities using the Borgnakke–Larsen model laws (2.43) and to extend the definition of the cross-section and its upper bound.

2.4.3 Transport step

In the second time step Δt, the particles move in free flow. Given the particles $\{(x_i, v_i) : i = 1, \ldots, N\}$, at the end of the step their positions are given by:

$$\tilde{x}_i^{n+1} = x_i^n + \hat{v}_i^{n+1}\Delta t$$

where $\hat{v}_i^{n+1}$ represents the post-collision velocity.

If the particles remain within the computational domain, the update is straightforward $x_i^{n+1} = \tilde{x}_i^{n+1}$ and $v_i^{n+1} = \hat{v}_i^{n+1}$.

When particles exit the domain, depending on the phenomenon being simulated, it is possible to re-inject molecules to simulate the flow of particles from the external region, a flow governed by a known density.

If, instead, the particles hit a solid wall, such as an obstacle, it is necessary to simulate boundary conditions, such as diffusive reflections, specular reflections, or a convex combination of these.

To implement diffuse reflection, it is essential to introduce one of the classical techniques for generating random variables with a known cumulative distribution function (CDF).

Inverse Transform Method

Let $U \sim U(0,1)$ be a uniform random variable. Given a cumulative distribution function (CDF) F such that $X = F^{-1}(U)$, then the CDF of X coincides with F ($F_X \equiv F$).

Therefore, to simulate the random variable X, we can determine the inverse of its CDF and generate a sample of uniform variables $\{u_i\}$ to compute the random realizations as follows:

$$x_i = F_X^{-1}(u_i). \tag{2.69}$$

Therefore, to simulate the diffuse reflection condition, we have already observed that while the number density distribution is given by (2.9), we must instead sample from the particle flux. The flux of particles leaving the surface per unit time and unit area is weighted by the normal velocity component $v_n = v \cdot n$, where n is the unit normal vector to the wall. Let v_{t_1} and v_{t_2} denote the velocity components tangential to the surface at the point of impact.

The probability density function for the particle flux is expressed as [15]:

$$P(v_n, v_{t_1}, v_{t_2}) = \underbrace{2\beta^2 v_n \exp(-\beta^2 v_n^2)}_{=:P(v_n)} \cdot \underbrace{\frac{\beta^2}{\pi} \exp(-\beta^2(v_{t_1}^2 + v_{t_2}^2))}_{=:F(v_{t_1})F(v_{t_2})} \tag{2.70}$$

where $\beta^2 = \frac{1}{2RT_w}$. Since the components are statistically independent, the joint

distribution can be separated as follows:

- Tangential components v_{t_1}, v_{t_2}: These follow the standard Maxwellian distribution for a surface at temperature T_w:

$$P(v_{t_1}) = \frac{\beta^2}{\pi} \exp(-\beta^2 v_{t_1}^2). \tag{2.71}$$

  These can be sampled using standard normal distribution generators.

- Normal component (u): The distribution is weighted by the normal velocity:

$$P(v_n) = 2\beta^2 v_n \exp(-\beta^2 v_n^2), \quad v_n > 0. \tag{2.72}$$

$$\Rightarrow P_{\beta^2 v_n^2} = \exp(-\beta^2 v_n^2).$$

In this case, it is necessary to apply the inverse transform method. Given the probability density function for the normal component, its cumulative distribution function (CDF) is:

$$F_{\beta^2 v_n^2} = 1 - \exp(-\beta^2 v_n^2.)$$

Exploiting the fact that if u is uniformly distributed in $[0, 1]$, then $1 - u$ is also a uniform random variable $u' \sim U(0, 1)$, we obtain:

$$v_n = \frac{1}{\beta}(-\log(u))^{\frac{1}{2}}.$$

Chapter 3

Theoretical results

3.1 Existence and uniqueness results

At an altitude of 400 km, the physical properties of the atmosphere allow for some fundamental simplifications in the kinetic model. In this region, the chemical composition is characterized by a predominance of atomic oxygen (O), allowing the system to be approximated as a single monoatomic gas species. Furthermore, the analysis of the mean free path indicates that collisional interactions are negligible.

To model this phenomenon, we consider the satellite $\Omega \subset \mathbb{R}^3$ an open, bounded and convex set with C^1 boundary and assume that the gas occupies the exterior domain. Therefore, the gas density f is defined in the exterior domain:

$$f : \mathbb{R}_+ \times (\mathbb{R}^3 \setminus \Omega) \times \mathbb{R}^3 \to [0, +\infty).$$

$$\text{Let } D := \mathbb{R}^3 \setminus \Omega, \qquad \mathcal{D}_T := (0, T) \times D \times \mathbb{R}^3;$$

therefore, the density satisfies the following system with initial and boundary conditions:

$$\begin{cases} \dfrac{\partial f}{\partial t} + v \cdot \nabla_x f = 0 & \text{for } (t, x, v) \in \mathcal{D}_T, \\ f(0, x, v) = f_{in}(x, v) & \text{for } (x, v) \in D \times \mathbb{R}^3, \\ f(t, x, v) = f_b(t, x, v) & \text{for } (t, x, v) \in \mathbb{R}_+ \times \Gamma_+. \end{cases} \tag{3.1}$$

where $n(x)$ denotes the outward normal to Ω (so it is inward with respect to the gas domain) and, consequently, $\Gamma_\pm$ represents the incoming and outgoing boundaries of the domain $D = D$, respectively.

We now further examine the forms of f_{in} and f_b that ensure the problem is physically consistent. Regarding the boundary condition, we assume diffuse

reflections. Therefore, we have:

$$f_b(t,x,v) = \frac{m^2}{2\pi(k_B T_w(x,t))^2} \exp\left(-\frac{m|v|^2}{2k_B T_w(x,t)}\right) \times \\ \times \int_{u\cdot n(x)<0} |u\cdot n(x)| f(t,x,u)\, du \qquad \text{for } (t,x,v) \in \mathbb{R}_+ \times \Gamma_+.$$

Given a point $(t,x) \in \partial\Omega$, the incoming and outgoing fluxes with respect to the domain $\mathbb{R}^3 \setminus \Omega$ at point x and time t are defined as:

$$\Phi_{in}(t,x) := \int_{v\cdot n(x)>0} f(t,x,v)|v\cdot n(x)|dv$$

$$\Phi_{out}(t,x) := \int_{v\cdot n(x)<0} f(t,x,v)|v\cdot n(x)|dv$$

Accordingly, the boundary distribution f_b can be rewritten as:

$$f_b(t,x,v) = \Phi_{out}(t,x) \frac{m^2}{2\pi(k_B T_w(x,t))^2} \exp\left(-\frac{m|v|^2}{2k_B T_w(x,t)}\right)$$

Note that the Maxwellian prefactor in the boundary condition ensures conservation of normal flux at the surface. Indeed, for $(t,x) \in \mathbb{R}_+ \times \partial\Omega$, choosing a local coordinate system where the x-axis is aligned with the inward normal unit vector $n(x)$, the calculation yields:

$$\begin{aligned}
&\Phi_{in}(t,x) = \Phi_{out}(t,x) \int_0^\infty \int_{-\infty}^\infty \int_{-\infty}^\infty \frac{m^2}{2\pi(k_B T_w)^2} v_x e^{-\frac{m(v_x^2+v_y^2+v_z^2)}{2k_B T_w}} dv_x dv_y dv_z \\
&= \Phi_{out}(t,x) \left[\int_0^\infty \frac{m v_x}{k_B T_w} e^{-\frac{m v_x^2}{2k_B T_w}} dv_x\right] \left[\int_{-\infty}^\infty \sqrt{\frac{m}{2\pi k_B T_w}} e^{-\frac{m v_y^2}{2k_B T_w}} dv_y\right] \times \\
&\qquad \times \left[\int_{-\infty}^\infty \sqrt{\frac{m}{2\pi k_B T_w}} e^{-\frac{m v_z^2}{2k_B T_w}} dv_z\right] = \\
&= \Phi_{out}(t,x) \cdot \underbrace{\left[-e^{-\frac{m v_x^2}{2k_B T_w}}\right]_0^\infty}_{=1} \underbrace{\left[\sqrt{\frac{m}{2\pi k_B T_w}} \cdot \sqrt{\frac{2\pi k_B T_w}{m}}\right]}_{=1} \underbrace{\left[\sqrt{\frac{m}{2\pi k_B T_w}} \cdot \sqrt{\frac{2\pi k_B T_w}{m}}\right]}_{=1} = \\
&= \Phi_{out}(t,x)
\end{aligned} \tag{3.2}$$

By virtue of the rotational invariance and symmetry of the Maxwellian distribution, this result can be generalized to any arbitrary direction of the normal vector.

Let

$$M(t,x,v) := \frac{m^2}{2\pi(k_B T_w(x,t))^2} \exp\left(-\frac{m|v|^2}{2k_B T_w(x,t)}\right).$$

From the calculations in the previous observation and by exploiting the parity of the Maxwellian distribution, it follows that:

$$\int_{v\cdot n(x)>0} M(t,x,v)|v\cdot n(x)|dv = 1. \tag{3.3}$$

Regarding the initial condition, we suppose that: f_{in} is the product of a spatial density $\rho_0(x) \geq 0$, such that $\rho_0(x) \in L^1D \cap L^\infty D$, and the free-space equilibrium Maxwellian distribution:

$$f_{in}(x,v) = \rho_0(x)\left(\frac{m}{2\pi k_B T_{gas}}\right)^{3/2} \exp\left(-\frac{m|v|^2}{2k_B T_{gas}}\right).$$

However, we shall prove existence and uniqueness for a more general form of f_{in}, which is also satisfied by the expression above.

Theorem: Existence and uniqueness theorem

Let $\Omega \subset \mathbb{R}^3$ be a bounded convex domain with C^1 boundary. Set

$$D := \mathbb{R}^3 \setminus \Omega.$$

Assume the wall temperature satisfies

$$T_w \in C^1([0,\infty) \times \partial\Omega; (0,\infty)), \qquad 0 < T_{\min} \leq T_w(t,x) \leq T_{\max} < \infty.$$

Define the diffuse kernel

$$M(t,x,v) := \frac{m^2}{2\pi(k_B T_w(t,x))^2} \exp\left(-\frac{m|v|^2}{2k_B T_w(t,x)}\right). \tag{3.4}$$

Let $f_{in} \in L^1(D \times \mathbb{R}^3) \cap L^\infty(D \times \mathbb{R}^3)$, $f_{in} \geq 0$ a.e. and such that

$$\tilde{J} := \sup_{(t,x)\in\mathbb{R}_+\times\partial\Omega} \int_{u\cdot n(x)<0} |u \cdot n(x)| f_{in}(x - tu, u) du < \infty. \tag{3.5}$$

Then there exists a unique nonnegative mild solution

$$f \in L^\infty\left(\mathbb{R}_+; L^1(D \times \mathbb{R}^3) \cap L^\infty(D \times \mathbb{R}^3)\right)$$

to the free transport equation

$$\partial_t f + v \cdot \nabla_x f = 0 \quad \text{in } \mathbb{R}_+ \times D \times \mathbb{R}^3, \tag{3.6}$$

with initial condition $f(0,x,v) = f_{in}(x,v)$ in $D\times\mathbb{R}^3$, and diffuse reflection boundary condition

$$f(t,x,v) = f_b(t,x,v) := M(t,x,v) \int_{u\cdot n(x)<0} |u \cdot n(x)| f_{in}(x - tu, u) du, \tag{3.7}$$

for a.e. $(t,x,v) \in \mathbb{R}_+ \times \Gamma_+$.
The boundary condition is understood a.e. with respect to the kinetic boundary measure

$$d\eta := |v \cdot n(x)| dv d\sigma(x),$$

and Γ_0 is negligible for $d\eta$.

We underline that this result has been tailored for our goal, namely the study of the interaction between a CubeSat and the atomic oxygen in upper atmosphere. In what follows, we suppose that the region Ω representing the satellite is convex but not strictly convex. This means that flat surfaces are allowed but, for avoiding technicalities originated by the lack of a normal vector to the surface, we will suppose that $\partial\Omega$ is of class C^1, hence we suppose that the vertices and angles of the domain are smoothed.

The proof consists of several steps. First of all, we recall, from (3.3), that,

for every $(t, x) \in \mathbb{R}_+ \times \partial\Omega$,

$$\int_{v \cdot n(x) > 0} M(t, x, v)(v \cdot n(x))dv = 1$$

and that, moreover, $M \in L^\infty(\mathbb{R}_+ \times \partial\Omega \times \mathbb{R}^3)$.

The first step consist in studying the negligibility of the grazing set Γ_0 2.4. The following lemma holds:

Lemma 1. *Let $\eta := |v \cdot n(x)|dvd\sigma(x)$ on $\partial\Omega \times \mathbb{R}^3$. Then $\eta(\Gamma_0) = 0$. In fact, for any measurable $\psi \geq 0$,*

$$\int_{\Gamma_0} \psi(x, v)d\eta = 0.$$

Moreover, for each fixed $x \in \partial\Omega$, the set $\{v \in \mathbb{R}^3 : v \cdot n(x) = 0\}$ has Lebesgue measure zero in $\mathbb{R}^3$.

Proof. The proof is a direct consequence of Bardos' Lemma [2]. □

Lemma 2. *Assume Ω is convex with C^1 boundary. Let $x \in \partial\Omega$ and $v \in \mathbb{R}^3$ such that $(x, v) \in \Gamma_-$. Then $x - sv \in D$ for all $s > 0$. In particular the ray $\{x - sv : s > 0\}$ does not meet $\partial\Omega$.*

Proof. Convexity implies that the tangent plane at x is a supporting hyperplane:

$$\Omega \subset \{y \in \mathbb{R}^3 : (y - x) \cdot n(x) \leq 0\}.$$

For $y = x - sv$ with $s > 0$:

$$(y - x) \cdot n(x) = (-sv) \cdot n(x) = -sv \cdot n(x) > 0.$$

Hence $y \notin \overline{\Omega}$, i.e. $y \in D$. This holds for all $s > 0$. □

We hence have that the characteristic curves intersect $\partial\Omega$ only once when $\tau(x, v) < +\infty$ and do not intersect $\partial\Omega$ when $\tau(x, v) = +\infty$. Note that, after hitting, the diffuse boundary condition force the ray going outside Ω.

For $(t, x, v) \in \mathbb{R}_+ \times D \times \mathbb{R}^3$ define

$$f(t, x, v) := f_{in}(x - tv, v)\mathbb{1}_{\{t < \tau(x,v)\}} + f_b(t - \tau(x, v), x - \tau(x, v)v, v)\mathbb{1}_{\{t \geq \tau(x,v)\}}, \tag{3.8}$$

where $\tau(x, v) \in [0, +\infty]$ is the backward exit time. On the grazing set (i.e. when $v \cdot n(x) = 0$), f may be defined arbitrarily.

The map τ is measurable (it is an infimum of measurable sets), hence f is measurable. Since $f_{in} \geq 0$, $M \geq 0$, and $J \geq 0$, we also have $f \geq 0$. Moreover,

for all $t \geq 0$,

$$\|f(t)\|_{L^\infty(D\times\mathbb{R}^3)} \leq \max\Big\{\|f_{in}\|_{L^\infty},\ \|M\|_{L^\infty}\tilde{J}\Big\},$$

thanks to the estimate

$$0 \leq M(t,x,v) \leq \frac{m^2}{2\pi(k_B T_{\min})^2} \quad \text{for all } (t,x,v),$$

and the hypothesis $0 < T_{\min} \leq T_w$. Finally, $f \in L^\infty(\mathbb{R}_+; L^1(D\times\mathbb{R}^3))$ and satisfies the mass estimate

$$\|f(t)\|_{L^1(D\times\mathbb{R}^3)} \leq \|f_{in}\|_{L^1(D\times\mathbb{R}^3)} \qquad \forall t \geq 0.$$

Indeed, the transport equation conserves mass in the bulk, and the diffuse boundary condition is conservative in the kinetic sense (see Chapter 2).

Lemma 3. *Let f be defined by* (3.8)*. Then f is a generalized solution of the free transport equation* (3.6)*, i.e., for a.e. $(t,x,v) \in \mathbb{R}_+ \times D \times \mathbb{R}^3$ and for all s such that $(t+s, x+sv) \in \mathbb{R}_+^* \times D$, one has*

$$\frac{d}{ds} f(t+s, x+sv, v) = 0.$$

Proof. Fix $(t,x,v) \in \mathbb{R}_+ \times D \times \mathbb{R}^3$ outside a negligible set, and let s be such that $x + sv \in D$ and $t + s > 0$. We claim that

$$\tau(x+sv, v) = \tau(x,v) + s \quad \text{in } [0, +\infty], \tag{3.9}$$

with the convention $+\infty + s = +\infty$. Indeed,

$$\tau(x+sv,v) = \inf\{\theta \geq 0 :\ (x+sv) - \theta v \notin \overline{D}\} = \inf\{\theta \geq 0 :\ x + (s-\theta)v \notin \overline{D}\}.$$

Setting $\theta = s + r$ (with $r \geq 0$) gives $x - rv \notin \overline{D}$, hence the infimum is $s + \tau(x,v)$.

We now distinguish two cases.

When $t < \tau(x,v)$, using (3.9), we have

$$t + s < \tau(x,v) + s = \tau(x+sv, v),$$

so by (3.8),

$$f(t+s, x+sv, v) = f_{in}\big((x+sv) - (t+s)v,\ v\big) = f_{in}(x - tv, v),$$

which is independent of s. Hence $s \mapsto f(t+s, x+sv, v)$ is constant (therefore C^1) and its derivative is 0.

On the other hand, if $t \geq \tau(x,v)$, we have, again by (3.9),

$$t + s \geq \tau(x,v) + s = \tau(x+sv, v),$$

so the second branch in (3.8) applies:

$$f(t+s,x+sv,v)=f_b\Big((t+s)-\tau(x+sv,v),\ (x+sv)-\tau(x+sv,v)v,\ v\Big).$$

Using (3.9) we obtain

$$(t+s)-\tau(x+sv,v)=t-\tau(x,v),\qquad (x+sv)-\tau(x+sv,v)v=x-\tau(x,v)v,$$

so

$$f(t+s,x+sv,v)=f_b\big(t-\tau(x,v),x-\tau(x,v)v,v\big),$$

which is again independent of s.

In both cases the trajectory $s\mapsto f(t+s,x+sv,v)$ is constant (hence C^1) and satisfies

$$\frac{d}{ds}f(t+s,x+sv,v)=0.$$

□

We now recover the initial datum as a limit.

Lemma 4. *Let f be defined by (3.8). Then for a.e. $(x,v)\in D\times\mathbb{R}^3$,*

$$\lim_{t\to 0^+} f(t,x,v)=f_{in}(x,v).$$

Proof. Fix (x,v) with $x\in D$. Since D is open, there exists $\delta>0$ such that $x-tv\in D$ for all $t\in[0,\delta]$. In particular, for $t\in(0,\delta)$ one has $t<\tau(x,v)$, hence by (3.8), $f(t,x,v)=f_{in}(x-tv,v)$. Since translations are continuous in L^1_{loc} and $f_{in}\in L^\infty$, we deduce $f_{in}(x-tv,v)\to f_{in}(x,v)$ for a.e. (x,v) as $t\to 0^+$. □

In order to recover the boundary condition, we define boundary values through interior limits along the normal direction.

For $(t,x,v)\in\mathbb{R}_+\times\partial\Omega\times\mathbb{R}^3$ such that the limit exists, set

$$f^*(t,x,v):=\lim_{\varepsilon\to 0^+} f\big(t,x+\varepsilon n(x),v\big).$$

The following result holds.

Lemma 5. *Let f be defined by (3.8). Then, for a.e. $(t,x,v)\in\mathbb{R}_+\times\Gamma_-$, the boundary limit $f^*(t,x,v)$ exists and satisfies*

$$f^*(t,x,v)=f_{in}(x-tv,v).$$

Consequently, for a.e. $(t,x)\in\mathbb{R}_+\times\partial\Omega$,

$$\int_{u\cdot n(x)<0}|u\cdot n(x)|f^*(t,x,u)du=\int_{u\cdot n(x)<0}|u\cdot n(x)|f_{in}(x-tu,u)du=:J(t,x),$$

Proof. Fix $(t,x,v) \in \mathbb{R}_+ \times \Gamma_-$, so $v \cdot n(x) < 0$. For $\varepsilon > 0$, let $x_\varepsilon = x + \varepsilon n(x) \in D$. By Lemma 2, the backward ray $x - sv$ starting at the boundary with $v \cdot n(x) < 0$ remains in D for all $s > 0$. By continuity of the geometry, the same holds for x_ε when ε is small, hence $\tau(x_\varepsilon, v) = +\infty$ for ε small, and therefore

$$f(t, x_\varepsilon, v) = f_{in}(x_\varepsilon - tv, v).$$

Letting $\varepsilon \to 0^+$ yields $f^*(t,x,v) = f_{in}(x - tv, v)$ a.e. on Γ_-. The flux identity follows by integrating against $|u \cdot n(x)|$ and using the definition of J. □

Lemma 6. *Let f be defined by (3.8). Then, for a.e. $(t,x,v) \in \mathbb{R}_+ \times \Gamma_+$, the boundary limit $f^*(t,x,v)$ exists and satisfies*

$$f^*(t,x,v) = f_b(t,x,v).$$

In particular, using Lemma 5, f^* satisfies the diffuse reflection boundary condition (3.7) for a.e. on $\mathbb{R}_+ \times \Gamma_+$.

Proof. Fix $(t,x,v) \in \mathbb{R}_+ \times \Gamma_+$, so $v \cdot n(x) > 0$. For $\varepsilon > 0$, set again $x_\varepsilon = x + \varepsilon n(x) \in D$. Since $v \cdot n(x) > 0$, the backward ray $x_\varepsilon - sv$ points toward Ω and hits $\partial\Omega$ in a time $\tau(x_\varepsilon, v) \to 0$ as $\varepsilon \to 0^+$, and the footpoint satisfies $x_\varepsilon - \tau(x_\varepsilon, v)v \to x$.

For each fixed $\varepsilon \geq 0$, since $t \geq \tau(x_\varepsilon, v)$ for ε small, the second branch of (3.8) applies:

$$f(t, x_\varepsilon, v) = f_b\big(t - \tau(x_\varepsilon, v), x_\varepsilon - \tau(x_\varepsilon, v)v, v\big).$$

Because M is continuous and bounded, and J is bounded and measurable, the function $f_b(t,x,v) = M(t,x,v)J(t,x)$ is defined for a.e. (t,x) and is locally integrable on $\mathbb{R}_+ \times \partial\Omega$. Therefore, for a.e. (t,x,v) (i.e., at Lebesgue points of $(t,x) \mapsto J(t,x)$),

$$f_b(t - \tau(x_\varepsilon, v), x_\varepsilon - \tau(x_\varepsilon, v)v, v) \to f_b(t,x,v) \quad \text{as } \varepsilon \to 0^+,$$

hence $f^*(t,x,v) = f_b(t,x,v)$ for a.e. on Γ_+.

Finally, by Lemma 5, for a.e. (t,x),

$$J(t,x) = \int_{u \cdot n(x) < 0} |u \cdot n(x)| f^*(t,x,u) du,$$

so for a.e. $(t,x,v) \in \mathbb{R}_+ \times \Gamma_+$,

$$f^*(t,x,v) = f_b(t,x,v) = M(t,x,v) \int_{u \cdot n(x) < 0} |u \cdot n(x)| f^*(t,x,u) du,$$

which is exactly (3.7). □

We can conclude by proving existence and uniqueness of the generalized solution.

By Lemma 3, f is a generalized solution of (3.6) in D. By Lemma 4, f recovers the initial datum f_{in} as $t \to 0^+$. By Lemma 6 and Lemma 5, f recovers the diffuse reflection boundary condition (3.7) on Γ_+ as an interior limit for a.e. boundary point. Therefore, f is a nonnegative generalized solution in the stated class.

In order to prove uniqueness, suppose by contradiction that $f^{(1)}$ and $f^{(2)}$ are two generalized solutions in the same class with the same initial datum. Set $g = f^{(1)} - f^{(2)}$. Then g is a generalized solution of free transport with zero initial datum and homogeneous diffuse boundary condition.

By linearity, g solves the transport equation and hence is constant along characteristics inside D. Using the initial limit, $g(0,\cdot,\cdot) = 0$ implies $g = 0$ on all characteristics that do not hit the boundary backward. For characteristics that hit Γ_+ backward, the boundary limit and the homogeneous diffuse condition force $g^* = 0$ on Γ_+; then constancy along characteristics yields $g = 0$ everywhere. Hence $f^{(1)} = f^{(2)}$ a.e.

Particular case: Let us consider f_{in} as the product of a spatial density $\rho_0(x) \geq 0$, such that $\rho_0(x) \in L^1(D) \cap L^\infty(D)$, and the free-space equilibrium Maxwellian distribution:

$$f_{in}(x,v) = \rho_0(x) \left(\frac{m}{2\pi k_B T_{gas}}\right)^{3/2} \exp\left(-\frac{m|v|^2}{2k_B T_{gas}}\right),$$

We show that f_{in} satisfies the hypotheses of Theorem 3.1. Indeed, given $(t,x) \in \mathbb{R}_+ \times \partial\Omega$:

$$\begin{aligned}
&\int_{u\cdot n(x)<0} |u\cdot n(x)| f_{in}(x-ut,u)du = \\
&\quad = \left(\frac{m}{2\pi k_B T_{gas}}\right)^{3/2} \int_{u\cdot n(x)<0} \rho_0(x-ut) \exp\left(-\frac{m|u|^2}{2k_B T_{gas}}\right) |u\cdot n(x)| du = \\
&\quad \leq \|\rho_0\|_{L_\infty(D)} \left(\frac{m}{2\pi k_B T_{gas}}\right)^{3/2} \left(\int_{-\infty}^{0} -u_x \exp\left(-\frac{mu_x^2}{2k_B T_{gas}}\right) du_x\right) \times \\
&\qquad\qquad \times \left(\int_{\mathbb{R}} \exp\left(-\frac{mu_y^2}{2k_B T_{gas}}\right) du_y\right)^2 = \\
&\quad \leq \|\rho_0\|_{L_\infty(D)} \left(\frac{m}{2\pi k_B T_{gas}}\right)^{3/2} \left(\frac{k_B T_{gas}}{m}\right) \left(\frac{2\pi k_B T_{gas}}{m}\right) = \\
&\quad \leq \|\rho_0\|_{L_\infty(D)} \left(\frac{k_B T_{gas}}{2\pi m}\right)^{\frac{1}{2}} < \infty \ \forall (t,x) \in \mathbb{R}_+ \times \partial\Omega
\end{aligned} \tag{3.10}$$

$$\begin{aligned}
\|f_{in}\|_{L^1(D\times\mathbb{R}^3)} &= \iint_{D\times\mathbb{R}^3} f_{in}(x,v)dvdx = \\
&= \left(\int_D \rho_0(x)dx\right)\left(\frac{m}{2\pi k_B T_{gas}}\right)^{3/2}\int_{\mathbb{R}^3}\exp\left(-\frac{m|v|^2}{2k_B T_{gas}}\right)dv = \\
&= \|\rho_0\|_{L^1(D)}\left(\frac{m}{2\pi k_B T_{gas}}\right)^{3/2}\left(\int_{-\infty}^{+\infty}\exp\left(-\frac{mv_i^2}{2k_B T_{gas}}\right)dv_i\right)^3 = \\
&= \|\rho_0\|_{L^1(D)}\left(\frac{m}{2\pi k_B T_{gas}}\right)^{3/2}\left(\sqrt{\frac{2\pi k_B T_{gas}}{m}}\right)^3 = \\
&= \|\rho_0\|_{L^1(D)} < \infty
\end{aligned} \tag{3.11}$$

Therefore, given this initial datum and the remaining hypotheses of the theorem, the existence of a solution is established.

3.2 Two-scale convergence

Let $\Omega \subset \mathbb{R}^3$ be an open convex set with C^1 boundary and assume that Ω is bounded.

Suppose moreover that the temperature of the boundary of Ω oscillates rapidly in time with period $P \in (0,T]$. We therefore introduce a scaling parameter ϵ such that, as $\epsilon \to 0^+$, the oscillation frequency tends to infinity.

A possible form for the temperature profile is given by:

$$T_w\left(\frac{t}{\epsilon},x\right) = \bar{T} + A(x)\cos\left(\frac{2\pi}{P}\frac{t}{\epsilon}+\phi\right) > 0; \tag{3.12}$$

assuming $\bar{T} > \sup_{x\in\partial\Omega}|A(x)|$, we ensure that the boundary temperature remains strictly positive.

We also assume that $A \in C^1(\partial\Omega)$, so that, for every $\varepsilon > 0$, the map $(t,x) \mapsto T_w(t/\varepsilon, x)$ is of class C^1 on $[0,T]\times\partial\Omega$.

Let $n(x)$ denote the outward unit normal to Ω (thus inward with respect to the gas domain D). We define:

$$\Gamma_\pm := \{(x,v) \in \partial\Omega\times\mathbb{R}^3 : \ \pm n(x)\cdot v > 0\}.$$

We also set

$$D := \mathbb{R}^3 \setminus \Omega, \qquad \mathcal{D}_T := (0,T)\times D\times\mathbb{R}^3.$$

We consider the family of solutions $\{f_\epsilon\}_{\epsilon>0}$ to the following transport problems:

$$\begin{cases}
\dfrac{\partial f_\epsilon}{\partial t} + v\cdot\nabla_x f_\epsilon = 0 & \text{for } (t,x,v)\in\mathcal{D}_T, \\
f_\epsilon(0,x,v) = f_{in}(x,v) & \text{for } (x,v)\in D\times\mathbb{R}^3, \\
f_\epsilon(t,x,v) = f_{b,\epsilon}(t,x,v) & \text{for } (t,x,v)\in\mathbb{R}_+\times\Gamma_+
\end{cases} \tag{3.13}$$

where:

$$f_{b,\epsilon}(t,x,v) = \frac{m^2}{2\pi(k_B T_w(\frac{t}{\epsilon},x))^2}\exp\left(-\frac{m|v|^2}{2k_B T_w(\frac{t}{\epsilon},x)}\right) \times \int_{u\cdot n(x)<0} |u\cdot n(x)| f_{in}(x-ut,u)du \quad \text{for } (x,v)\in\Gamma_+; \tag{3.14}$$

and the initial datum satisfies $f_{in}\in L^1(D\times\mathbb{R}^3)\cap L^\infty(D\times\mathbb{R}^3)$ with $f_{in}(x,v)\geq 0$ a.e and

$$\tilde{J} = \sup_{(t,x)\in\mathbb{R}_+\times\partial\Omega}\left(\int_{u\cdot n(x)<0}|u\cdot n(x)|f_{in}(x-ut,u)du\right)<\infty.$$

We recall that, due to the convexity of Ω and to the exterior geometry of the domain, the incoming boundary datum on Γ_+ admits an explicit representation in terms of the initial datum along backward characteristics.

For later use, we introduce the oscillatory diffuse kernel

$$M^{\#}(s,x,v) := \frac{m^2}{2\pi(k_B T_w(s,x))^2}\exp\left(-\frac{m|v|^2}{2k_B T_w(s,x)}\right), \qquad (s,x,v)\in\mathbb{T}_P\times\partial\Omega\times\mathbb{R}^3. \tag{3.15}$$

Then (3.14) can be rewritten as

$$f_{b,\varepsilon}(t,x,v) = M^{\#}\left(\frac{t}{\varepsilon},x,v\right)J(t,x), \qquad J(t,x) := \int_{u\cdot n(x)<0}|u\cdot n(x)|f_{in}(x-ut,u)\,du. \tag{3.16}$$

Since T_w is continuous and strictly positive on the compact set $\mathbb{T}_P\times\partial\Omega$, there exist constants $0<T_{\min}\leq T_{\max}<\infty$ such that

$$0<T_{\min}\leq T_w(s,x)\leq T_{\max} \qquad \forall (s,x)\in\mathbb{T}_P\times\partial\Omega. \tag{3.17}$$

In particular,

$$0\leq M^{\#}(s,x,v)\leq \frac{m^2}{2\pi(k_B T_{\min})^2} \qquad \forall (s,x,v)\in\mathbb{T}_P\times\partial\Omega\times\mathbb{R}^3. \tag{3.18}$$

The general solution of the family of problems (3.14) can be written in integral form:

$$f_\epsilon(t,x,v) = f_{in}(x-vt,v)\mathbb{1}_{\{t<\tau(x,v)\}} + f_{b,\epsilon}(t-\tau(x,v),x-\tau(x,v)v,v)\mathbb{1}_{\{t\geq\tau(x,v)\}}. \tag{3.19}$$

Here $\tau(x,v)\in[0,+\infty]$ denotes the backward hitting time. If $\tau(x,v)=+\infty$, then the second term is identically zero for all $t>0$.

3.2.1 Weak convergence along characteristics of the gas density

Let $\Omega \subset \mathbb{R}^3$ be a bounded open convex set with C^1 boundary, and set

$$D := \mathbb{R}^3 \setminus \overline{\Omega}, \qquad \mathcal{D}_T := (0,T) \times D \times \mathbb{R}^3.$$

We denote by $n(x)$ the outward unit normal to Ω (hence inward with respect to the gas domain D), and define

$$\Gamma_\pm := \{(x,v) \in \partial\Omega \times \mathbb{R}^3 : \pm n(x) \cdot v > 0\}.$$

We assume that the wall temperature oscillates rapidly in time with period $P \in (0,T]$. In particular, we assume that there exists a profile

$$T_w \in C(\mathbb{T}_P; C^1(\partial\Omega)), \qquad \inf T_w > 0.$$

which is P-periodic in the first variable, and such that the wall temperature is given by

$$(t,x) \mapsto T_w\left(\frac{t}{\varepsilon}, x\right).$$

A typical example is

$$T_w\left(\frac{t}{\varepsilon}, x\right) = \bar{T} + A(x)\cos\left(\frac{2\pi}{P}\frac{t}{\varepsilon} + \phi\right), \qquad (t,x) \in [0,T] \times \partial\Omega,$$

where $\bar{T} > \sup_{x\in\partial\Omega} |A(x)|$, so that the temperature remains strictly positive. We assume moreover that $A \in C^1(\partial\Omega)$, hence for every $\varepsilon > 0$ the map

$$(t,x) \mapsto T_w\left(\frac{t}{\varepsilon}, x\right)$$

is of class C^1 on $[0,T] \times \partial\Omega$.

We consider the family $\{f_\varepsilon\}_{\varepsilon>0}$ solving

$$\begin{cases} \partial_t f_\varepsilon + v \cdot \nabla_x f_\varepsilon = 0 & \text{in } \mathcal{D}_T, \\ f_\varepsilon(0,x,v) = f_{in}(x,v) & \text{for } (x,v) \in D \times \mathbb{R}^3, \\ f_\varepsilon(t,x,v) = f_{b,\varepsilon}(t,x,v) & \text{for } (t,x,v) \in \mathbb{R}_+ \times \Gamma_+, \end{cases} \tag{3.20}$$

where the boundary datum is given by

$$f_{b,\varepsilon}(t,x,v) = \frac{m^2}{2\pi(k_B T_w(\frac{t}{\varepsilon},x))^2} \exp\left(-\frac{m|v|^2}{2k_B T_w(\frac{t}{\varepsilon},x)}\right) \times \\ \times \int_{u\cdot n(x)<0} |u \cdot n(x)|\, f_{in}(x-ut,u)\, du, \qquad (x,v) \in \Gamma_+. \tag{3.21}$$

The initial datum is assumed to satisfy

$$f_{in} \in L^1(D \times \mathbb{R}^3) \cap L^\infty(D \times \mathbb{R}^3), \qquad f_{in} \geq 0 \quad \text{a.e.},$$

and

$$\widetilde{J} := \sup_{(t,x)\in\mathbb{R}_+\times\partial\Omega} \int_{u\cdot n(x)<0} |u\cdot n(x)|\, f_{in}(x-ut,u)\, du < +\infty.$$

Since $f_{in} \in L^1(D\times\mathbb{R}^3)\cap L^\infty(D\times\mathbb{R}^3)$, Hölder's inequality implies $f_{in} \in L^2(D\times\mathbb{R}^3)$ and

$$\|f_{in}\|^2_{L^2(D\times\mathbb{R}^3)} \le \|f_{in}\|_{L^1(D\times\mathbb{R}^3)}\, \|f_{in}\|_{L^\infty(D\times\mathbb{R}^3)}.$$

Since Ω is bounded, convex, and has C^1 boundary, the incoming boundary contribution can be explicitly reconstructed from the initial datum along backward characteristics. In order to simplify the notation, we introduce the oscillatory diffuse kernel

$$M^{\#}(s,x,v) := \frac{m^2}{2\pi(k_B T_w(s,x))^2} \exp\left(-\frac{m|v|^2}{2k_B T_w(s,x)}\right), \qquad (s,x,v)\in \mathbb{T}_P\times\partial\Omega\times\mathbb{R}^3, \tag{3.22}$$

where $\mathbb{T}_P := \mathbb{R}/(P\mathbb{Z})$. Then (3.21) can be rewritten as

$$f_{b,\varepsilon}(t,x,v) = M^{\#}\left(\frac{t}{\varepsilon},x,v\right)\, J(t,x), \qquad J(t,x) := \int_{u\cdot n(x)<0} |u\cdot n(x)|\, f_{in}(x-ut,u)\, du. \tag{3.23}$$

Since T_w is continuous and strictly positive on the compact set $\mathbb{T}_P\times\partial\Omega$, there exist constants

$$0 < T_{\min} \le T_{\max} < +\infty$$

such that

$$T_{\min} \le T_w(s,x) \le T_{\max} \qquad \forall (s,x)\in\mathbb{T}_P\times\partial\Omega. \tag{3.24}$$

In particular,

$$0 \le M^{\#}(s,x,v) \le \frac{m^2}{2\pi(k_B T_{\min})^2} \qquad \forall (s,x,v)\in\mathbb{T}_P\times\partial\Omega\times\mathbb{R}^3, \tag{3.25}$$

and

$$0 \le M^{\#}(s,x,v) \le \frac{m^2}{2\pi(k_B T_{\min})^2} \exp\left(-\frac{m|v|^2}{2k_B T_{\max}}\right) \qquad \forall (s,x,v)\in\mathbb{T}_P\times\partial\Omega\times\mathbb{R}^3. \tag{3.26}$$

Let $\tau(x,v)\in[0,+\infty]$ denote the backward hitting time, namely

$$\tau(x,v) := \inf\{\, s>0 :\ x - sv \in \partial\Omega\,\},$$

with the convention $\tau(x,v) = +\infty$ if the set is empty. We also introduce the grazing set

$$\Sigma_0 := \{(x,v)\in D\times\mathbb{R}^3 :\ \tau(x,v) < +\infty,\ n(x-\tau(x,v)v)\cdot v = 0\}.$$

By the Sard-type argument of Bardos (see Proposition 2.3 in [3]), the set of characteristics tangent to $\partial\Omega$ is negligible. Σ_0 is negligible in $D\times\mathbb{R}^3$, all identities below are understood up to this negligible set.

Then the solution to (3.20) admits the representation

$$f_\varepsilon(t,x,v) = f_{in}(x-vt,v)\,\mathbb{1}_{\{t<\tau(x,v)\}} + f_{b,\varepsilon}(t-\tau(x,v),x-\tau(x,v)v,v)\,\mathbb{1}_{\{t\geq\tau(x,v)\}} \tag{3.27}$$

for a.e. $(t,x,v)\in\mathcal{D}_T$. If $\tau(x,v)=+\infty$, then the second term is identically zero for all $t>0$.

We intend to identify the weak limit of $\{f_\varepsilon\}_{\varepsilon>0}$ in $L^2(\mathcal{D}_T)$. In the present setting, the rapidly oscillating wall temperature generates an oscillatory boundary contribution along characteristics, whose weak limit is obtained by periodic averaging.

We first introduce the set of phase points whose backward characteristic hits the obstacle non-tangentially,

$$E := \{(x,v)\in D\times\mathbb{R}^3 :\ \tau(x,v)<+\infty,\ n(x-\tau(x,v)v)\cdot v>0\}, \tag{3.28}$$

and, for $(x,v)\in E$, the associated boundary footpoint

$$x_b(x,v) := x-\tau(x,v)v\in\partial\Omega. \tag{3.29}$$

With this notation, (3.27) decomposes as

$$f_\varepsilon = f^{(\mathrm{free})} + f_\varepsilon^{(\mathrm{bd})}, \tag{3.30}$$

where

$$f^{(\mathrm{free})}(t,x,v) := f_{in}(x-vt,v)\,\mathbb{1}_{\{t<\tau(x,v)\}}, \tag{3.31}$$

and

$$f_\varepsilon^{(\mathrm{bd})}(t,x,v) := J(t-\tau(x,v),x_b(x,v))\,M^{\#}\!\left(\frac{t-\tau(x,v)}{\varepsilon},x_b(x,v),v\right)\mathbb{1}_{\{t\geq\tau(x,v)\}}\,\mathbb{1}_E(x,v). \tag{3.32}$$

We next recall the geometric parametrization of the hitting set by boundary rays.

Lemma 7. *Recall the set E defined in (3.28). For $(y,v) \in \Gamma_+$ and $s > 0$, define*

$$\Phi(y,v,s) := (y + sv, v).$$

Then, for every $(y,v) \in \Gamma_+$ and every $s > 0$,

$$y + sv \in D, \qquad \tau_{y+sv,v} = s, \qquad x_b(y + sv, v) = y.$$

In particular,

$$\Phi : \Gamma_+ \times (0, +\infty) \to E$$

is a measurable bijection, whose inverse is given by

$$\Phi^{-1}(x,v) = \big(x_b(x,v),\, v,\, \tau(x,v)\big).$$

Moreover, for every nonnegative measurable function $H : E \to [0, +\infty]$,

$$\int_E H(x,v)\, dx\, dv = \int_{\Gamma_+} \int_0^{+\infty} H(y + sv, v)\, |n(y) \cdot v|\, ds\, d\sigma(y)\, dv. \tag{3.33}$$

Proof. We first show that $\Phi(\Gamma_+ \times (0,\infty)) \subset E$.

Let $(y,v) \in \Gamma_+$ and $s > 0$. Set $w := -v$. Since $n(y) \cdot v > 0$, one has

$$n(y) \cdot w = -\, n(y) \cdot v < 0,$$

hence $(y,w) \in \Gamma_-$. By Lemma 2,

$$y - rw \in D \qquad \forall r > 0.$$

Since $y - rw = y + rv$, this yields

$$y + rv \in D \qquad \forall r > 0.$$

In particular, if we set

$$x := y + sv,$$

then $x \in D$.

Moreover, for every $0 < r < s$,

$$x - rv = y + (s - r)v \in D,$$

while

$$x - sv = y \in \partial\Omega.$$

Therefore the first backward hitting time of (x,v) is exactly

$$\tau(x,v) = s,$$

and the corresponding boundary footpoint is

$$x_b(x,v) = x - \tau(x,v)v = y.$$

Since $n(y)\cdot v > 0$, we conclude that $(x,v) \in E$. This proves

$$\Phi(\Gamma_+ \times (0,\infty)) \subset E.$$

We now prove surjectivity. Let $(x,v) \in E$. By definition,

$$\tau(x,v) < +\infty, \qquad y := x - \tau(x,v)v \in \partial\Omega, \qquad n(y)\cdot v > 0.$$

Thus $(y,v) \in \Gamma_+$ and

$$x = y + \tau(x,v)v,$$

hence

$$(x,v) = \Phi(y,v,\tau(x,v)).$$

So Φ is surjective onto E.

Injectivity is now immediate. If

$$\Phi(y_1,v,s_1) = \Phi(y_2,v,s_2) =: (x,v),$$

then from the first part of the proof we know that

$$\tau(x,v) = s_1 = s_2, \qquad x_b(x,v) = y_1 = y_2.$$

Hence $(y_1,v,s_1) = (y_2,v,s_2)$.

The measurability of Φ is immediate. Formula (3.33) follows from the standard local change of variables on $\partial\Omega$: in local coordinates $y = \chi(\theta)$,

$$(\theta,s) \mapsto \chi(\theta) + sv$$

has Jacobian

$$|(\partial_{\theta_1}\chi \times \partial_{\theta_2}\chi)\cdot v| = |n(y)\cdot v|\,|\partial_{\theta_1}\chi \times \partial_{\theta_2}\chi|,$$

which gives the factor $|n(y)\cdot v|\,d\sigma(y)\,ds$. □

We also need a periodic averaging lemma in L^2.

Lemma 8. *Let (Ξ, μ) be a σ-finite measure space, and let*

$$Q : \mathbb{T}_P \times \Xi \to \mathbb{R}$$

be measurable, P-periodic and continuous with respect to the first variable. Assume that

$$q(\xi) := \sup_{s \in \mathbb{T}_P} |Q(s, \xi)| \in L^2(\Xi, d\mu).$$

For $\varepsilon > 0$, define

$$Q_\varepsilon(r, \xi) := Q\left(\frac{r}{\varepsilon}, \xi\right), \qquad \overline{Q}(\xi) := \frac{1}{P} \int_0^P Q(s, \xi)\, ds.$$

Then

$$Q_\varepsilon \rightharpoonup \overline{Q} \qquad \text{weakly in } L^2((0,T) \times \Xi, dr \otimes d\mu).$$

Proof. We first test against tensor-product functions

$$\Psi(r, \xi) = \alpha(r)\beta(\xi), \qquad \alpha \in L^2(0,T), \quad \beta \in L^2(\Xi, d\mu).$$

Since $T < +\infty$, one also has $\alpha \in L^1(0,T)$. For almost every $\xi \in \Xi$, the function

$$s \mapsto Q(s, \xi)$$

is P-periodic and continuous. Hence the standard periodic averaging argument yields

$$\int_0^T Q\left(\frac{r}{\varepsilon}, \xi\right) \alpha(r)\, dr \to \overline{Q}(\xi) \int_0^T \alpha(r)\, dr \qquad \text{as } \varepsilon \to 0.$$

Moreover,

$$\left| \int_0^T Q\left(\frac{r}{\varepsilon}, \xi\right) \alpha(r)\, dr \right| \le q(\xi)\, \|\alpha\|_{L^1(0,T)}.$$

Therefore

$$\left| \beta(\xi) \int_0^T Q\left(\frac{r}{\varepsilon}, \xi\right) \alpha(r)\, dr \right| \le |\beta(\xi)|\, q(\xi)\, \|\alpha\|_{L^1(0,T)},$$

and the right-hand side belongs to $L^1(\Xi)$ thanks to the Cauchy–Schwarz inequality, since $\beta, q \in L^2(\Xi)$. The dominated convergence theorem therefore implies

$$\int_\Xi \int_0^T Q_\varepsilon(r, \xi)\Psi(r, \xi)\, dr\, d\mu(\xi) \to \int_\Xi \int_0^T \overline{Q}(\xi)\Psi(r, \xi)\, dr\, d\mu(\xi).$$

We know moreover that finite linear combinations of tensor products are dense in $L^2((0,T) \times \Xi)$, and

$$\|Q_\varepsilon\|_{L^2((0,T)\times\Xi)} \le \sqrt{T}\, \|q\|_{L^2(\Xi)}.$$

The conclusion follows by density. □

We next prove the uniform L^2 bound.

Lemma 9. *The family $\{f_\varepsilon\}_{\varepsilon>0}$ is uniformly bounded in $L^2(\mathcal{D}_T)$.*

Proof. By (3.30),

$$f_\varepsilon = f^{(\mathrm{free})} + f_\varepsilon^{(\mathrm{bd})}.$$

We first estimate the free-flight part. Since

$$f^{(\mathrm{free})}(t,x,v) = f_{in}(x-vt,v)\,\mathbb{1}_{\{t<\tau(x,v)\}},$$

we have

$$\|f^{(\mathrm{free})}\|^2_{L^2(\mathcal{D}_T)} \le \int_0^T \int_{D\times\mathbb{R}^3} |f_{in}(x-vt,v)|^2\,dx\,dv\,dt.$$

For each fixed $t \in (0,T)$ and $v \in \mathbb{R}^3$, the map $x \mapsto x - vt$ is a translation, hence preserves Lebesgue measure; moreover, the set

$$\{x \in D :\ t < \tau(x,v)\}$$

is sent into D. Therefore

$$\int_D |f_{in}(x-vt,v)|^2\,\mathbb{1}_{\{t<\tau(x,v)\}}\,dx \le \int_D |f_{in}(y,v)|^2\,dy,$$

and integrating in (t,v) gives

$$\|f^{(\mathrm{free})}\|^2_{L^2(\mathcal{D}_T)} \le T\,\|f_{in}\|^2_{L^2(D\times\mathbb{R}^3)}.$$

We now estimate the boundary-generated part. By Lemma 7, for $(x,v) = (y+sv,v)$ with $(y,v)\in\Gamma_+$ and $s>0$, one has

$$\tau(x,v) = s, \qquad x_b(x,v) = y.$$

Hence

$$\|f_\varepsilon^{(\mathrm{bd})}\|^2_{L^2(\mathcal{D}_T)} = \int_0^T \int_{\Gamma_+} \int_0^t |J(t-s,y)|^2 \left| M^{\#}\Big(\frac{t-s}{\varepsilon}, y, v\Big)\right|^2 |n(y)\cdot v|\,ds\,d\sigma(y)\,dv\,dt.$$

Setting $r = t-s$ yields

$$\begin{aligned}\|f_\varepsilon^{(\mathrm{bd})}\|^2_{L^2(\mathcal{D}_T)} &= \int_{\Gamma_+} \int_0^T \int_0^{T-r} |J(r,y)|^2 \left| M^{\#}\Big(\frac{r}{\varepsilon}, y, v\Big)\right|^2 |n(y)\cdot v|\,ds\,dr\,d\sigma(y)\,dv \\ &\le T\,\widetilde{J}^2 \int_{\Gamma_+} \sup_{s\in\mathbb{T}_P} |M^{\#}(s,y,v)|^2 |n(y)\cdot v|\,d\sigma(y)\,dv.\end{aligned}$$

By (3.26), there exist two constants $C, c > 0$ such that

$$\sup_{s\in\mathbb{T}_P} |M^{\#}(s,y,v)|^2 \le C\,e^{-c|v|^2} \qquad \forall (y,v)\in\Gamma_+.$$

Since $\partial\Omega$ is compact and

$$\int_{\mathbb{R}^3} |v|\, e^{-c|v|^2}\, dv < +\infty,$$

it follows that

$$\int_{\Gamma_+} \sup_{s\in\mathbb{T}_P} |M^{\#}(s,y,v)|^2 |n(y)\cdot v|\, d\sigma(y)\, dv < +\infty.$$

This proves the uniform bound for $\|f_\varepsilon^{(\mathrm{bd})}\|_{L^2(\mathcal{D}_T)}$, and therefore for $\|f_\varepsilon\|_{L^2(\mathcal{D}_T)}$. □

The next result identifies the weak limit.

Proposition 1. *Per $\varepsilon \to 0^+$, si ha la convergenza:*

$$f_\varepsilon \rightharpoonup \bar{f} \qquad \textit{debolmente in } L^2(\mathcal{D}_T),$$

dove $\overline{M}$ è definita da:

$$\overline{M}(y,v) := \frac{1}{P}\int_0^P M^{\#}(s,y,v)\, ds, \qquad (y,v)\in\partial\Omega\times\mathbb{R}^3, \tag{3.34}$$

e la funzione limite $\bar{f}$ soddisfa la seguente relazione:

$$\begin{aligned}\bar{f}(t,x,v) = {} & f_{in}(x-vt,v)\,\mathbb{1}_{\{t<\tau(x,v)\}} + \\ & + J(t-\tau(x,v),x-\tau(x,v)v)\,\overline{M}(x-\tau(x,v)v,v)\,\mathbb{1}_{\{t\geq\tau(x,v)\}}\,\mathbb{1}_E(x,v).\end{aligned} \tag{3.35}$$

Proof. By Lemma 9, the family $\{f_\varepsilon\}_{\varepsilon>0}$ is bounded in $L^2(\mathcal{D}_T)$.

The free-flight part

$$f^{(\mathrm{free})}(t,x,v) = f_{in}(x-vt,v)\,\mathbb{1}_{\{t<\tau(x,v)\}}$$

does not depend on ε, hence converges strongly in $L^2(\mathcal{D}_T)$ to itself.

It remains to treat the boundary-generated part. Let $\phi\in L^2(\mathcal{D}_T)$. Using Lemma 7, we obtain

$$\begin{aligned}&\int_{\mathcal{D}_T} f_\varepsilon^{(\mathrm{bd})}(t,x,v)\,\phi(t,x,v)\,dt\,dx\,dv = \\ &\quad = \int_0^T\int_{\Gamma_+}\int_0^t J(t-s,y)\,M^{\#}\Big(\frac{t-s}{\varepsilon},y,v\Big)\,\phi(t,y+sv,v)\,|n(y)\cdot v|\,ds\,d\sigma(y)\,dv\,dt.\end{aligned}$$

We now set

$$r := t-s.$$

Since the region $\{(t,s) : 0 < s < t < T\}$ is mapped onto

$$\{(r,s) : 0 < r < T,\ 0 < s < T - r\},$$

we obtain

$$\int_{\mathcal{D}_T} f_\varepsilon^{(\mathrm{bd})}(t,x,v)\,\phi(t,x,v)\,dt\,dx\,dv = \int_{\Gamma_+}\int_0^T M^{\#}\left(\frac{r}{\varepsilon}, y, v\right)\,A_\phi(r,y,v)\,|n(y)\cdot v|\,dr\,d\sigma(y)\,dv, \tag{3.36}$$

where

$$A_\phi(r,y,v) := J(r,y)\int_0^{T-r}\phi(r+s, y+sv, v)\,ds. \tag{3.37}$$

We claim that:

$$A_\phi \in L^2\big((0,T)\times\Gamma_+,\ dr\otimes|n(y)\cdot v|\,d\sigma(y)\,dv\big).$$

Indeed, by Cauchy–Schwarz,

$$\begin{aligned}|A_\phi(r,y,v)|^2 &\le |J(r,y)|^2\,(T-r)\int_0^{T-r}|\phi(r+s,y+sv,v)|^2\,ds\\ &\le T\,\widetilde{J}^2\int_0^{T-r}|\phi(r+s,y+sv,v)|^2\,ds.\end{aligned}$$

Integrating this estimate and using Fubini's theorem gives

$$\begin{aligned}&\int_{\Gamma_+}\int_0^T |A_\phi(r,y,v)|^2\,|n(y)\cdot v|\,dr\,d\sigma(y)\,dv\\ &\quad\le T\,\widetilde{J}^2\int_{\Gamma_+}\int_0^T\int_0^{T-r}|\phi(r+s,y+sv,v)|^2|n(y)\cdot v|\,ds\,dr\,d\sigma(y)\,dv\\ &\quad= T\,\widetilde{J}^2\int_0^T\int_{\Gamma_+}\int_0^t|\phi(t,y+sv,v)|^2|n(y)\cdot v|\,ds\,d\sigma(y)\,dv\,dt\\ &\quad= T\,\widetilde{J}^2\int_0^T\int_E \mathbb{1}_{\{\tau(x,v)<t\}}\,|\phi(t,x,v)|^2\,dx\,dv\,dt\\ &\quad\le T\,\widetilde{J}^2\,\|\phi\|^2_{L^2(\mathcal{D}_T)}.\end{aligned}$$

This proves the claim.

We now apply Lemma 8 on the measure space

$$\Xi := \Gamma_+, \qquad d\mu(y,v) := |n(y)\cdot v|\,d\sigma(y)\,dv,$$

with

$$Q(s,y,v) := M^{\#}(s,y,v).$$

By (3.26), there exist constants $C, c > 0$ such that

$$\sup_{s\in\mathbb{T}_P}|Q(s,y,v)| \le C\,e^{-c|v|^2},$$

hence

$$(y,v) \mapsto \sup_{s\in\mathbb{T}_P} |Q(s,y,v)| \in L^2(\Gamma_+, d\mu).$$

Therefore

$$M^{\#}\left(\frac{r}{\varepsilon}, y, v\right) \rightharpoonup \overline{M}(y,v) \qquad \text{weakly in } L^2((0,T)\times\Gamma_+, dr\otimes d\mu).$$

Since $A_\phi \in L^2((0,T)\times\Gamma_+, dr\otimes d\mu)$, passing to the limit in (3.36) yields

$$\lim_{\varepsilon\to 0}\int_{\mathcal{D}_T} f_\varepsilon^{(\mathrm{bd})}(t,x,v)\,\phi(t,x,v)\,dt\,dx\,dv = \int_{\Gamma_+}\int_0^T \overline{M}(y,v)\,A_\phi(r,y,v)\,|n(y)\cdot v|\,dr\,d\sigma(y)\,dv.$$

Using the definition (3.37) and reverting the change of variables

$$(x,v) = (y+sv, v),$$

we obtain

$$\begin{aligned}
&\lim_{\varepsilon\to 0}\int_{\mathcal{D}_T} f_\varepsilon^{(\mathrm{bd})}(t,x,v)\,\phi(t,x,v)\,dt\,dx\,dv = \\
&\quad = \int_0^T\int_{\Gamma_+}\int_0^t J(t-s,y)\,\overline{M}(y,v)\,\phi(t,y+sv,v)\,|n(y)\cdot v|\,ds\,d\sigma(y)\,dv\,dt = \\
&\quad = \int_{\mathcal{D}_T} J(t-\tau(x,v), x_b(x,v))\,\overline{M}(x_b(x,v),v)\,\mathbb{1}_{\{t\ge\tau(x,v)\}}\,\mathbb{1}_E(x,v)\,\phi(t,x,v)\,dt\,dx\,dv.
\end{aligned}$$

Since $x_b(x,v) = x - \tau(x,v)v$, this proves that

$$f_\varepsilon^{(\mathrm{bd})} \rightharpoonup J(t-\tau(x,v), x-\tau(x,v)v)\,\overline{M}(x-\tau(x,v)v,v)\,\mathbb{1}_{\{t\ge\tau(x,v)\}}\,\mathbb{1}_E(x,v)$$

weakly in $L^2(\mathcal{D}_T)$.

Adding the strong convergence of the free-flight part yields (3.35). □

3.2.2 Two-scale description and convergence of a degradation model

VLEO is an attractive regime for satellite missions because it enables higher-resolution observations and lower-latency communications, but it also exposes spacecraft surfaces to a denser residual atmosphere and stronger aerodynamic drag. As seen in Chapter 1, atomic oxygen (AO) is abundant at these altitudes and is known to react with exposed materials, producing oxidation, erosion, and changes in surface properties.

Other physical effects may also influence material degradation, such as ultraviolet radiation, thermal cycling, contamination, and gas–surface interaction mechanisms. In the present section we focus only on the role of AO and its interaction with the wall temperature.

Throughout this subsection, we assume that $\Omega \subset \mathbb{R}^3$ is bounded, convex, and has C^1 boundary. In particular, the outward unit normal $n(x)$ is defined for every $x \in \partial\Omega$, and the surface measure $|\partial\Omega|$ is finite.

For each $\varepsilon > 0$, we introduce a degradation function

$$u_\varepsilon : [0,T] \times \partial\Omega \to \mathbb{R}_+,$$

where $u_\varepsilon(t,x)$ measures the cumulative AO-induced surface degradation at time t and boundary point x.

The value $u_\varepsilon = 0$ corresponds to an initially intact surface, whereas $u_\varepsilon \geq 1$ represents complete oxidation (or, more generally, complete degradation of the reactive surface layer). We model the evolution of u_ε through the incoming particle flux and a temperature-dependent efficiency factor.

We assume that the wall temperature admits a two-scale description

$$T_w : [0,T] \times \partial\Omega \times \mathbb{T}_P \to (0,\infty),$$

such that

$$T_w \in L^\infty\big((0,T) \times \partial\Omega; C_\#(\mathbb{T}_P)\big), \qquad 0 < T_{\min} \leq T_w(t,x,\theta) \leq T_{\max} < \infty$$

for a.e. $(t,x,\theta) \in (0,T) \times \partial\Omega \times \mathbb{T}_P$. The rapidly oscillating wall temperature is then given by

$$T_w^\varepsilon(t,x) := T_w\left(t, x, \frac{t}{\varepsilon}\right).$$

In the present reduced model, the degradation is driven only by the incoming free-stream particles described by f_{in}. Since Ω is convex, a particle emitted from the boundary into the exterior domain does not hit the obstacle again, so no multiple boundary recollisions need to be taken into account.

We define u_ε by

$$u_\varepsilon(t,x) = \int_0^t \kappa\left(T_w\left(s, x, \frac{s}{\varepsilon}\right)\right)\left(\int_{v\cdot n(x)<0} f_{in}(x - vs, v)\,|v \cdot n(x)|\,dv\right) ds. \tag{3.38}$$

We assume that the degradation efficiency satisfies

$$\kappa \in C_b(\mathbb{R}_+), \qquad \kappa(r) \geq 0 \quad \text{for all } r \in [T_{\min}, T_{\max}].$$

This modelling choice accounts for the increase in the degradation rate as the satellite temperature rises.

Since Ω is assumed to be convex, multiple reflections of a single particle with the boundary are not possible. Consequently, the degradation process is driven exclusively by particles originating from infinity.

In this framework, we consider the incoming flux associated with f_{in}, where $f_{in} \in L^1(D \times \mathbb{R}^3) \cap L^\infty(D \times \mathbb{R}^3)$, $f_{in}(x,v) \geq 0$ a.e., and

$$\tilde{J} := \sup_{(t,x)\in\mathbb{R}_+\times\partial\Omega}\left(\int_{u\cdot n(x)<0} |u \cdot n(x)|\, f_{in}(x - ut, u)\,du\right) < \infty. \tag{3.39}$$

Defining the incoming flux on the boundary at time t as

$$J(t,x) := \int_{v\cdot n(x)<0} f_{in}(x-vt,v)\,|v\cdot n(x)|\,dv, \tag{3.40}$$

we immediately have

$$0 \le J(t,x) \le \tilde{J} \qquad \text{for a.e. } (t,x)\in(0,T)\times\partial\Omega, \tag{3.41}$$

hence

$$J \in L^\infty((0,T)\times\partial\Omega).$$

By (3.38), using the boundedness of κ and (3.41), we obtain

$$\begin{aligned}
\|u_\varepsilon\|^2_{L^2((0,T)\times\partial\Omega)} &= \int_0^T\int_{\partial\Omega}\left[\int_0^t \kappa\left(T_w\left(s,x,\frac{s}{\varepsilon}\right)\right)J(s,x)\,ds\right]^2 dt\,d\sigma(x)\\
&\le \|\kappa\|^2_{L^\infty(\mathbb{R}_+)}\int_0^T\int_{\partial\Omega}\left(\int_0^t J(s,x)\,ds\right)^2 dt\,d\sigma(x)\\
&\le \|\kappa\|^2_{L^\infty(\mathbb{R}_+)}\int_0^T\int_{\partial\Omega}\left(\int_0^t \tilde{J}\,ds\right)^2 dt\,d\sigma(x)\\
&= \|\kappa\|^2_{L^\infty(\mathbb{R}_+)}\tilde{J}^2\int_0^T\int_{\partial\Omega} t^2\,dt\,d\sigma(x)\\
&= \|\kappa\|^2_{L^\infty(\mathbb{R}_+)}\tilde{J}^2|\partial\Omega|\frac{T^3}{3} < \infty.
\end{aligned}$$

Therefore, the family $\{u_\varepsilon\}_{\varepsilon>0}$ is bounded in $L^2((0,T)\times\partial\Omega)$.

We now identify directly the two-scale limit of the whole sequence.

Proposition 2. *Define*

$$a(t,x,\theta) := \kappa(T_w(t,x,\theta)), \qquad a_\varepsilon(t,x) := a\left(t,x,\frac{t}{\varepsilon}\right). \tag{3.42}$$

Let

$$\overline{\kappa}(t,x) := \frac{1}{P}\int_0^P \kappa(T_w(t,x,\theta))\,d\theta. \tag{3.43}$$

Then, for every

$$\psi \in L^2((0,T)\times\partial\Omega; C_\#(\mathbb{T}_P)),$$

one has

$$\begin{aligned}
\lim_{\varepsilon\to 0+}\int_{\partial\Omega}\int_0^T u_\varepsilon(t,x)\,\psi\left(t,x,\frac{t}{\varepsilon}\right)\,dt\,d\sigma(x) =\\
= \frac{1}{P}\int_0^P\int_{\partial\Omega}\int_0^T u(t,x)\,\psi(t,x,\theta)\,dt\,d\sigma(x)\,d\theta,
\end{aligned} \tag{3.44}$$

where:

$$u(t,x) := \int_0^t \overline{\kappa}(s,x)J(s,x)\,ds.$$

In particular, u_ε two-scale converges to the limit u, which is independent of the fast variable θ.

Proof. Since $T_w \in L^\infty((0,T)\times\partial\Omega; C_\#(\mathbb{T}_P))$ and $\kappa \in C_b(\mathbb{R}_+)$, it follows that

$$a \in L^\infty((0,T)\times\partial\Omega; C_\#(\mathbb{T}_P)).$$

Hence, by the standard identification theorem for periodic oscillating sequences (see, e.g., [1]),

$$a_\varepsilon(t,x) = a\left(t,x,\frac{t}{\varepsilon}\right) \rightharpoonup \bar{a}(t,x) := \frac{1}{P}\int_0^P a(t,x,\theta)\,d\theta \qquad \text{weakly in } L^2((0,T)\times\partial\Omega).$$

By definition of a, this weak limit is precisely

$$\bar{a}(t,x) = \overline{\kappa}(t,x) = \frac{1}{P}\int_0^P \kappa(T_w(t,x,\theta))\,d\theta. \tag{3.45}$$

Let now

$$\psi \in L^2((0,T)\times\partial\Omega; C_\#(\mathbb{T}_P)).$$

Set

$$I_\varepsilon := \int_{\partial\Omega}\int_0^T u_\varepsilon(t,x)\,\psi\left(t,x,\frac{t}{\varepsilon}\right)\,dt\,d\sigma(x).$$

Using (3.38), we obtain

$$I_\varepsilon = \int_{\partial\Omega}\int_0^T \left(\int_0^t a_\varepsilon(s,x)J(s,x)\,ds\right)\psi\left(t,x,\frac{t}{\varepsilon}\right)\,dt\,d\sigma(x).$$

The integrand is absolutely integrable on

$$\{(s,t)\in(0,T)^2 :\ 0\le s\le t\le T\}\times\partial\Omega,$$

because a_ε and J are bounded, and

$$(t,x)\mapsto \sup_{\theta\in\mathbb{T}_P}|\psi(t,x,\theta)|$$

belongs to $L^2((0,T)\times\partial\Omega)$, hence also to $L^1((0,T)\times\partial\Omega)$ since $(0,T)\times\partial\Omega$ has finite measure. Therefore, Fubini's theorem applies and gives

$$I_\varepsilon = \int_0^T\int_{\partial\Omega} a_\varepsilon(s,x)J(s,x)\left(\int_s^T \psi\left(t,x,\frac{t}{\varepsilon}\right)\,dt\right)d\sigma(x)\,ds. \tag{3.46}$$

Define

$$\Psi_\varepsilon(s,x) := \int_s^T \psi\left(t,x,\frac{t}{\varepsilon}\right)\,dt, \qquad \bar{\psi}(t,x) := \frac{1}{P}\int_0^P \psi(t,x,\theta)\,d\theta,$$

and

$$\Psi_0(s,x) := \int_s^T \bar{\psi}(t,x)\,dt.$$

We claim that

$$\Psi_\varepsilon \to \Psi_0 \qquad \text{strongly in } L^2((0,T)\times\partial\Omega). \tag{3.47}$$

To prove this, define

$$\widetilde{\psi}(t,x,\theta) := \psi(t,x,\theta) - \bar{\psi}(t,x).$$

Then $\widetilde{\psi} \in L^2((0,T)\times\partial\Omega; C_\#(\mathbb{T}_P))$ and

$$\frac{1}{P}\int_0^P \widetilde{\psi}(t,x,\theta)\,d\theta = 0 \qquad \text{for a.e. } (t,x).$$

Moreover,

$$\Psi_\varepsilon(s,x) - \Psi_0(s,x) = \int_s^T \widetilde{\psi}\Big(t,x,\frac{t}{\varepsilon}\Big)\,dt.$$

Hence it is enough to show that

$$\int_s^T \widetilde{\psi}\Big(t,x,\frac{t}{\varepsilon}\Big)\,dt \to 0 \qquad \text{strongly in } L^2((0,T)\times\partial\Omega)$$

whenever $\widetilde{\psi}$ has zero average in the fast variable.

We first consider tensorized functions of the form

$$\widetilde{\psi}(t,x,\theta) = g(t,x)\,q(\theta),$$

with $g \in L^2((0,T)\times\partial\Omega)$ and $q \in C_\#(\mathbb{T}_P)$ satisfying

$$\frac{1}{P}\int_0^P q(\theta)\,d\theta = 0.$$

Define

$$(K_\varepsilon^q g)(s,x) := \int_s^T g(t,x)\,q\Big(\frac{t}{\varepsilon}\Big)\,dt.$$

For a.e. (s,x), by Cauchy–Schwarz,

$$\begin{aligned}
|K_\varepsilon^q g(s,x)| &\le \|q\|_{L^\infty(\mathbb{T}_P)} \int_s^T |g(t,x)|\,dt,\\
|K_\varepsilon^q g(s,x)|^2 &\le \|q\|_{L^\infty(\mathbb{T}_P)}^2 (T-s)\int_s^T |g(t,x)|^2\,dt\\
&\le T\|q\|_{L^\infty(\mathbb{T}_P)}^2 \int_s^T |g(t,x)|^2\,dt.
\end{aligned}$$

Integrating in (s,x) and using Fubini's theorem, we obtain

$$\|K_\varepsilon^q g\|_{L^2((0,T)\times\partial\Omega)}^2 \le T^2\|q\|_{L^\infty(\mathbb{T}_P)}^2 \|g\|_{L^2((0,T)\times\partial\Omega)}^2, \tag{3.48}$$

hence

$$\|K_\varepsilon^q g\|_{L^2((0,T)\times\partial\Omega)} \le T\|q\|_{L^\infty(\mathbb{T}_P)} \|g\|_{L^2((0,T)\times\partial\Omega)}, \tag{3.49}$$

uniformly in ε.

Assume now that $g \in C_c^1(0,T;L^2(\partial\Omega))$. For $s \in (0,T)$, define

$$K_\varepsilon^q g(s) := \int_s^T g(t)\, q\Big(\frac{t}{\varepsilon}\Big)\, dt,$$

where the integral is understood in the Bochner sense in $L^2(\partial\Omega)$.

Since q is continuous, periodic, and has zero average, there exists $Q \in C_\#^1(\mathbb{T}_P)$ such that $Q' = q$. Hence

$$q\Big(\frac{t}{\varepsilon}\Big) = \varepsilon\, \frac{d}{dt} Q\Big(\frac{t}{\varepsilon}\Big).$$

Integrating by parts in the Bochner sense, we obtain in $L^2(\partial\Omega)$

$$K_\varepsilon^q g(s) = -\varepsilon g(s)\, Q\Big(\frac{s}{\varepsilon}\Big) - \varepsilon \int_s^T \partial_t g(t)\, Q\Big(\frac{t}{\varepsilon}\Big)\, dt,$$

since $g(T) = 0$.

Taking the $L^2(\partial\Omega)$ norm and using the boundedness of Q,

$$\|K_\varepsilon^q g(s)\|_{L^2(\partial\Omega)} \le \varepsilon \|Q\|_{L^\infty(\mathbb{T}_P)} \left(\|g(s)\|_{L^2(\partial\Omega)} + \int_s^T \|\partial_t g(t)\|_{L^2(\partial\Omega)}\, dt \right).$$

By integrating with respect to $s \in (0,T)$ and using the Cauchy–Schwarz inequality, we infer that there exists a constant $C > 0$, independent of ε, such that

$$\|K_\varepsilon^q g\|_{L^2((0,T)\times\partial\Omega)} \le C\,\varepsilon \left(\|g\|_{L^2((0,T)\times\partial\Omega)} + \|\partial_t g\|_{L^2((0,T)\times\partial\Omega)} \right). \tag{3.50}$$

In particular,

$$K_\varepsilon^q g \to 0 \qquad \text{strongly in } L^2((0,T)\times\partial\Omega)$$

for every $g \in C_c^1(0,T;L^2(\partial\Omega))$.

By density of $C_c^1(0,T;L^2(\partial\Omega))$ in $L^2((0,T)\times\partial\Omega)$ and the uniform estimate (3.49), the above convergence extends to every $g \in L^2((0,T)\times\partial\Omega)$.

We now pass to the general case. Consider the linear operator

$$(\mathcal{T}_\varepsilon \varphi)(s,x) := \int_s^T \varphi\Big(t, x, \frac{t}{\varepsilon}\Big)\, dt.$$

For a.e. (s,x),

$$|\mathcal{T}_\varepsilon \varphi(s,x)| \le \int_s^T \sup_{\theta\in\mathbb{T}_P} |\varphi(t,x,\theta)|\, dt,$$

and therefore, arguing exactly as above,

$$\|\mathcal{T}_\varepsilon \varphi\|_{L^2((0,T)\times\partial\Omega)} \le T \|\varphi\|_{L^2((0,T)\times\partial\Omega;C_\#(\mathbb{T}_P))}. \tag{3.51}$$

Since $C_\#(\mathbb{T}_P)$ is a separable Banach space, finite sums of tensor products are dense in $L^2((0,T)\times\partial\Omega;C_\#(\mathbb{T}_P))$. Hence, given $\widetilde{\psi}$ with zero average in θ,

there exists a sequence $(\widetilde{\psi}_n)_n$ of finite sums of tensor products such that

$$\widetilde{\psi}_n \to \widetilde{\psi} \qquad \text{in } L^2((0,T)\times\partial\Omega; C_\#(\mathbb{T}_P)).$$

After replacing each $\widetilde{\psi}_n$ by

$$\widetilde{\psi}_n - \frac{1}{P}\int_0^P \widetilde{\psi}_n(\,\cdot\,,\,\cdot\,,\theta)\,d\theta,$$

we may assume that every $\widetilde{\psi}_n$ has zero average in θ. For each fixed n, by the tensorized case proved above,

$$\mathcal{T}_\varepsilon\widetilde{\psi}_n \to 0 \qquad \text{strongly in } L^2((0,T)\times\partial\Omega).$$

Using the uniform estimate (3.51), we infer that

$$\begin{aligned}\|\mathcal{T}_\varepsilon\widetilde{\psi}\|_{L^2} &\le \|\mathcal{T}_\varepsilon(\widetilde{\psi}-\widetilde{\psi}_n)\|_{L^2} + \|\mathcal{T}_\varepsilon\widetilde{\psi}_n\|_{L^2}\\ &\le T\|\widetilde{\psi}-\widetilde{\psi}_n\|_{L^2((0,T)\times\partial\Omega;C_\#(\mathbb{T}_P))} + \|\mathcal{T}_\varepsilon\widetilde{\psi}_n\|_{L^2}.\end{aligned}$$

Passing first to the limit as $\varepsilon\to 0$ and then as $n\to\infty$, we conclude that

$$\mathcal{T}_\varepsilon\widetilde{\psi} \to 0 \qquad \text{strongly in } L^2((0,T)\times\partial\Omega).$$

This proves (3.47).

Since $J\in L^\infty((0,T)\times\partial\Omega)$, multiplication by J is continuous on $L^2((0,T)\times\partial\Omega)$. Therefore,

$$J(s,x)\Psi_\varepsilon(s,x) \to J(s,x)\Psi_0(s,x) \qquad \text{strongly in } L^2((0,T)\times\partial\Omega).$$

Moreover, by (3.42),

$$|a_\varepsilon(s,x)| \le \|\kappa\|_{L^\infty(\mathbb{R}_+)} \qquad \text{for a.e. } (s,x)\in(0,T)\times\partial\Omega.$$

Using (3.46), we may write

$$\begin{aligned}I_\varepsilon &= \int_0^T\int_{\partial\Omega} a_\varepsilon(s,x)J(s,x)\Psi_\varepsilon(s,x)\,d\sigma(x)\,ds =\\ &= \int_0^T\int_{\partial\Omega} a_\varepsilon(s,x)J(s,x)\big(\Psi_\varepsilon(s,x)-\Psi_0(s,x)\big)\,d\sigma(x)\,ds+\\ &\quad+\int_0^T\int_{\partial\Omega} a_\varepsilon(s,x)J(s,x)\Psi_0(s,x)\,d\sigma(x)\,ds.\end{aligned}$$

The first term tends to zero as $\varepsilon\to 0$, since

$$\begin{aligned}&\left|\int_0^T\int_{\partial\Omega} a_\varepsilon(s,x)J(s,x)\big(\Psi_\varepsilon(s,x)-\Psi_0(s,x)\big)\,d\sigma(x)\,ds\right|\\ &\quad\le \|a_\varepsilon\|_{L^\infty((0,T)\times\partial\Omega)}\|J\|_{L^2((0,T)\times\partial\Omega)}\|\Psi_\varepsilon-\Psi_0\|_{L^2((0,T)\times\partial\Omega)}\to 0.\end{aligned}$$

For the second term, using the weak convergence of a_ε to $\overline{\kappa}$ in $L^2((0,T)\times\partial\Omega)$

and the fact that

$$J\Psi_0 \in L^2((0,T)\times\partial\Omega),$$

we obtain

$$\int_0^T \int_{\partial\Omega} a_\varepsilon(s,x)J(s,x)\Psi_0(s,x)\,d\sigma(x)\,ds \to \int_0^T \int_{\partial\Omega} \overline{\kappa}(s,x)J(s,x)\Psi_0(s,x)\,d\sigma(x)\,ds.$$

Hence

$$\lim_{\varepsilon\to 0} I_\varepsilon = \int_0^T \int_{\partial\Omega} \overline{\kappa}(s,x)J(s,x)\Psi_0(s,x)\,d\sigma(x)\,ds.$$

Substituting the expression of Ψ_0 and applying Fubini's theorem once again on $\{(s,t) : 0 \le s \le t \le T\}$, we obtain

$$\begin{aligned}\lim_{\varepsilon\to 0} I_\varepsilon &= \int_0^T \int_{\partial\Omega} \overline{\kappa}(s,x)J(s,x)\left(\int_s^T \bar{\psi}(t,x)\,dt\right) d\sigma(x)\,ds \\ &= \int_{\partial\Omega}\int_0^T \left(\int_0^t \overline{\kappa}(s,x)J(s,x)\,ds\right)\bar{\psi}(t,x)\,dt\,d\sigma(x).\end{aligned}$$

Since

$$\bar{\psi}(t,x) = \frac{1}{P}\int_0^P \psi(t,x,\theta)\,d\theta,$$

the right-hand side can be rewritten as

$$\frac{1}{P}\int_0^P \int_{\partial\Omega}\int_0^T \left(\int_0^t \overline{\kappa}(s,x)J(s,x)\,ds\right)\psi(t,x,\theta)\,dt\,d\sigma(x)\,d\theta.$$

Therefore,

$$\lim_{\varepsilon\to 0}\int_{\partial\Omega}\int_0^T u_\varepsilon(t,x)\,\psi\left(t,x,\frac{t}{\varepsilon}\right)\,dt\,d\sigma(x) = \frac{1}{P}\int_0^P\int_{\partial\Omega}\int_0^T u(t,x)\psi(t,x,\theta)\,dt\,d\sigma(x)\,d\theta,$$

where

$$u(t,x) := \int_0^t \overline{\kappa}(s,x)J(s,x)\,ds.$$

This proves (3.44). Since the limit is uniquely identified, the whole sequence u_ε two-scale converges to u, and not only a subsequence. □

Chapter 4

Numerical Results

This chapter presents and discusses the numerical results obtained through the implementation of the DSMC method in MATLAB R2024b.
The simulations were carried out on an AMD Ryzen 7 5700U processor (8 physical cores, 16 threads, 1.80 GHz base frequency) equipped with 16 GB of RAM. To enhance computational efficiency, the code was parallelized using the parfor construct from the Parallel Computing Toolbox, thereby enabling multi-core execution and maximizing the utilization of the available CPU threads.

The numerical results of interest are divided into two main cases. In the first case, involving a multi-species polyatomic gas, the goal is the study of the relaxation of a gaseous mixture surrounding a satellite to the equilibrium configuration of the Boltzmann equation under specific initial and boundary conditions.

In the second case, concerning free molecular transport, the objective is to provide a numerical method for simulating some possible mechanisms of surface erosion of satellite components caused by the action of atomic oxygen.

4.1 Convergence to the equilibrium configuration for a polyatomic gas mixture

Using the DSMC method, we simulate a cube with side length 10 cm (representing our CubeSat) at an altitude of 100 km above the Earth.

Recalling the atmospheric conditions at this altitude, the gas is assumed to consist of diatomic molecules of N_2 (78%) and O_2 (22%), with a non-negligible mean free path.

$$\begin{cases} \dfrac{\partial f_i}{\partial t} + v \cdot \nabla_x f_i = \displaystyle\sum_{j \in \{\mathrm{N}_2, \mathrm{O}_2\}} Q_{ij}(f_i, f_j) & (t, x, v, I) \in \mathbb{R}_+ \times (\mathbb{R}^3 \setminus \Omega) \times \mathbb{R}^3 \times \mathbb{R}_+, \\ f_i(0, x, v, I) = f_{i,in}(x, v, I) & (x, v, I) \in (\mathbb{R}^3 \setminus \Omega) \times \mathbb{R}^3 \times \mathbb{R}_+ \\ f_i(t, x, v, I) = f_{i,b}(t, x, v, I) & (t, x, v) \in \mathbb{R}_+ \times \Gamma_+ \times \mathbb{R}_+ \end{cases} \tag{4.1}$$

where $i \in \{\mathrm{N}_2, \mathrm{O}_2\}$. The initial distribution is given by:

$$f_{i,in}(x, v, I) = n_i(t, x) \left(\frac{m_i}{2\pi k_B T_{gas}(t, x)} \right)^{3/2} \frac{1}{k_B T_{gas}(t, x)} \times \\ \times \exp\left(-\frac{m_i |v|^2}{2 k_B T_{gas}(t, x)} - \frac{I}{k_B T_{gas}(t, x)} \right)$$

while the boundary condition at the satellite surface is defined as:

$$f_{i,b}(t, x, v, I) = J(t, x) \frac{m_i^2}{2\pi (k_B T_w(x))^2} \exp\left(-\frac{m_i |v|^2}{2 k_B T_w(x)} \right) \times \\ \times \frac{1}{k_B T_w(x)} \exp\left(-\frac{I}{k_B T_w(x)} \right) \quad \text{for } (t, x, v.I) \in \mathbb{R}_+ \times \Gamma_+ \times \mathbb{R}_+;$$

where:

$$J(t, x) = \int_{v \cdot n(x) < 0} f_{in}(x, v) |v \cdot n(x)| \, dv$$

The primary objective is to simulate the system of Boltzmann equations in the immediate vicinity of the satellite. To this end, the computational domain is defined as a larger cube with side length 18 cm, which entirely encloses the CubeSat, as illustrated in Figure 4.1.

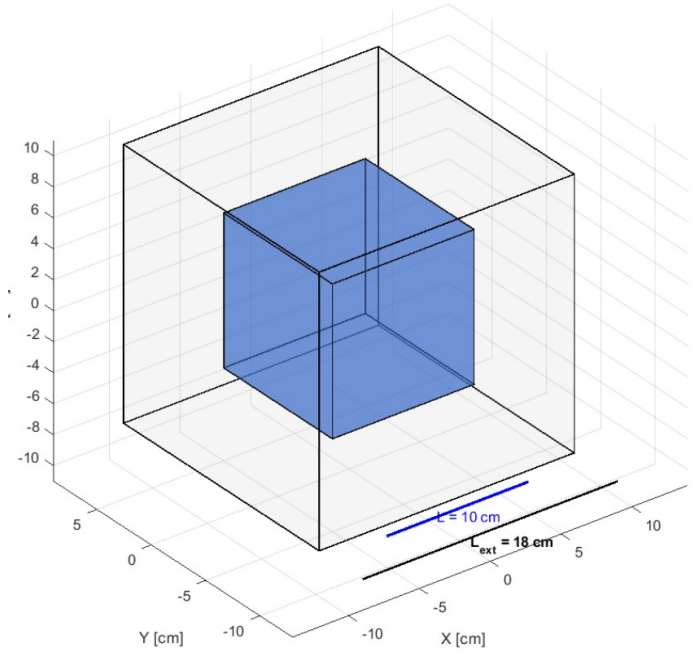

Figure 4.1: Representation of the satellite body (inner cube) and the surrounding computational gas domain

A sample of 500,000 particles is considered within the domain, and the space is discretized into cubic cells of size $dx = 1\,\text{cm}$. This configuration yields a total of $n_{cells} = 18^3 - 10^3 = 4832$ cells; consequently, the average population is around 100 particles per cell.

For the satellite surfaces we assume that the face $Y = -\frac{L}{2}$ is oriented towards the Sun with temperature $T_{satSun} = 330\,\text{K}$, the opposite face $Y = \frac{L}{2}$ has temperature $T_{satShadow} = 250\,\text{K}$, while all the remaining faces are set to $T_{SatSide} = 280\,\text{K}$.

We employ a splitting approach: in the first step, $N_c = 5$ collisions per cell are simulated using the Nanbu–Babovsky algorithm 2.4.2, followed by the transport step with the corresponding reflections. This procedure is iterated in time; using a time step $\Delta t = 10^{-5}\,\text{s}$ over the time interval $[0,\, 0.01]\,\text{s}$.

For the temperature of the gas in the domain and the initial conditions of the system, we consider two different cases:

- *Case I:* We impose different temperatures for the two gas species in the domain. In particular, we set $T_{gas_{N_2}} = 180\,\text{K}$ and $T_{gas_{O_2}} = 220\,\text{K}$, thereby forcing the system to be initially out of equilibrium.

  The internal energy is taken to be constant for each species and equal to

$$I_{in} = k_B T_{gas_{\text{species}}},$$

while the velocities are sampled uniformly in the interval $[-v_{\max}, v_{\max}]$, with

$$v_{\max} = \sqrt{3}\,\sigma_{\text{species}},$$

so as to obtain an initial kinetic temperature consistent with the imposed value.

Although this initial sampling is not physically realistic, it is useful for investigating how the model evolves from an arbitrary distribution toward the equilibrium predicted by the H-theorem.

- *Case II:* We impose the same temperature for both gas species, $T_{gas} = 200\,\text{K}$, corresponding to the equilibrium atmospheric temperature outside the computational domain.

  Both the initial internal energy and the velocities are sampled from the distributions given in (2.56), i.e. a Maxwellian distribution for the velocities and a negative exponential distribution for the internal energy.

  This sampling procedure is physically consistent with the equilibrium state.

In both cases, the same number of particles leaving the computational domain are reintroduced, representing particles arriving from infinity in the equilibrium state (2.56), we assume an atmospheric equilibrium temperature of $T_{gas} = 200\,\text{K}$. Therefore, the velocities are sampled from a flux Maxwellian, in agreement with the methodology described in Section 2.4.3. This approach governs not only the inflow of new particles into the computational domain, but also the interaction with the satellite surface, where a purely diffuse reflection model is assumed. In this case, the re-emitted particles are sampled from a flux Maxwellian distribution corresponding to the local wall temperature.

As for the internal energy, since its equilibrium distribution is a negative exponential law, it is sampled by means of the inverse transform method. It is therefore assumed that each impacting particle loses memory of its previous energy state and is re-emitted with an internal energy consistent with thermal equilibrium at the local wall temperature.

As for the cross section and the collisional kernel, we adopt a *Variable Hard Sphere* (VHS) model extended to the multispecies case. For simplicity, we assume identical molecular diameters for both species, setting the interaction parameters $C_{ij} = 1$ and $\alpha_{ij} = 1$ for all interacting pairs.

Regarding the upper bound of the collision kernel Σ, its estimation depends on the nature of the interacting particles. If the molecules involved in the collision belong to the same species, we employ the monoatomic estimate:

$$\Sigma = \mathcal{B}(2\Delta v_{\text{species}}) \tag{4.2}$$

If, instead, the collision involves two different species, we approximate the upper bound as:

$$\Sigma = \mathcal{B}(\Delta v_{O_2} + \Delta v_{N_2} + |\bar{v}_{O_2} - \bar{v}_{N_2}|), \tag{4.3}$$

where:

$$\Delta v_{specie} = \max_{i \in specie} |v_i - \bar{v}_{specie}| \qquad \bar{v}_{secie} = \frac{1}{N} \sum_{i \in specie} v_i.$$

This choice follows from the fact that, assuming we have a particle of species O_2 with pre-collisional velocity $\mathbf{v}$ and a particle of species N_2 with pre-collisional velocity $\mathbf{v}_*$, we have:

$$|v - v_*| \leq |v - \bar{v}_{O_2}| + |v_* - \bar{v}_{N_2}| + |\bar{v}_{O_2} - \bar{v}_{N_2}| \leq \Delta v_{O_2} + \Delta v_{N_2} + |\bar{v}_{O_2} - \bar{v}_{N_2}|.$$

Case I: initial uniform sampling

In this section, the results obtained using uniform distribution for the initial particle sampling are presented.

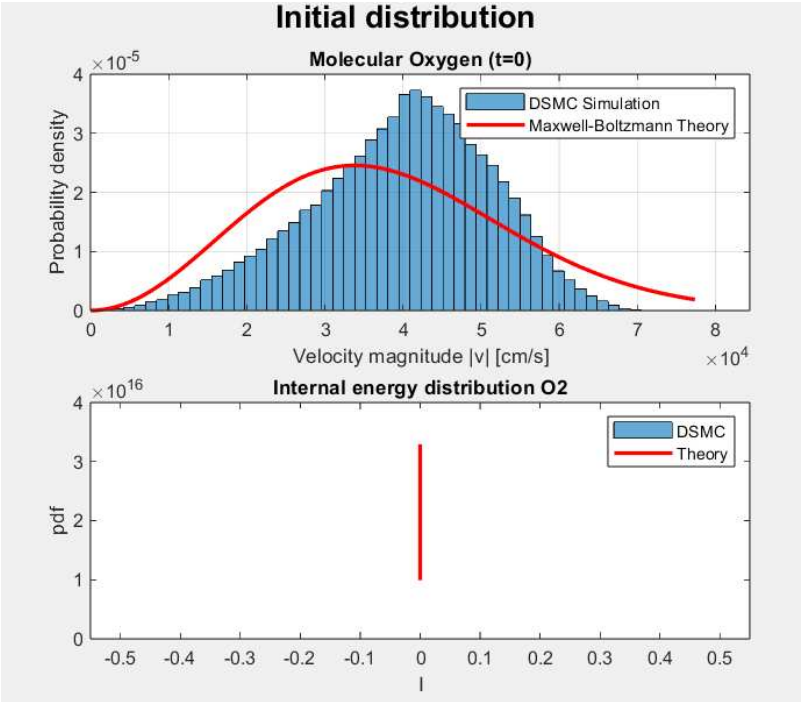

Figure 4.2: Initial velocity and internal energy distributions for O_2.

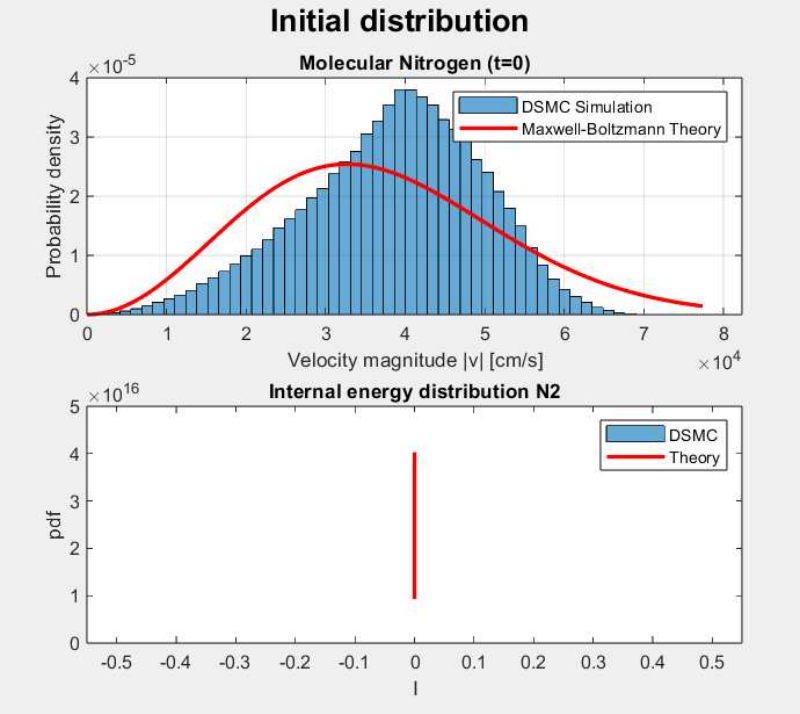

Figure 4.3: Initial velocity and internal energy distributions for N_2.

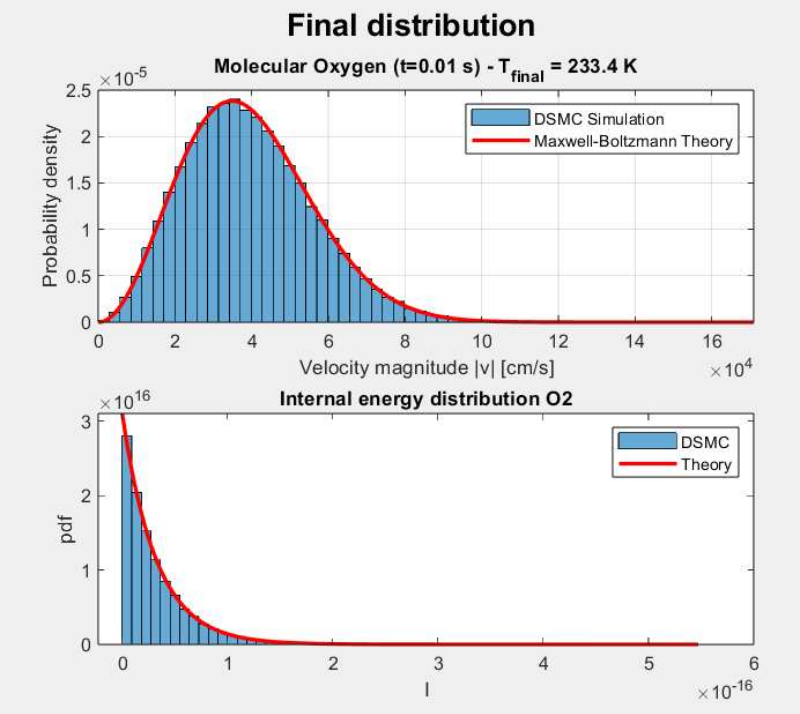

Figure 4.4: Final velocity distributions for Molecular Oxygen after $t_{max} = 0.01s$.

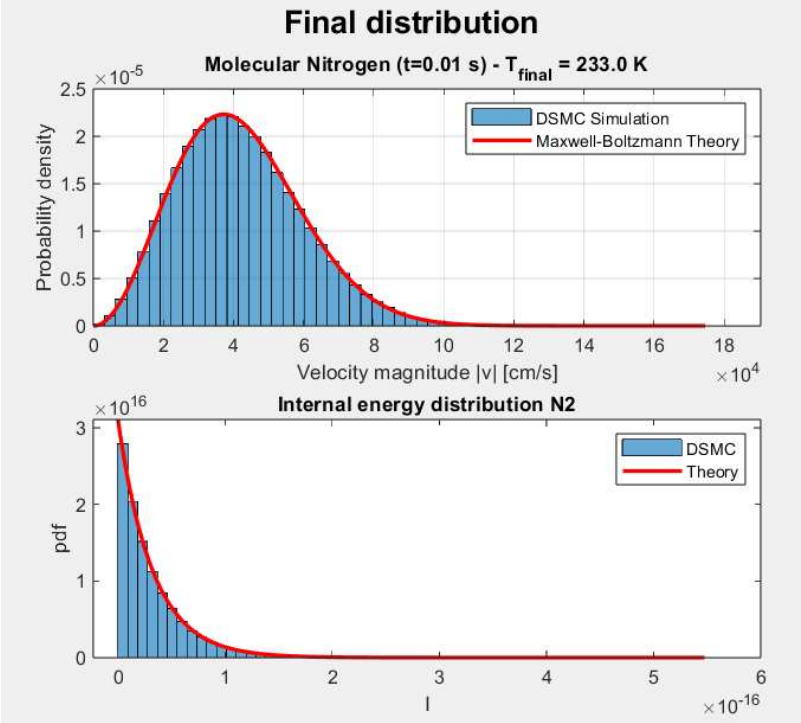

Figure 4.5: Final velocity distributions for Molecular Nitrogen after $t_{max} = 0.01s$.

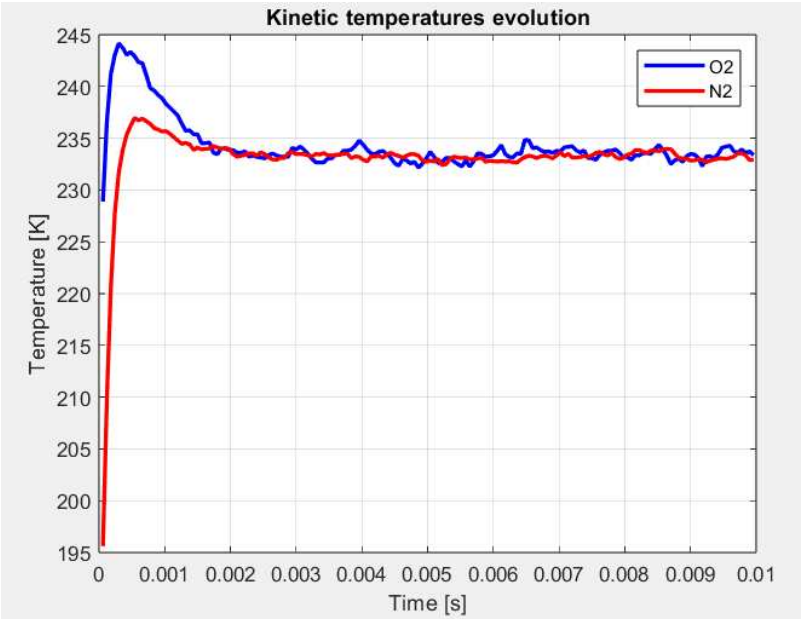

Figure 4.6: Evolution of the kinetic temperature throughout the simulation domain.

We observe that the final distribution is Maxwellian, with a kinetic temperature of approximately $T_{eq} = 233\,\mathrm{K}$, despite the fact that the system was

initialized with non-Maxwellian distributions.

Another important aspect is that the two gas species, due to the continuous injection of particles at equilibrium (i.e., with the same temperature), eventually reach a common temperature; this temperature, however, is higher than the atmospheric equilibrium temperature. This increase is a consequence of the presence of the satellite: the diffuse reflection of particles on its warmer surfaces leads to a local heating of the gas, thereby raising the effective equilibrium temperature in the region surrounding the cube.

Case II: Initial Maxwellian Sampling

In this section, the results obtained using a Maxwellian distribution for the initial particle sampling are presented.

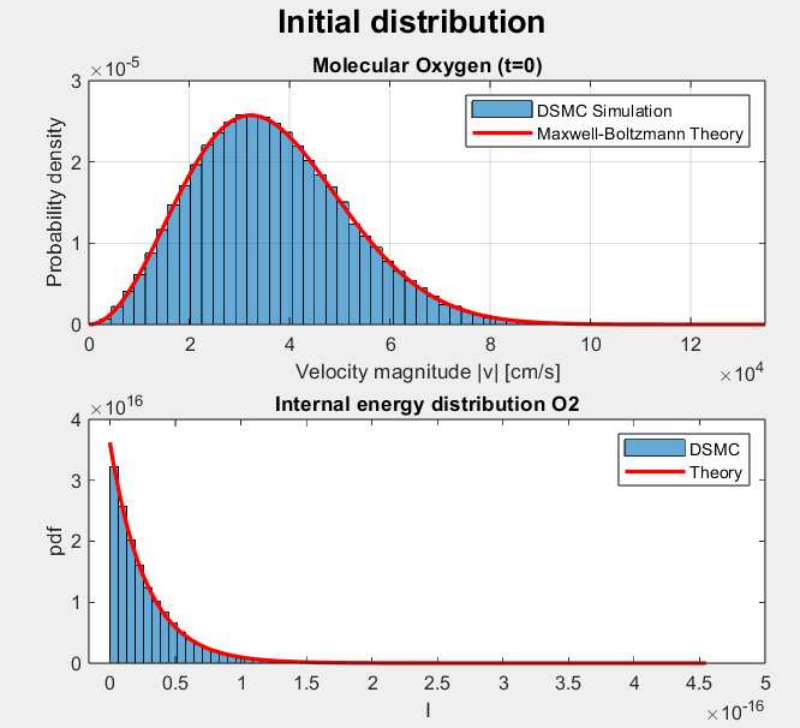

Figure 4.7: Initial velocity and internal energy distributions for O_2.

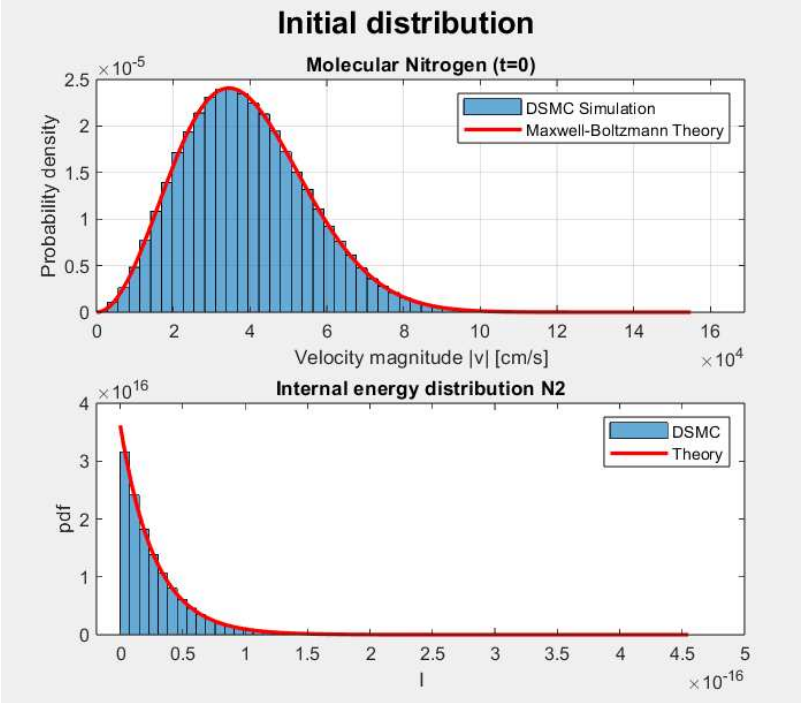

Figure 4.8: Initial velocity and internal energy distributions for N_2.

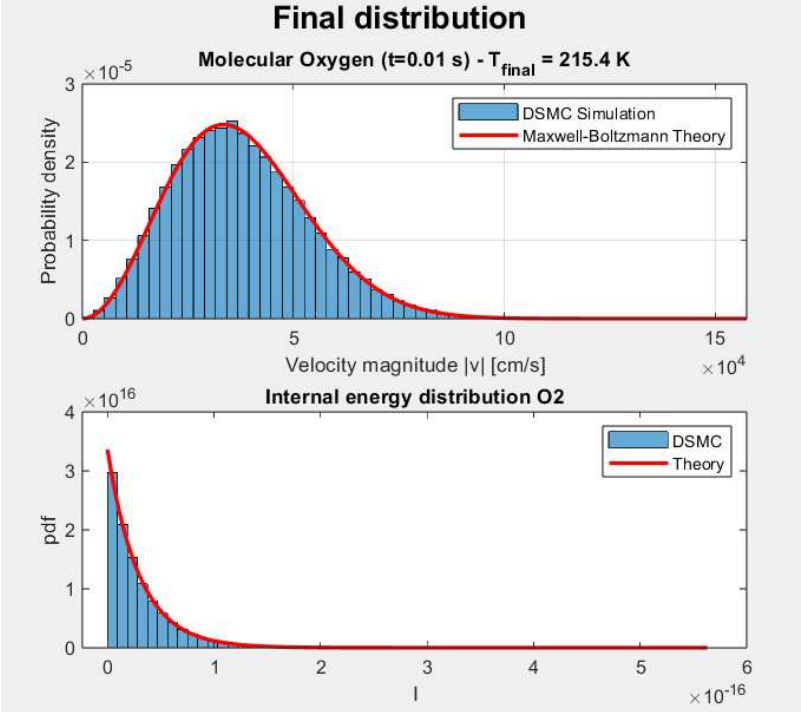

Figure 4.9: Final velocity and internal energy distributions for Molecular Oxygen after t_{max}.

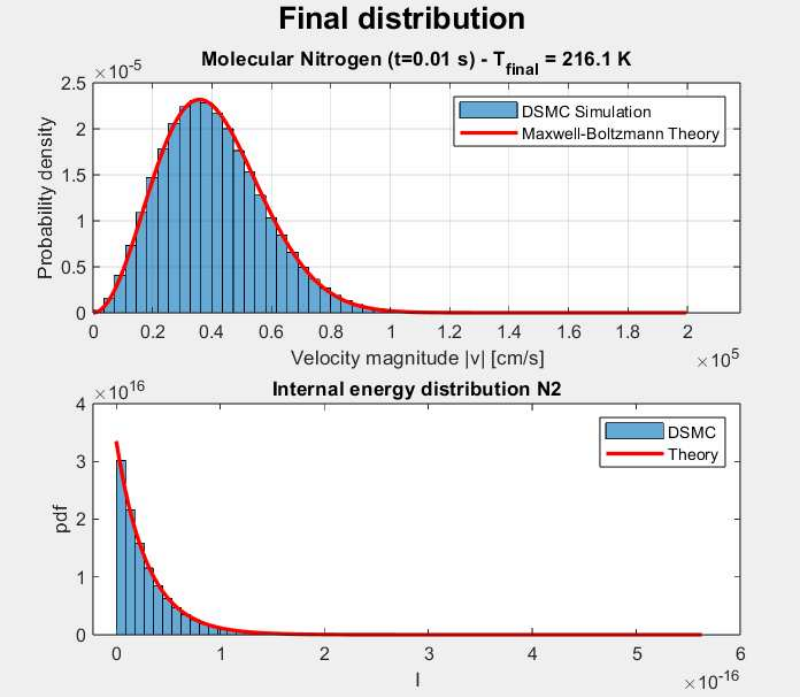

Figure 4.10: Final velocity and internal energy distributions for Molecular Nitrogen after t_{max}.

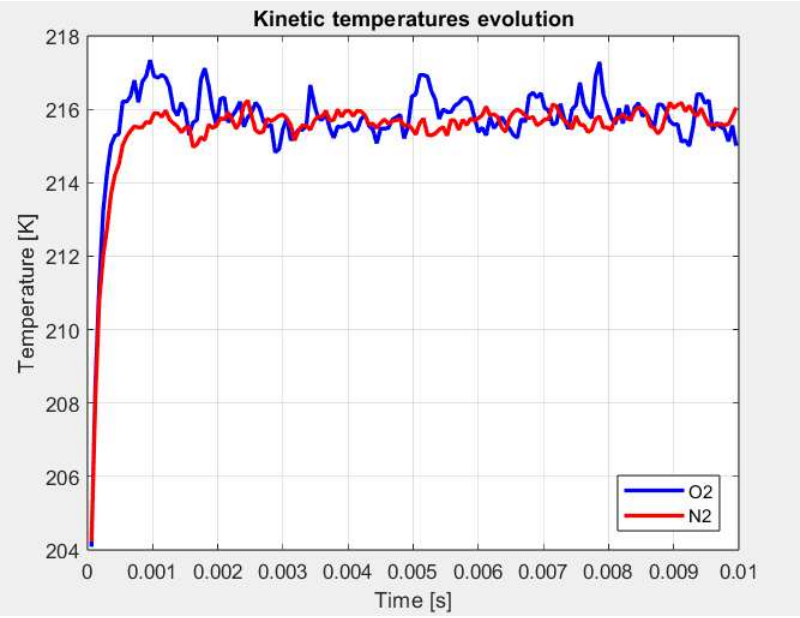

Figure 4.11: Evolution of the kinetic temperature throughout the simulation domain.

From the analysis of the plots, it can be observed that both gaseous species, under both initial conditions, progressively approach thermodynamic equilib-

rium, in agreement with the predictions of Boltzmann's H-theorem for polyatomic gas mixtures.

Moreover, the diffuse reflection mechanism at the satellite surfaces, which are maintained at a higher temperature than the surrounding gas, induces a progressive heating of the gas in the vicinity of the solid boundaries.

In both cases, the two species reach a kinetic temperature that oscillates around approximately 216 K, which is higher than the initial atmospheric gas temperature.

4.2 Numerical study of the degradation model

In this section, we simulate a CubeSat located at an altitude of approximately 400 km above the Earth. At these altitudes, the dominant species is atomic oxygen (with a kinetic temperature of approximately $T_{gas} = 1000K$), which interacts with the satellite surface and leads to degradation effects.

Therefore, the objective is to develop a DSMC model capable of reproducing the degradation patterns on the satellite surfaces. At such altitudes, as previously discussed, the mean free path is very large; consequently, the regime can be considered collisionless. It is therefore sufficient to simulate free transport and reflections at the boundaries, which are assumed to be purely diffuse, as described in Section 2.4.3. We also account for the reinjection of particles leaving the computational domain by sampling the incoming particles from a flux Maxwellian distribution.
The physical phenomenon is governed by the following system of equations:

$$\begin{cases} \dfrac{\partial f}{\partial t} + v \cdot \nabla_x f = 0 & (t,x,v) \in \mathbb{R}_+ \times (\mathbb{R}^3 \setminus \Omega) \times \mathbb{R}^3 \\ f(0,x,v) = f_{in}(x,v) & (x,v) \in (\mathbb{R}^3 \setminus \Omega) \times \mathbb{R}^3 \\ f(t,x,v) = f_b(t,x,v) & (t,x,v) \in \mathbb{R}_+ \times \Gamma_+ \end{cases} \tag{4.4}$$

The initial distribution is given by:

$$f_{in}(x,v) = n \left(\frac{m}{2\pi k_B T_{gas}} \right)^{3/2} \exp\left(-\frac{m|v-u_\infty|^2}{2k_B T_{gas}} \right),$$

where $u_\infty \in \mathbb{R}^3$ represents the satellite's drift velocity relative to the atmosphere.

While the boundary condition at the satellite surface is defined as:

$$f_b(t,x,v) = J(t,x) \frac{m^2}{2\pi (k_B T_w(t,x))^2} \exp\left(-\frac{m|v|^2}{2k_B T_w(t,x)} \right) \quad \text{for} (t,x,v) \in \mathbb{R}_+ \times \Gamma_+;$$

where:

$$J(t,x) = \int_{v \cdot n(x) < 0} f_{in}(x,v) |v \cdot n(x)| \, dv$$

We consider a cubic domain representing the CubeSat, with side length 10 cm, centered inside a spherical computational domain of radius $R = 50$, as shown in Figure 4.12. Unlike the previous simulation, where the focus was on the equilibrium configuration near the satellite, here a larger external domain is considered in order to account for particles arriving from all directions.

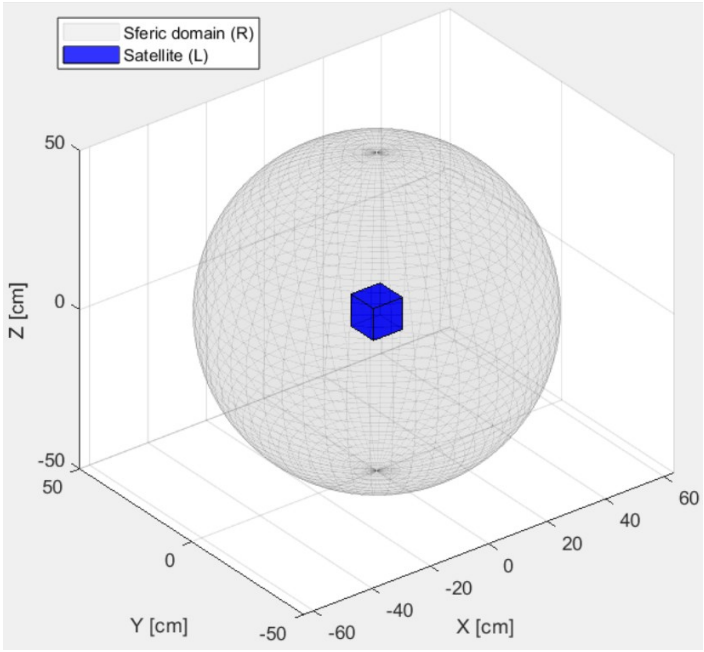

Figure 4.12: Representation of the satellite body (inner cube) and the surrounding computational gas domain.

To model degradation, each surface of the cube is discretized using a 100×100 grid. Each time one of the 500,000 particles within the domain impacts the cube, the corresponding surface cell is identified, and a degradation contribution is accumulated. In addition to the particle flux, the local degradation rate is weighted by several physical factors. Specifically, the contribution is scaled by the temperature following Arrhenius' law, the cosine of the impact angle θ between the surface normal $n(x)$ and the incident velocity vector v, as well as by the kinetic energy of the impinging molecule. These factors represent the primary causes of atomic oxygen degradation, as discussed in [7]. In the case of Kapton, the previously cited article reports that the dependence on kinetic energy follows a power law; specifically, the weight of the erosion function is proportional to $E_c^{0.68}$.

The Arrhenius law describes the rate at which the degradation process occurs, in our case driven by atomic oxygen, and illustrates how the reaction rate k directly depends on the temperature T_w of the exposed object. Specifically,

the relationship establishes that:

$$k \propto \exp\left(\frac{-E_a}{RT_w}\right);$$

where E_a represents the activation energy, which is the energy required to trigger the corrosive process, while R is the universal gas constant. For our simulation, we have adopted a value of $E_a = 0.4$ eV, which is the value reported in [7] for Kapton.

If a particle impacts an edge or a vertex (abbiamo assunto una tolleranza di 10^8), the degradation contribution is assumed to be distributed equally among the two or three corresponding adjacent cells, respectively. This approach prevents numerical singularities and ensures a more realistic representation of material degradation near the geometric discontinuities of the CubeSat.

The degradation values accumulated in the cells of the different faces of the cube were normalized, in these simulations, with respect to the maximum value recorded over the entire domain. This approach is appropriate for analyzing the relative distribution of erosion over limited time intervals. However, for long-term simulations, it is preferable to adopt a normalization based on a fixed degradation parameter; this allows one to monitor the saturation of the different faces or cells as they approach maximum degradation, independently of the evolution of values in the remaining portions of the CubeSat.

4.2.1 Case I: Fixed temperature

In this section, the satellite surface temperatures are assumed to be constant over time. This approximation is physically sound given the extremely short simulation interval of $[0, 0.1]s$.
Specifically, we assume that the face $Y = -L/2$ is oriented towards the Sun with a temperature $T_{satSun} = 330$ K, the opposite face $Y = L/2$ has a temperature $T_{satShadow} = 250$ K, while all the remaining lateral faces are set to $T_{satSide} = 280$ K.

Isotropic influx of atomic Oxygen

In this section, we consider a scenario where molecules enter the spherical domain isotropically; consequently, the drift velocity is set to $u_\infty = [0, 0, 0]$. With no preferred direction in the incoming flux, we can isolate the effects of the model parameters on the degradation process without any directional bias.

If we consider only the effect of the impact angle θ between the surface normal $n(x)$ and the incident velocity vector v, together with the kinetic energy of the impinging molecules, neglecting for now temperature effects, we obtain a degradation pattern as shown in the figure 4.13.

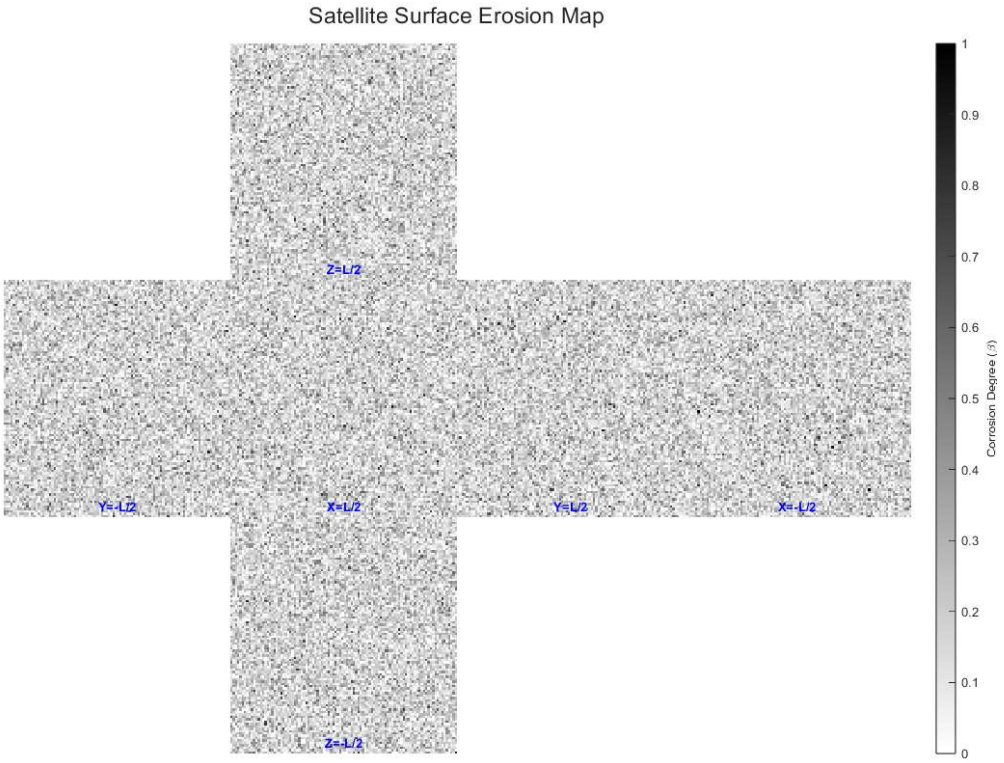

Figure 4.13: Final degradation plot on the CubeSat with zero drift and no temperature effects.

We observe that the degradation is distributed uniformly across all six faces of the CubeSat. This is consistent with the fact that the model depends solely on geometric parameters, while the incoming particles are isotropic, so no face is preferentially exposed.

If, in addition to the geometric contribution, we also include a temperature-dependent effect, the resulting degradation pattern is the one shown in the figure 4.14.

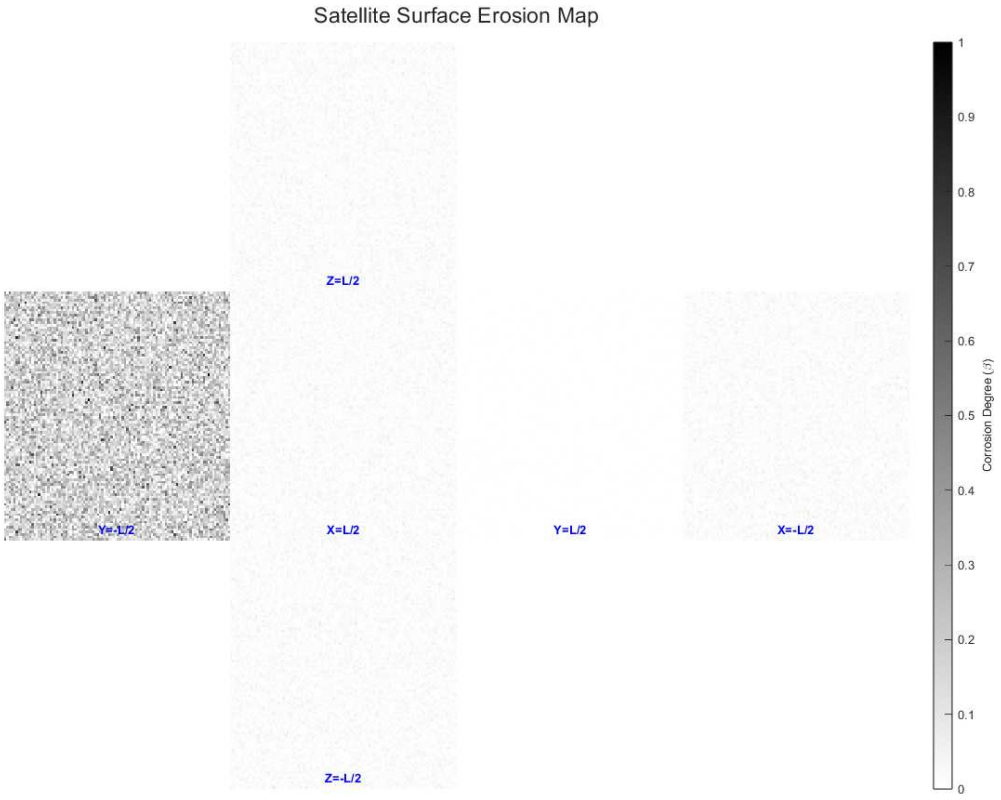

Figure 4.14: Final degradation plot on the CubeSat with zero drift and the temperature effects.

We immediately notice that the hottest face ($Y = -L/2$) exhibits the highest level of degradation. This is consistent with the Arrhenius law, which predicts higher reaction rates at higher temperatures. Another important observation is that faces with the same temperature are less corroded compared to the isotropic case. This is because the Arrhenius-type dependence of the degradation rate slows down the process on the cooler faces, reducing the overall erosion there.

Effect of satellite drift on atomic oxygen degradation

In this section, we also include a drift term $u_\infty = v_{magn}[1, 0, 0]$ with $v_{magn} = 7.7 \times 10^5$ cm/s, accounting for the motion of the satellite. Compared to the isotropic case, where geometric effects led to uniform degradation across the faces, we now observe a different behavior, as shown in the figure 4.15.

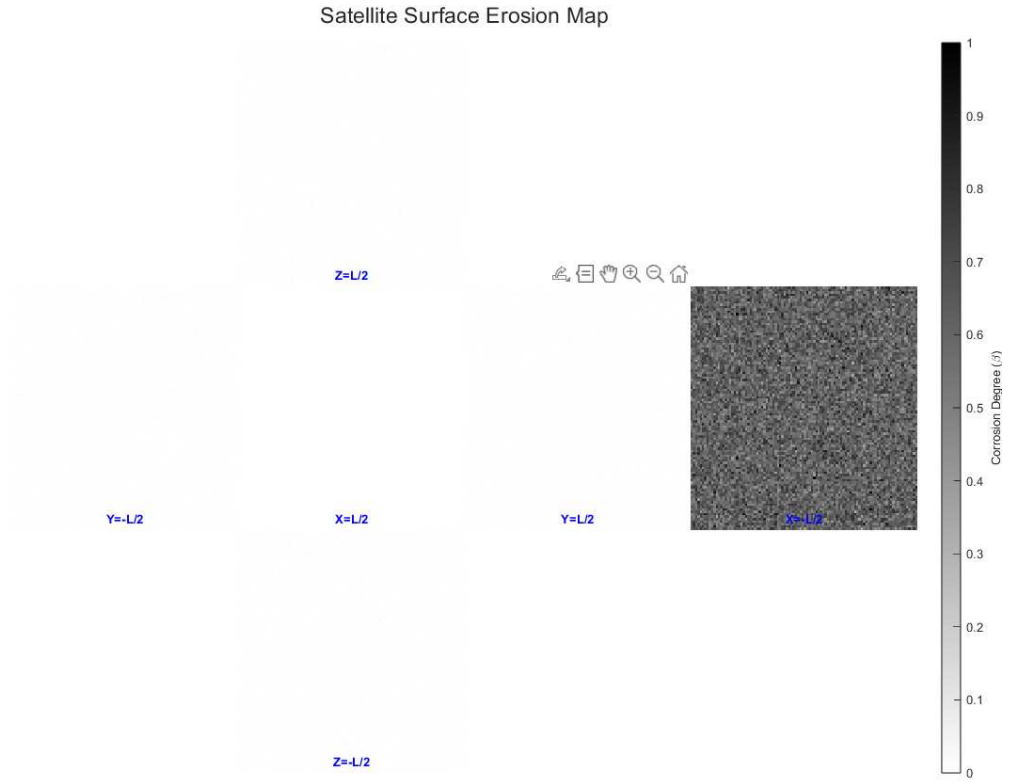

Figure 4.15: Final degradation plot on the CubeSat with drift and no temperature effects.

We note that particles tend to impact more frequently on the face ($X = -L/2$), which is directly exposed to the flow. Moreover, since the magnitude of the orbital velocity is of the order of 10^5, the particles colliding with the face oriented toward the flow possess very high kinetic energy, making degradation on the other faces practically negligible by comparison.

If, in addition to the drift term, we include the contribution of temperature to the degradation process, we obtain the CubeSat degradation profile shown in Figure 4.16.

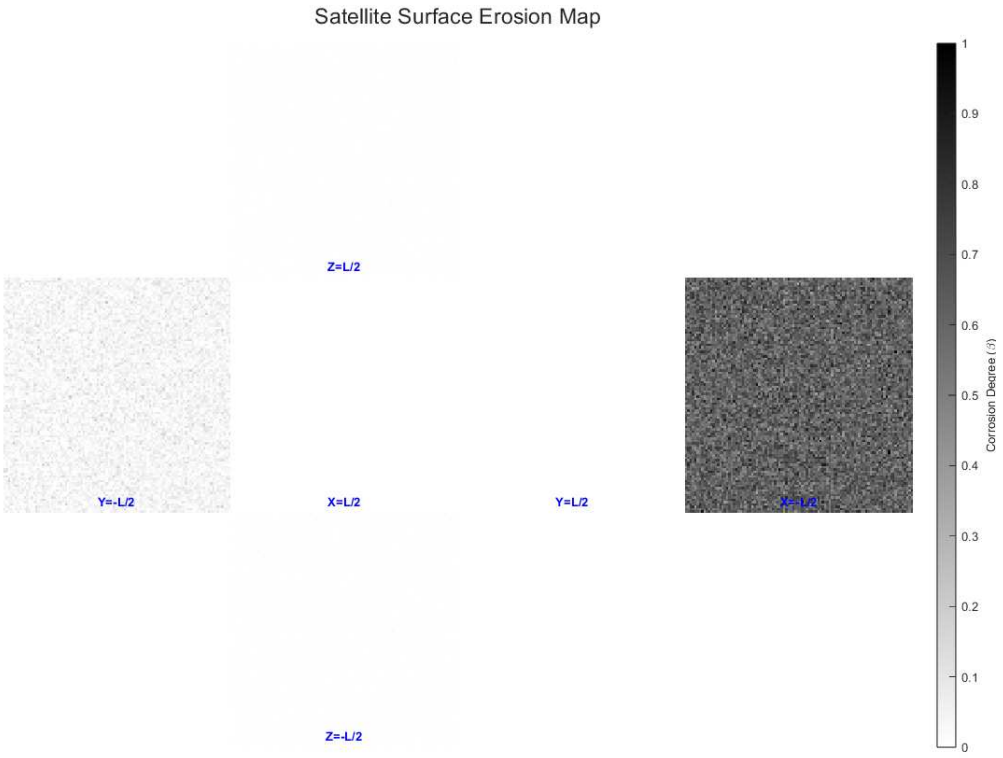

Figure 4.16: Final degradation plot on the CubeSat with drift and the temperature effects.

It is observed that, in addition to the degradation induced by the drift term, the contribution of the thermal gradient emerges; on the surface with the highest temperature, it is no longer completely dominated by the drift.

To further demonstrate the correct behavior of the DSMC method and to highlight the temporal evolution of the degradation, we also report, for this case, the degradation profile at half the final time, shown in Figure 4.17.

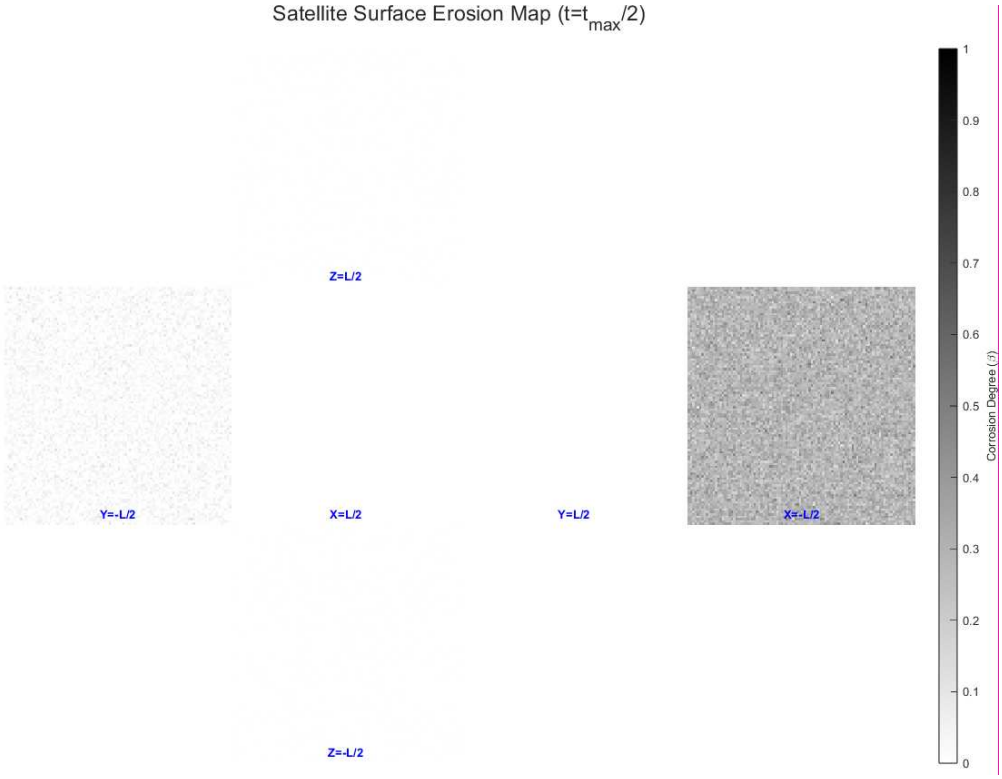

Figure 4.17: degradation plot on the CubeSat at intermediate time with drift and temperature effects.

In this case, the degradation values are normalized with respect to the maximum value attained at the final time, and the surface clearly appears less corroded, consistently with the expected temporal evolution.

4.2.2 Case II: Oscillating temperature

We now consider the case in which the satellite rotates around the z-axis with a period $P = 0.1\,\mathrm{s}$. As the Sun remains in a fixed position, this rotation induces a time-dependent oscillation of the surface temperature.

We therefore assume temperatures oscillating between $T_{\min} = 250\,\mathrm{K}$ and $T_{\max} = 330\,\mathrm{K}$, and we take the face exposed to the Sun to be $Y = -\frac{L}{2}$. In particular, we consider the following temperature distribution:

$$\begin{cases} T_{y_n}(t) = T_m + A\cos(\omega t) \\ T_{y_p}(t) = T_m + A\cos(\omega t + \pi) \\ T_{x_n}(t) = T_m + A\cos(\omega t - \frac{\pi}{2}) \\ T_{x_p}(t) = T_m + A\cos(\omega t + \frac{\pi}{2}) \\ T_{z_n}(t) = T_m \\ T_{z_p}(t) = T_m \end{cases} \tag{4.5}$$

where T_m and A denote the mean temperature and the amplitude, defined as

$$T_m = \frac{T_{\max} + T_{\min}}{2}, \quad A = \frac{T_{\max} - T_{\min}}{2},$$

and $\omega = \frac{2\pi}{P}$ is the angular frequency associated with the period P. Since the rotation occurs around the z-axis, the temperature of the faces $Z = \pm\frac{L}{2}$ is kept constant, as their orientation with respect to the Sun does not change.

Using a DSMC approach, we simulate the degradation of the CubeSat by considering the wall temperature, the cosine of the angle between the incident velocity and the surface normal, and the kinetic energy as the main contributing factors. The result is shown in Figure 4.18.

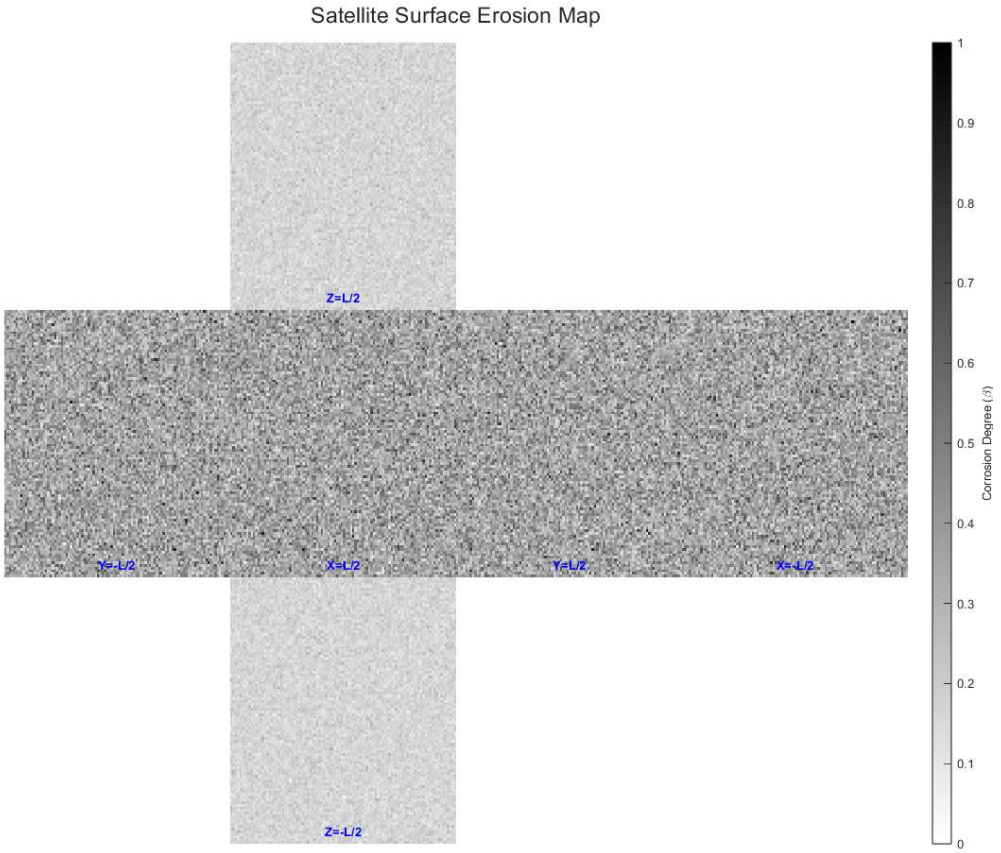

Figure 4.18: Final degradation pattern on the CubeSat rotating around the z-axis

As can be observed, the oscillating temperature leads to a more uniform degradation over the four lateral faces, which are periodically exposed to the Sun during the rotation. Moreover, the nonlinear dependence of the Arrhenius law implies that the faces undergoing temperature fluctuations (X and Y) experience a higher average degradation rate than the Z faces, which remain at a constant mean temperature.

Conclusions

In the present thesis work, the interaction between the atmosphere in Very Low Earth Orbit (VLEO) and a CubeSat has been analyzed. Due to the rarefied nature of the atmosphere within the VLEO regime, the continuum hypothesis is no longer applicable, necessitating a kinetic description in place of classical fluid dynamic models, such as the Euler equations. Consequently, the adoption of kinetic theory proved indispensable.
Furthermore, since atmospheric composition varies significantly with altitude, a polyatomic Boltzmann model for mixtures was employed for altitudes near 100 km, where the mean free path is small relative to the characteristic dimensions of the satellite and the species are non reactive. Conversely, for altitudes around 400 km, where the mean free path is such that particle collisions become negligible compared to the characteristic dimensions of the satellite, a monoatomic free molecular flow model was adopted, accounting for the predominance of highly reactive atomic oxygen.

Regarding the monoatomic case at 400 km, we investigated an existence and uniqueness theorem for the solution of the differential system, supplemented with boundary conditions on a convex body (smoothing the edges of the CubeSat). Moreover, we established the existence and the two-scale limit of the solution for cases where the surface temperature oscillates, consistently with the satellite's orbital motion.

Polyatomic gas mixtures and their interaction with the CubeSat were simulated through a DSMC method, allowing for an analysis of the convergence to equilibrium in the region immediately surrounding the satellite. The results demonstrated how diffuse reflections and intermolecular collisions influence the gas convergence toward a Maxwellian distribution, with the temperature shifting as a result of reflections with the warmer boundaries.

The predominance of reactive atomic oxygen leads to degradation phenomena on satellite surfaces. Consequently, the degradation process was simulated in a DSMC and its behavior analyzed in relation to relevant physical factors, such as particle flux, temperature, drift, and impact angle. Furthermore, the two-scale convergence of a degradation functional, characterized by a temperature-dependent kernel, was rigorously studied.

As an outlook, the present framework could be extended to incorporate

chemical reactions within the polyatomic gas model, allowing for a more accurate description of high altitude atmospheric interactions. Furthermore, in the context of end of life satellite scenarios, where the objective is to minimize space debris, the satellite is typically accelerated to induce re-entry, and in such regimes the assumptions underlying both Boltzmann and free transport models progressively lose validity, making a description based on plasma dynamics necessary.
Moreover, the DSMC-based degradation model could be further refined by accounting for the material-dependent response of the satellite surface, enabling a more realistic characterization of degradation processes. Finally, the degradation functional, here modeled through a kernel monotonically increasing with temperature, could be generalized by incorporating additional environmental factors, such as particle energy distribution and incident flux, thereby providing a more comprehensive description of the degradation dynamics.

Appendices

Appendix A

Useful data and tables

A.1 Chapman and Cowling molecular diameters

We report Table 11 extracted from [6], containing the viscosities and molecular diameters of gases. In particular, we focus on the diameters (fourth column) of diatomic oxygen (O_2) and diatomic nitrogen (N_2).

Table 11. ***Viscosities and molecular diameters of gases at*** **S.T.P.**

Gas	Molecular weight	$10^7 \times \mu$ (poise)†	$10^8 \times \sigma$ (cm.)
Hydrogen	2·016	845	2·745
Deuterium	4·029	1191	2·751
Helium	4·003	1865	2·193
Methane	16·043	1024	4·187
Ammonia	17·031	923	4·477
Neon	20·183	2975	2·602
Acetylene	26·038	948	4·912
Carbon monoxide	28·011	1635	3·810
Nitrogen	28·013	1656	3·784
Ethylene	28·054	927	5·062
Air	—	1719	—
Nitric oxide	30·007	1774	3·720
Ethane	30·070	858	5·353
Oxygen	32	1919	3·636
Hydrogen sulphide	34·080	1163	4·743
Hydrogen chloride	36·461	1328	4·514
Argon	39·944	2117	3·659
Carbon dioxide	44·011	1380	4·643
Nitrous oxide	44·013	1351	4·692
Methyl chloride	50·488	968	5·737
Sulphur dioxide	64·064	1164	5·551
Chlorine	70·906	1233	5·534
Krypton	83·80	2328	4·199
Xenon	131·30	2107	4·939

* See, for example, reference (1) in the list at the end of this chapter. Later references to this list will be indicated by figures in the text, as (1).
† 1 poise = 1 g./cm. sec.

Figure A.1: Original table [6] of viscosities μ and molecular diameters σ of gases.

Bibliography

[1] G. Allaire. Homogenization and two-scale convergence. SIAM Journal on Mathematical Analysis, 23(6):1482–1518, 1992.

[2] G. Allaire, X. Blanc, B. Despres, and F. Golse. Transport et diffusion. Editions de l'Ecole de polytechnique, 2018.

[3] C. Bardos. Problèmes aux limites pour les équations aux dérivées partielles du premier ordre à coefficients réels; théorèmes d'approximation; application à l'équation de transport. Annales scientifiques de l'École normale supérieure (4), 3(2):185–233, 1970.

[4] E. Bernard, F. Golse, and F. Salvarani. Homogenization of transport problems and semigroups. Mathematical Methods in the Applied Sciences, 33(10):1228–1234, 2010.

[5] C. Burkhard and S. Weston. The evolution of cubesat spacecraft platforms. In NATO Science and Technology Organization, Moffett Field, CA, 2021.

[6] S. Chapman and T. G. Cowling. The Mathematical Theory of Non-uniform Gases: An Account of the Kinetic Theory of Viscosity, Thermal Conduction and Diffusion in Gases. Cambridge Mathematical Library. Cambridge University Press, Cambridge, 3rd edition, 1970.

[7] A. de Rooij. Corrosion in space. Technical report, European Space Agency (ESA), Materials and Components Technology Division, Noordwijk, The Netherlands.

[8] L. Desvillettes, R. Monaco, and F. Salvarani. A kinetic model allowing to obtain the energy law of polytropic gases in the presence of chemical reactions. European Journal of Mechanics B/Fluids, 24(2):219–236, 2005.

[9] ESA. Esa seeks space applications ideas in very low earth orbit, 2023.

[10] NASA. What is a satellite?, 2023.

[11] NASA. What are smallsats and cubesats?, 2024.

[12] NASA CubeSat Launch Initiative. CubeSat 101: Basic Concepts and Processes for First-Time CubeSat Developers. National Aeronautics and Space Administration (NASA), Washington, DC, 2017. Revisione di Ottobre 2017. Prodotto in collaborazione con California Polytechnic State University.

[13] L. Pareschi and G. Russo. An introduction to the numerical analysis of the boltzmann equation. Rivista di Matematica della Università di Parma, 4(7):145–250, 2005.

[14] M. Rupin, F. Lemoult, G. Lerosey, and P. Roux. Experimental demonstration of ordered and disordered multiresonant metamaterials for lamb waves. Physical Review Letters, 112(23):234301, 2014.

[15] C. Shen. Rarefied Gas Dynamics: Fundamentals, Simulations and Micro Flows. Springer Science & Business Media, Berlin, Heidelberg, 2005.

[16] L. Tartar. Compensated compactness and applications to partial differential equations. In Nonlinear Analysis and Mechanics: Heriot-Watt Symposium, volume 39 of Research Notes in Mathematics, pages 136–212. Pitman, Boston, MA, London, 1979.

[17] L. Tartar. An Introduction to Navier–Stokes Equation and Oceanography, volume 1 of Lecture Notes of the Unione Matematica Italiana. Springer, Berlin, Heidelberg, New York, 2006.

[18] U.S. Committee on Extension to the Standard Atmosphere. U.s. standard atmosphere, 1976. Technical Report NOAA-S/T 76-1562, National Oceanic and Atmospheric Administration, National Aeronautics and Space Administration, United States Air Force, Washington, D.C., 1976.